

21966052



This is to certify that the

dissertation entitled

A THREE-DIHENSIONAL FINITE ELEMENT ANALYSIS OF THE TEMPERATURE DISTRIBUTION ON THE FLOOR OF A FARROWING HOUSE

presented by

Heeseung Choi

has been accepted towards fulfillment of the requirements for

Ph. D degree in Agri. Engineering

Date Oct. 3 , 1988

Jane Segoline



RETURNING MATERIALS: Place in book drop to remove this checkout from your record. FINES will be charged if book is returned after the date stamped below.

A THREE-DIMENSIONAL FINITE ELEMENT ANALYSIS OF THE TEMPERATURE DISTRIBUTION ON THE FLOOR OF A FARROWING HOUSE

Ву

Heeseung Choi

A DISSERTATION

Submitted to

Michigan State University

in partial fulfillment of the requirements

for the degree of

DOCTOR OF PHILOSOPHY

in

Agricultural Engineering

Department of Agricultural Engineering

1988

ABSTRACT

A THREE-DIMENSIONAL FINITE ELEMENT ANALYSIS OF THE TEMPERATURE DISTRIBUTION ON THE FLOOR OF A FARROWING HOUSE

By

Heeseung Choi

The typical hot water floor heating system for a solid floor farrowing house has a complicated pipe circuit that heats the pig creep area but avoids the area beneath the sow. The typical system is costly to construct, has a relatively high pumping resistance and provides a less-than-desirable temperature distribution in the creep area. An improved hot water heating circuit that runs beneath the sow and the creep area has been used to eliminate some of the problems. This improved system uses insulation around the pipe and between the pipe and floor surface in the area beneath the sow to obtain the desired floor temperature in the sow area.

No design method exists for the improved system. The floor temperature provided by the improved pipe system is a function of the number, size, depth and spacing of the heat pipes, the insulation size and the placement, and the size of the fins that can be attached to the pipes. A three-dimensional finite element heat transfer program was used to calculate the temperature distribution on the floor surface for various arrangements of the new heating system. The finite element method was also used to find a design condition for each of three possible

Heeseung Choi

arrangements. A three-dimensional finite element grid generation program was written specifically for this study to generate the large volume of input data required in a solution.

Three different arrangements were studied: (1) three hot water pipes without fins, (2) three pipes with a steel fin attached, and (3) three pipes with a copper fin attached. Prototype designs that gave the most desirable temperature distribution on the floor were recommended for each case. The recommended heating systems provide six places in the creep area with the desired piglet temperature range and a sow area within the desired temperature range. The heat input of the sow to the floor was not incorporated into this study. The structural strength of the floor resulting from the placement of flat sheets of insulation in the concrete also was not investigated. The new designs reduce operation costs and the pumping energy requirements. The farrowing areas near the cooler end of the hot water pipe line can be heated to the desired temperature by adjusting the size of the fins attached to the pipes.

Approved

Approved

Department Chairman

Copyright by
HEESEUNG CHOI
1988

To my wife Yangjin and our son Sungwoo and my father and mother in Korea

ACKNOWLEDGMENT

The author wishes to express the deep gratitude and appreciation to his major professor, Dr. Larry J. Segerlind (Agricultural Engineering) for the guidance, knowledge and encouragement throughout the graduate program.

To the other members of the guidance committee, Dr. Thomas H. Burkhardt (Agricultural Engineering), Dr. Howard L. Person (Agricultural Engineering), and Dr. Gary L. Cloud (Metallurgy, Mechanics and Material Science), the author owes a debt of their inspiration and advices.

Gratitude is extented to Dr. John B. Gerrish (Agricultural Engineering) and Andy Thulin (Animal Science) for constructive suggestions and criticisms. Author also wish to thank Dr. John D. Carlson (Agricultural Engineering) for his encourage in Christianity.

TABLE OF CONTENTS

	List	of Tabl	es	ix
	List	of Figu	res	x
Cha	pter		P	age
I.	INT	RODUC	CTION	1
II.	LIT	ERATU	RE REVIEW	4
	2.1	Farrow	ing House	4
	2.2	Three-I	Dimensional Finite Element Analysis	6
	2.3	Finite I	Element Formulation	8
m.	AN	ALYSIS	OF A TYPICAL FARROWING HOUSE	17
	3.1	Farrow	ing Crate Dimensions and Finite Element Model	17
	3.2	Calcula	ted Temperature Values	21
IV.	CA	LCULAT	TIONS RELATED TO THE DESIGN OF A HOT WATER	
	HE.	ATING	SYSTEM	26
	4.1	Finite I	Element Grid Generation	27
	4.2	Calcula	tions Related to the Design of a Piping System	30
		4.2.1	Placement depth of flat insulation (D)	32
		4.2.2	Thickness of flat insulation (tF)	32
		4.2.3	Width of flat insulation (W)	36
		4.2.4	Thickness of perimeter insulation (tP)	36
		4.2.5	Thickness of flat insulation above the perimeter insulated	
			pipe	42
		4.2.6	Width of flat insulation above the perimeter insulated pipe	42

	4.2.7 Su	mmary	42
V.	PROTOTYPE	MODELS FOR HOT WATER HEATING SYSTEM	
	IN A FARROV	VING HOUSE	46
	5.1 Three Hea	ting Pipes without Fins	46
	5.1.	Thickness of flat insulation	48
	5.1.5	2 Width of flat insulation	50
	5.1.3	B Length of perimeter insulation	50
	5.1.4	Recommended model	53
	5.2 Three Hea	ting Pipes with Steel Fins	58
	5.2.	1 Length of fin	58
	5.2.	2 Thickness of fin	61
	5.2.3	Recommended model	61
	5.3 Three Hea	ting Pipes with Copper Fins	66
	5.3.	1 Length of fin	70
	5.3.	2 Thickness of fin	70
	5.3.3	3 Width of flat insulation	7 5
	5.3.	4 Recommended model	75
	5.4 Effect of F	Room and Hot Water Temperature	81
VI.	DISCUSSION	AND SUMMARY	86
VII	CONCLUSION	VS	89
	APPENDIX A	GRID GENERATION PROGRAM	91
	APPENDIX B	FINITE ELEMENT HEAT TRANSFER PROGRAM	98
	APPENDIX C	PIPE HEAD LOSS	109
	BIBLIOGRAP	HY	119

LIST OF TABLES

Table	I	Page
2.1	Shape functions and derivatives for eight node hexahedron	. 13

LIST OF FIGURES

Figure	P	age
1.1	Pipe arrangement in a typical hot water heating system of the farrowing	
	house which has 10 pens	3
1.2	Pipe arrangement in a modified hot water heating system	3
2.1	Location of eight nodes in natural and Cartesian coordinates	12
3.1	Typical cross - section of concrete floor heated with hot water	18
3.2	Typical crate dimensions	19
3.3	Temperature distribution on the floor of the typical farrowing house	
	heated with hot water.	22
3.4	Temperature contour on the floor of the typical farrowing house	
	heated with hot water.	24
3.5	Temperature distribution on the floor when 1.3 cm thick and 5.1 cm	
	wide flat insulation is applied over the hot water pipes	2 5
4.1	Element for the model of three heat pipes without fin and the location	
	of coordinates (Dimension of z-axis is expanded)	29
4.2	Variables for the test model	31
4.3	Effect of D, the placement depth of flat insulation	
	(tF = 1.3 cm, W = 15.2 cm)	33
4.4	Effect of tF, the thickness of flat insulation	
	(D = 2.5 cm, W = 15.2 cm)	34
4.5	Temperature drop according to the thickness of flat insulation	35
4.6	Effect of W, the width of flat insulation (tF = 1.3 cm , D = 2.5 cm)	37

4.7	Effect of W, the width of flat insulation (tF = 2.5 cm , D = 2.5 cm)	3 8
4.8	Temperature drop according to the width of flat insulation	
	(tF = 1.3 cm, D = 2.5 cm)	39
4.9	Temperature drop according to the width of flat insulation	
	(tF = 2.5 cm, D = 2.5 cm)	40
4.10	Effect of the thickness of perimeter insulation (No flat insulation)	41
4.11	Effect of the thickness of flat insulation on the perimeter insulated pipe	
	(D = 2.5 cm, W = 15.2 cm, tP = 1.0 cm)	43
4.12	Effect of the width of flat insulation on the perimeter insulated pipe	
	(tF = 1.3 cm, D = 2.5 cm, tP = 1.0 cm)	44
5.1	Variables for the model of three pipes without fin	47
5.2	Effect of the thickness of flat insulation	
	$(L_1 = 50.8 \text{ cm}, W_1 = W_2 = 15.2 \text{ cm}, L_2 = 76.2 \text{ cm})$	49
5.3	Effect of the width of flat insulation	
	$(L_1 = L_2 = 50.8 \text{ cm}, W_1 = 15.2 \text{ cm}, TI = 1.3 \text{ cm})$	51
5.4	Effect of the length of perimeter insulation	
	$(L_1 = 50.8 \text{ cm}, W_1 = 15.2 \text{ cm}, W_2 = 5.1 \text{ cm}, TI = 0.64 \text{ cm})$	52
5.5	Recommended model for three pipes without fin	54
5.6	Temperature distribution on the floor of recommended model for	
	three pipes without fin	55
5.7	Temperature contour on the floor of the recommended model for	
	three pipes without fin	56
5.8	Three-dimensional temperature distribution of recommended model	
	for three pipes without fin	57
5.9	Variables of fin and insulation for model of three pipes with fin	59
5.10	Effect of the length of steel fin (LI = 76.2 cm, WI = 15.2 cm,	
	TI = 1.3 cm WF = 25.4 cm, TF = 0.5 cm)	60

5.11	Temperature change on the steel fin	62
5.12	Effect of the thickness of flat insulation on 22.9 cm long steel fin	63
5.13	Effect of the thickness of steel fins	64
5.14	Recommended model for three pipes with steel fins	65
5.15	Temperature distribution on the floor of recommended model for	
	three pipes with steel fins	67
5.16	Temperature contour on the floor of the recommended model for	
	three pipes with steel fins	68
5.17	Three-dimensional temperature distribution of recommended model	
	for three pipes with steel fins.	69
5.18	Effect of the length of copper fin (LI = 76.2 cm, WI = 15.2 cm,	
	TI = 1.3 cm, WF = 25.4 cm, TF = 0.5 cm)	71
5.19	Temperature change on the copper fin	72
5.20	Effect of the thickness of flat insulation on 15.2 cm long copper fin	73
5.21	Effect of the thickness of copper fin	74
5.22	Effect of the width of flat insulation on 22.9 cm long copper fin	76
5.23	Recommended model for three pipes with copper fin	77
5.24	Temperature distribution on the floor of recommended model for	
	three pipes with copper fins	78
5.25	Temperature contour on the floor of the recommended model for	
	three pipes with copper fins	79
5.26	Three-dimensional temperature distribution of recommended model	
	for three pipes with copper fins	80
5.27	Effect of the hot water temperature at the room temperature 15.6 °C	82
5.28	Effect of the room temperature at the water temperature 60°C	83
5.29	Temperature distribution in condition of 13.9 °C (57 °F) room	
	temperature and 62.8 °C (145 °F) water temperature	85

I. INTRODUCTION

The farrowing house must provide a comfortable environmental condition for the young piglets and the sows at the same time. The new-born piglet needs a temperature of 29.4°C to 32.2°C (85°F to 90°F) to protect it from chilling, because it is poorly endowed with hair, has a low amount of body fat and a thin skin. Since chilling is a major cause of death in baby pigs, the new born piglet must be kept warm enough to survive the first three days of life. On the contrary, the sow prefers a temperature of 15.6°C to 18.3°C (60°F to 65°F) to optimize feed intake, milk production, and sow condition. Two separate thermal environments are needed in a relatively small region of a farrowing house.

To provide the environment for the piglets, additional heat sources are added in the baby pig creep area. Suspended infra-red lamps and suspended electric bar heaters are often used in solid floor systems while heat pads are used to provide a warm micro-climate for the baby pigs on slotted floors. The use of these devices allows the remainder of the room to be maintained at a condition better for the sow. A hot water floor heating system is also used in farrowing houses to provide extra heat for the litter without excessive heating of the entire building. The hot water pipe system shown in Figure 1.1 by a dotted line is the typical arrangement used in farrowing buildings. This arrangement has many elbows that increase the construction time and cost, the likelihood of leaks, and

the operating cost of a swine facility. This complicated pipe line has been simplified to the one shown in Figure 1.2 where the heating pipes that cross the sow area are insulated to provide the proper temperature for the sow. The amount of insulation needed beneath the sow is not known.

There are many variables that affect the temperature distribution on the floor of a farrowing house. Some of these include the number, spacing and depth of the pipes, the insulation size and placement over the pipes and around the pipes, and the effect of fins that could be attached to the pipes. The temperature distribution on the floor surface of a farrowing house can not be calculated analytically. A numerical procedure must be used. The finite element method appears to be the powerful tool available to study the temperature distribution of such a complicate model.

The general objective for this study was to calculate the temperature distribution on the floor of a farrowing house for specified hot water pipe arrangements and insulation placement. Another objective was to develop configurations that will provide comfortable temperature distribution for both the sow and baby pigs. Specific objectives relative to the design of a new hot water heating system evolved after the first analysis was completed; these are discussed later.

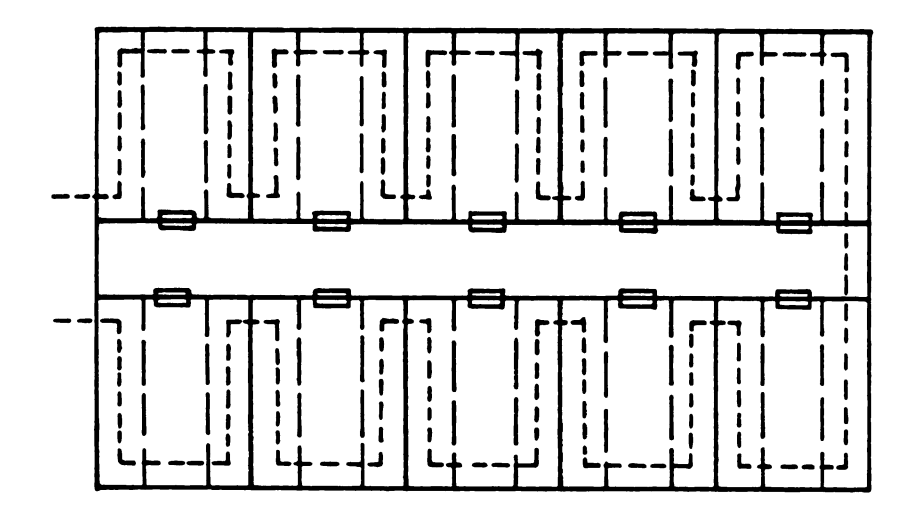


Figure 1.1 Pipe arrangement in a typical hot water heating system of the fallowing house which has 10 pens.

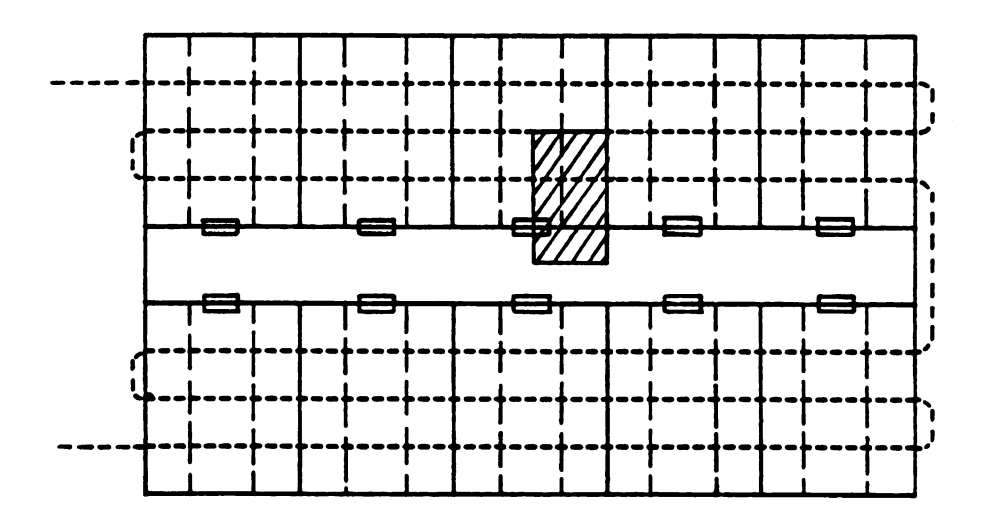


Figure 1.2 Pipe arrangement in a modified hot water heating system.

II. LITERATURE REVIEW

2.1 Farrowing House

Butchbaker and Shanklin (1965) studied the temperature regulating mechanisms of young pigs in the test chamber using four different room temperatures. They found a single newborn pig cannot maintain homeothermic status without supplemental heat despite a well-developed shiver mechanism. Karhnak and Aldrich (1971) measured the room temperature and floor temperature of a farrow-to-finish building equipped with an under floor heating system. The room temperature, measured using thermocouples, ranged from 16°C to 21°C (61°F to 69°F) in the winter time. The floor temperature ranged from 21°C to 39°C (69°F to 102°F). They observed that pigs usually laid across the front of the pen, although the warmest spots were along both sides of the pen beneath the guard rails. Spillman and Murphy (1976) found that producers with totally slotted floor creep areas tended to keep the room temperature around 27°C (80°F) while those with partially slotted or solid floor creep areas maintained room temperatures from 16°C to 24°C (60°F to 70°F). They observed that pigs more than 7 to 10 days old tend not to sleep under heat lamps.

Muehling and Stanislaw (1979) provided the important design factors for farrowing units whose floors are solid or slotted. They suggested the room tem-

perature of solid and slotted floors to be 15.6°C to 18.3°C (60°F to 65°F) and 21.1°C to 23.9°C (70°F to 75°F), respectively. The floor temperature for a litter at farrowing was suggested to be in the range of 29.4°C to 32.2°C (85°F to 90°F) for the first three days of life while the comfortable floor temperature for a sow was 15.6°C to 18.3°C (60°F to 65°F). Van Fossen and Overhult (1980) provided the fundamental information to select, design, install and operate an electric or a hot water floor heating system. They emphasized that heating pipes across the sow area must be insulated with a 1.3 cm to 2.5 cm (0.5 inch to 1.0 inch) thickness of rigid, non-deteriorating insulation. They recommended the heated floor area of from birth to weaning as 0.56 to 1.4 m^2 per litter (6 to 15 ft^2 per litter). England et al. (1987) stated that the baby pig areas, on solid or slotted floors without bedding, should be kept at 32.3°C to 35.0°C (90°F to 95°F) for the first few days, and then in the 21.2°C to 26.7°C (70°F to 80°F) range until weaning at three to six week of age.

The ideal floor temperature distribution in the farrowing house can be achieved based upon the literature. The floor temperature in the sow area should be kept uniform through the whole sow area in the range of 15.6° C to 18.3° C (60°F to 65° F) regardless the change of the hot water temperature and the age of baby pigs. The floor temperature in the baby pig area, however, should be controlled according to the age and the weight of baby pigs. Furthermore, it will be more desirable the baby pig area provides several micro temperature environments which baby pigs can choose by themselves because the individuals vary in their preferred temperature. It is not economical to keep the whole litter area (1.95 m^2 , 21 ft^2) warm in the temperature range of 29.4° C to 32.2° C (85° F to 90° F) for

the first few days of life (Muehling and Stanislaw, 1979). The small heated area $(0.56 \ m^2, 6 \ ft^2)$, only about 30 % of total baby pig area, is necessary for the new born pigs (Van Fossen and Overhult, 1980). The ideal floor temperature distribution in the baby pig area was assumed in this study as that of providing a uniform temperature in the range of 29.4 °C to 32.2 °C (85 °F to 90 °F) on the over 30 % of total baby pig area. Moreover, it should provide several temperature ranges to satisfy the baby pigs individually.

2.2 Three-Dimensional Finite Element Analysis

The finite element method was introduced at the mid 1950s as a method of analyzing structures with reinforcing coverings. The method has become a powerful computational tool in the field of structural mechanics, fluid mechanics, and heat transfer, especially for the analysis of irregularly-shaped objects having different materials or complex boundary conditions through extensive rearch.

For the case of three-dimensional steady state heat transfer, the procedure was completely described by Zienkiewicz et al. (1967). The transient heat conduction problem for two dimensions was performed by Wilson and Nickell (1966) using a variational principle. They also solved time dependent problems using a single step technique. A detailed description of the general theory of finite element method is given in several textbooks such as Zienkiewicz (1977), Segerlind (1984) and Allaire (1985).

The accuracy of the finite element method for steady state heat transfer was studied by Laura et al. (1974) who calculated the error between analytical and finite element results for two cases whose domains were extremely complicated. Good agreement, less than 1 % error, was obtained between the finite element results and the analytical solutions for a hexagonal model with a concentric, circular hole and a square model in a nonhomogeneous media.

Since the preparation of numerous input data is necessary and is a tedious task, automatic input data generation is nearly a necessity when solving a three-dimensional problem. Akyuz (1970) presented a scheme for generating input data in two- and three-dimensional space using the concept of natural coordinate systems. He divided the solution domain into subdomains depending on the field quantities and the complexity of the geometrical form. Cavendish et al. (1985) describe the algorithm for the computer generation of tetrahedral finite element meshes for solids. The proposed algorithm was separated into two independent modules. First, the node points were defined within and on the surface of the solid. Then, the node points were automatically connected to form wellproportioned tetrahedral finite elements. To minimize the memory space and computer time, a banded matrix solution technique is used. The matrix should have a bandwidth as small as possible. Grooms (1972) presented a simple and straightforward matrix bandwidth reduction procedure. The basic idea was to systematically move rows that are far apart and coupled closer together. He compared his method with other bandwidth reduction methods. Collins (1973) presented a method in which the engineer numbered the nodal points but the computer renumbered the nodes to minimize the bandwidth during calculations.

The computer restored the original numbering for output.

2.3 Finite Element Formulation

The finite element method can be viewed as a numerical procedure for solving differential equations. The finite element analysis in conjunction with a variational principal is a powerful method for the determination of the temperature distribution within a complex body that has different material properties, an irregular shape and mixed boundary conditions.

The governing partial differential equation for steady state threedimensional heat conduction (Kreith, 1965) is

$$\frac{\partial}{\partial x}\left(K_{xx}\frac{\partial T}{\partial x}\right) + \frac{\partial}{\partial y}\left(K_{yy}\frac{\partial T}{\partial y}\right) + \frac{\partial}{\partial z}\left(K_{xx}\frac{\partial T}{\partial z}\right) + Q = 0 \tag{2.1}$$

with the boundary conditions

$$T = T_B \qquad \qquad \text{on} \quad S_1 \tag{2.2}$$

and/or

$$K_{zz} \frac{\partial T}{\partial z} l_z + K_{yy} \frac{\partial T}{\partial y} l_y + K_{zz} \frac{\partial T}{\partial z} l_z + q + h \left(T - T_{\infty} \right) = 0 \text{ on } S_2 \qquad (2.3)$$

where T ('K) is a temperature that is a function of x, y, and z. K_{xx} , K_{yy} , and K_{xx} (kW/m 'K) are the thermal conductivities in the x, y, and z directions, Q (kW/m^3) is an internal heat source or sink, q (kW/m^2) is the heat flux over the surface, and h (kW/m^2 'K) is the convection coefficient. T_{∞} ('K) is the ambient temperature, and T_B ('K) is the known boundary temperature. The quantities of

 l_z , l_y and l_z are the direction cosines of a vector normal to the surface. S_1 is the boundary surface where temperature is known, and S_2 is the another surface where heat is gained or lost due to a convection heat transfer or a heat flux.

The functional formulation, that is derived from the variational calculus (Pars, 1962), for (2.1) and its boundary conditions (2.2) and (2.3) is

$$\Pi = \int_{V} \frac{1}{2} \left[K_{xx} \left(\frac{\partial T}{\partial x} \right)^{2} + K_{yy} \left(\frac{\partial T}{\partial y} \right)^{2} + K_{xx} \left(\frac{\partial T}{\partial z} \right)^{2} - 2 Q T \right] dV$$

$$+ \int_{S} \left[q T + \frac{1}{2} h \left(T - T_{\infty} \right)^{2} \right] dS$$
(2.4)

Functional, Π , must be minimized with respect to the set of nodal values $\{T\}$. The minimization of Π occurs when

$$\frac{\partial \Pi}{\partial \{T\}} = \frac{\partial}{\partial \{T\}} \sum_{\epsilon=1}^{E} \Pi^{(\epsilon)} = \sum_{\epsilon=1}^{E} \frac{\partial \Pi^{(\epsilon)}}{\partial \{T\}} = 0$$
 (2.5)

where E is the total number of elements.

The derivative $\frac{\partial \Pi^{(e)}}{\partial \{T\}}$ in (2.5) is given by Segerlind (1976) as

$$\frac{\partial \Pi^{(e)}}{\partial \{T\}} = \left(\int_{V^{(e)}} [B^{(e)}]^T \left[D^{(e)} \right] [B^{(e)}] dV + \int_{S_2^{(e)}} h \left[N^{(e)} \right]^T \left[N^{(e)} \right] dS \right) \{T\}$$

$$- \int_{V^{(e)}} Q \left[N^{(e)} \right]^T dV + \int_{S_2^{(e)}} q \left[N^{(e)} \right]^T dS - \int_{S_2^{(e)}} h T_{\infty} \left[N^{(e)} \right]^T dS$$
(2.6)

where $[D^{(e)}]$ contains the thermal conductivities

$$[D^{(e)}] = \begin{bmatrix} K_{zz} & 0 & 0 \\ 0 & K_{yy} & 0 \\ 0 & 0 & K_{zz} \end{bmatrix}$$

 $[N^{(e)}]$ contains the shape functions, and $[B^{(e)}]$ is related to the derivatives of the shape functions. The set of integrals in (2.6) can be condensed by using the element stiffness matrix $[K^{(e)}]$ and the element force vector $\{EF^{(e)}\}$ as

$$\frac{\partial \Pi^{(e)}}{\partial \{T\}} = [K^{(e)}] \{T\} - \{EF^{(e)}\}$$

$$(2.7)$$

where

$$[K^{(e)}] = \int_{V^{(e)}} [B^{(e)}]^T [D^{(e)}] [B^{(e)}] dV + \int_{S_2^{(e)}} h [N^{(e)}]^T [N^{(e)}] dS$$
 (2.8)

and

$$\{EF^{(e)}\} = \int_{V^{(e)}} Q [N^{(e)}]^T dV - \int_{S^{(e)}} q [N^{(e)}]^T dS + \int_{S^{(e)}} h T_{\infty} [N^{(e)}]^T dS \qquad (2.9)$$

The final system of equations is obtained by substituting (2.7) into (2.5), giving

$$\frac{\partial \Pi}{\partial \{T\}} = \sum_{e=1}^{E} ([K^{(e)}]\{T\} - \{EF^{(e)}\}) = 0$$
 (2.10)

or

$$[K] \{T\} = \{EF\}$$
 (2.11)

where

$$[K] = \sum_{e=1}^{E} [K^{(e)}]$$

$$\{EF\} = \sum_{e=1}^{E} \{EF^{(e)}\}\$$

Before evaluating the element stiffness matrix $[K^{(e)}]$ and the element force vector $\{EF^{(e)}\}$, equation (2.9) and matrix $[D^{(e)}]$ can be simplified with the condition of $K_{zz} = K_{yy} = K_{zz} = K_a$, Q = 0, and q = 0, because of the same thermal con-

ductivities in the x, y, and z direction, no internal heat source, and no heat flux over the surface for the models in this study. Therefore, the element force vector reduces to

$$\{EF^{(e)}\} = \int_{S_{\epsilon}^{(e)}} h \ T_{\infty} [N^{(e)}]^T \ dS \qquad (2.12)$$

while

$$[D^{(e)}] = K_a \begin{bmatrix} 1 & 0 & 0 \\ 0 & 1 & 0 \\ 0 & 0 & 1 \end{bmatrix}$$
 (2.13)

Since the three-dimensional element used in this study was an eight node hexahedron, the matrices $[N^{(e)}]$ and $[B^{(e)}]$ are

$$[N^{(e)}] = [N_1 \ N_2 \ N_3 \ \cdots \ N_8]$$

$$[B^{(e)}] = \begin{bmatrix} \frac{\partial N_1}{\partial x} & \frac{\partial N_2}{\partial x} & \frac{\partial N_3}{\partial x} & \dots & \frac{\partial N_8}{\partial x} \\ \frac{\partial N_1}{\partial y} & \frac{\partial N_2}{\partial y} & \frac{\partial N_3}{\partial y} & \dots & \frac{\partial N_8}{\partial y} \\ \frac{\partial N_1}{\partial z} & \frac{\partial N_2}{\partial z} & \frac{\partial N_3}{\partial z} & \dots & \frac{\partial N_8}{\partial z} \end{bmatrix}$$

The coordinate transformation, from the global to the natural coordinate system, allows the boundaries of elements to be distorted, and requires the integrals in equation (2.8) and (2.12) to be evaluated numerically using a Gauss-Legendre technique (Segerlind, 1976). The global coordinate system (x, y, z), the natural coordinate system (ξ, η, ζ) , and the location of the eight - node are shown in Figure 2.1. The shape functions and their derivatives for the natural coordinate system are given in Table 2.1.

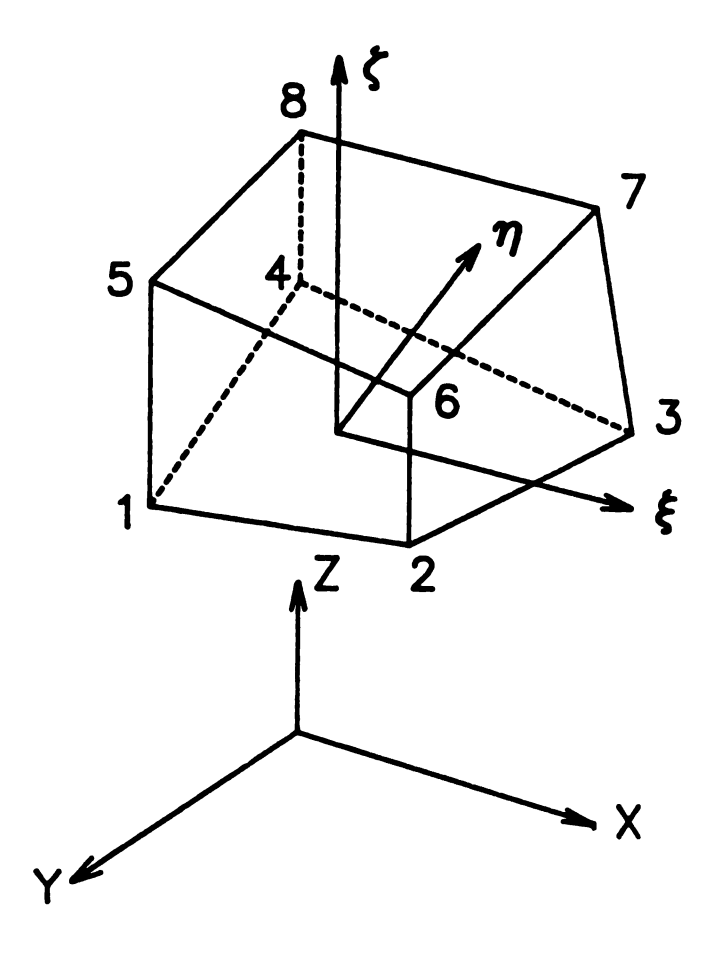


Figure 2.1 Location of eight nodes in natural and Cartesian coordinates.

Table 2.1 Shape functions and derivatives for eight node hexahedron.

	Shape functions	Derivatives		
Node		$\frac{\partial N_i}{\partial \xi}$	$rac{\partial N_i}{\partial \eta}$	$\frac{\partial N_i}{\partial \varsigma}$
N_1	$\frac{1}{8}(1-\xi)(1-\eta)(1-\zeta)$	$-\frac{1}{8}(1-\eta)(1-\varsigma)$	$-\frac{1}{8}(1-\xi)(1-\zeta)$	$-\frac{1}{8}(1-\xi)(1-\eta)$
N_2	$\frac{1}{8}(1+\xi)(1-\eta)(1-\zeta)$	$\frac{1}{8}(1-\eta)(1-\varsigma)$	$-\frac{1}{8}(1+\xi)(1-\zeta)$	$-\frac{1}{8}(1+\xi)(1-\eta)$
N_3	$\frac{1}{8}(1+\xi)(1+\eta)(1-\zeta)$	$\frac{1}{8}(1+\eta)(1-\zeta)$	$\frac{1}{8}(1+\xi)(1-\zeta)$	$-\frac{1}{8}(1+\xi)(1+\eta)$
N ₄	$\frac{1}{8}(1-\xi)(1+\eta)(1-\zeta)$	$-\frac{1}{8}(1+\eta)(1-\varsigma)$	$\frac{1}{8}(1-\xi)(1-\zeta)$	$-\frac{1}{8}(1-\xi)(1+\eta)$
N_5	$\frac{1}{8}(1-\xi)(1-\eta)(1+\zeta)$	$-\frac{1}{8}(1-\eta)(1+\varsigma)$	$-\frac{1}{8}(1-\xi)(1+\zeta)$	$\frac{1}{8}(1-\xi)(1-\eta)$
N_6	$\frac{1}{8}(1+\xi)(1-\eta)(1+\zeta)$	$\frac{1}{8}(1-\eta)(1+\varsigma)$	$-\frac{1}{8}(1+\xi)(1+\zeta)$	$\frac{1}{8}(1+\xi)(1-\eta)$
N ₇	$\frac{1}{8}(1+\xi)(1+\eta)(1+\zeta)$	$\frac{1}{8}(1+\eta)(1+\zeta)$	$\frac{1}{8}(1+\xi)(1+\zeta)$	$\frac{1}{8}(1+\xi)(1+\eta)$
N ₈	$\frac{1}{8}(1-\xi)(1+\eta)(1+\zeta)$	$-\frac{1}{8}(1+\eta)(1+\varsigma)$	$\frac{1}{8}(1-\xi)(1+\varsigma)$	$\frac{1}{8}(1-\xi)(1+\eta)$

The change in the increment volume dV is

$$dV = dx \, dy \, dz = |\det[J]| \, d\xi \, d\eta \, d\varsigma \tag{2.14}$$

where [J] is the Jacobian matrix of the transformation

$$[J] = \begin{bmatrix} \frac{\partial x}{\partial \xi} & \frac{\partial y}{\partial \xi} & \frac{\partial z}{\partial \xi} \\ \frac{\partial x}{\partial \eta} & \frac{\partial y}{\partial \eta} & \frac{\partial z}{\partial \eta} \\ \frac{\partial x}{\partial \zeta} & \frac{\partial y}{\partial \zeta} & \frac{\partial z}{\partial \zeta} \end{bmatrix}$$
(2.15)

and the limits of integration are from -1 to 1 for each coordinate variable.

The Cartesian coordinates are given by

$$x = \sum_{i=1}^{8} N_{i} X_{i}$$

$$y = \sum_{i=1}^{8} N_{i} Y_{i}$$

$$z = \sum_{i=1}^{8} N_{i} Z_{i}$$
(2.16)

where X_i , Y_i and Z_i are the nodal coordinates. Substitution into (2.15) yields

$$[J] = \begin{bmatrix} \frac{\partial N_1}{\partial \xi} & \frac{\partial N_2}{\partial \xi} & \cdots & \frac{\partial N_8}{\partial \xi} \\ \frac{\partial N_1}{\partial \eta} & \frac{\partial N_2}{\partial \eta} & \cdots & \frac{\partial N_8}{\partial \eta} \\ \frac{\partial N_1}{\partial \zeta} & \frac{\partial N_2}{\partial \zeta} & \cdots & \frac{\partial N_8}{\partial \zeta} \end{bmatrix} \begin{bmatrix} X_1 & Y_1 & Z_1 \\ X_2 & Y_2 & Z_2 \\ \vdots & \vdots & \vdots \\ X_n & \vdots & \vdots \\ X_n & \vdots & \vdots \\ X_n & Y_n & Z_n \end{bmatrix}$$
(2.17)

and each column of [B] is given by

$$[B^{(e)}(\xi,\eta,\zeta)] = \begin{bmatrix} \frac{\partial N_i}{\partial x} \\ \frac{\partial N_i}{\partial y} \\ \frac{\partial N_i}{\partial z} \end{bmatrix}_{i=1,8} = [J]^{-1} \begin{bmatrix} \frac{\partial N_i}{\partial \xi} \\ \frac{\partial N_i}{\partial \eta} \\ \frac{\partial N_i}{\partial \zeta} \end{bmatrix}_{i=1,8}$$
(2.18)

The change of variable in the surface integral is

$$dS = dx \ dy = |\det[J]| \ d\xi \ d\eta \tag{2.19}$$

Since convection heat loss in this study occurs only on the top surface, $\varsigma = 1$, the Jacobian matrix for the surface integral becomes

$$[J]_{on \varsigma=1} = \begin{bmatrix} \frac{\partial x}{\partial \xi} & \frac{\partial y}{\partial \xi} & \frac{\partial z}{\partial \xi} \\ \frac{\partial x}{\partial \eta} & \frac{\partial y}{\partial \eta} & \frac{\partial z}{\partial \eta} \\ 0 & 0 & 1 \end{bmatrix}$$
(2.20)

The unit value assigned to the diagonal allows the inverse matrix of [J] to be evaluated.

Substituting (2.14) through (2.20) into (2.8) and (2.12) gives

$$[K^{(e)}] = \int_{-1}^{1} \int_{-1}^{1} \int_{-1}^{1} [B^{(e)}(\xi, \eta, \zeta)]^{T} [D^{(e)}] [B^{(e)}(\xi, \eta, \zeta)] | \det[J] | d\xi d\eta d\zeta$$

$$+ \int_{-1}^{1} \int_{-1}^{1} h [N^{(e)}(\xi, \eta)]^{T} [N^{(e)}(\xi, \eta)] | \det[J] | d\xi d\eta$$
(2.21)

$$\{EF^{(e)}\} = \int_{-1}^{1} \int_{-1}^{1} h \ T_{\infty} [N^{(e)}(\xi, \eta)] \ | \det[J] \ | \ d\xi d\eta$$
 (2.22)

The Gauss - Legendre quadrature was applied to numerically evaluate the integration shown in (2.21) and (2.22). Since the highest order of the polynomials that occur in $[B^{(e)}]^T[D^{(e)}][B^{(e)}]$ and $[N^{(e)}]^T[N^{(e)}]$ of equation (2.21) is two, the

number of integration points (n) becomes two for each coordinate direction. The sampling points of ± 0.577350 and a weight coefficient $(H_{ijk} \text{ and } H_{ij})$ of 1.00 were used to evaluate the integrals. Eight integration points were required for the volume integral and four integrating points were required to evaluate the surface integral in (2.21). Since the highest order of polynomials in $[N^{(e)}]$ is one, one integration point is required for each direction. The sampling point for one integral point in the Gauss - Legendre is 0 and the weight coefficient (H_{ij}) is 2.0. One integration point is required in (2.22).

The numerical integration changes (2.21) and (2.22) to the following final

$$[K^{(e)}] = \sum_{i=1}^{2} \sum_{j=1}^{2} \sum_{k=1}^{2} [f_{1}(\xi_{i}, \eta_{j}, \zeta_{k}) H_{ijk}] | det[J] |$$
 (2.23)

+
$$\sum_{i=1}^{2} \sum_{j=1}^{2} [f_2(\xi_i, \eta_j) H_{ij}] | det[J] |$$

where

$$f_{1}(\xi_{i},\eta_{j},\zeta_{k}) = [B^{(e)}(\xi_{i},\eta_{j},\zeta_{k})]^{T} [D^{(e)}(\xi_{i},\eta_{j},\zeta_{k})] [B^{(e)}(\xi_{i},\eta_{j},\zeta_{k})]$$

$$f_{2}(\xi_{i},\eta_{j}) = h [N^{(e)}(\xi_{i},\eta_{j})]^{T} [N^{(e)}(\xi_{i},\eta_{j})]$$

$$H_{ijk} = H_{ij} = 1.0$$

and

$$\{EF^{(e)}\} = h \ T_{\infty} \sum_{i=1}^{1} \sum_{j=1}^{1} [f_{3}(\xi_{i}, \eta_{j}) H_{ij}] | det[J] |$$
 (2.24)

where

$$f_{3}(\xi_{i},\eta_{j}) = [0 \ 0 \ 0 \ \frac{1}{4} \ \frac{1}{4} \ \frac{1}{4} \ \frac{1}{4}]^{T}$$

$$H_{ij} = 2$$

III. ANALYSIS OF A TYPICAL FARROWING HOUSE

The first calculations performed were done on the typical pipe layout shown in Figure 1.1. The cross section of the concrete floor heated with hot water is shown in Figure 3.1. A two-dimensional analysis was performed. This assumed that the pipes extended an infinite distance parallel to the sow area. The pipes beneath the sow area were not include in this analysis.

3.1 Farrowing Crate Dimensions and Finite Element Model

Most farrowing crates have dimensions of 152.4 cm (5 feet) wide by 213.4 cm (7 feet) long. The width includes an 45.7 cm (1.5 feet) young pig area on both sides of a 61.0 cm (2 feet) sow stall as shown in Figure 3.2.

The repeated symmetry of farrowing crates reduces the region to be analyzed. The X - axis was defined as the direction of the alley, while the Y - axis was the perpendicular to the X - axis as shown in Figure 3.2. The Z - axis was defined as the direction of the floor depth, upward being positive.

Boundaries with respect to the X - axis were the center of the crate and the right side of the crate, while boundaries with respect to the Y - axis were the center of the crate and the center of the alley. Each boundary was an axis of

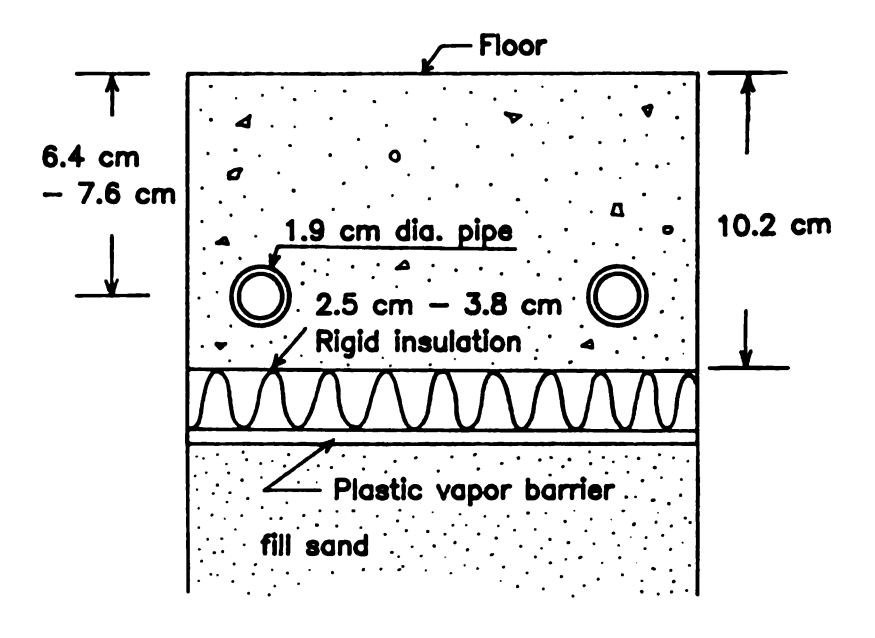


Figure 3.1 Typical cross - section of concrete floor heated with hot water.

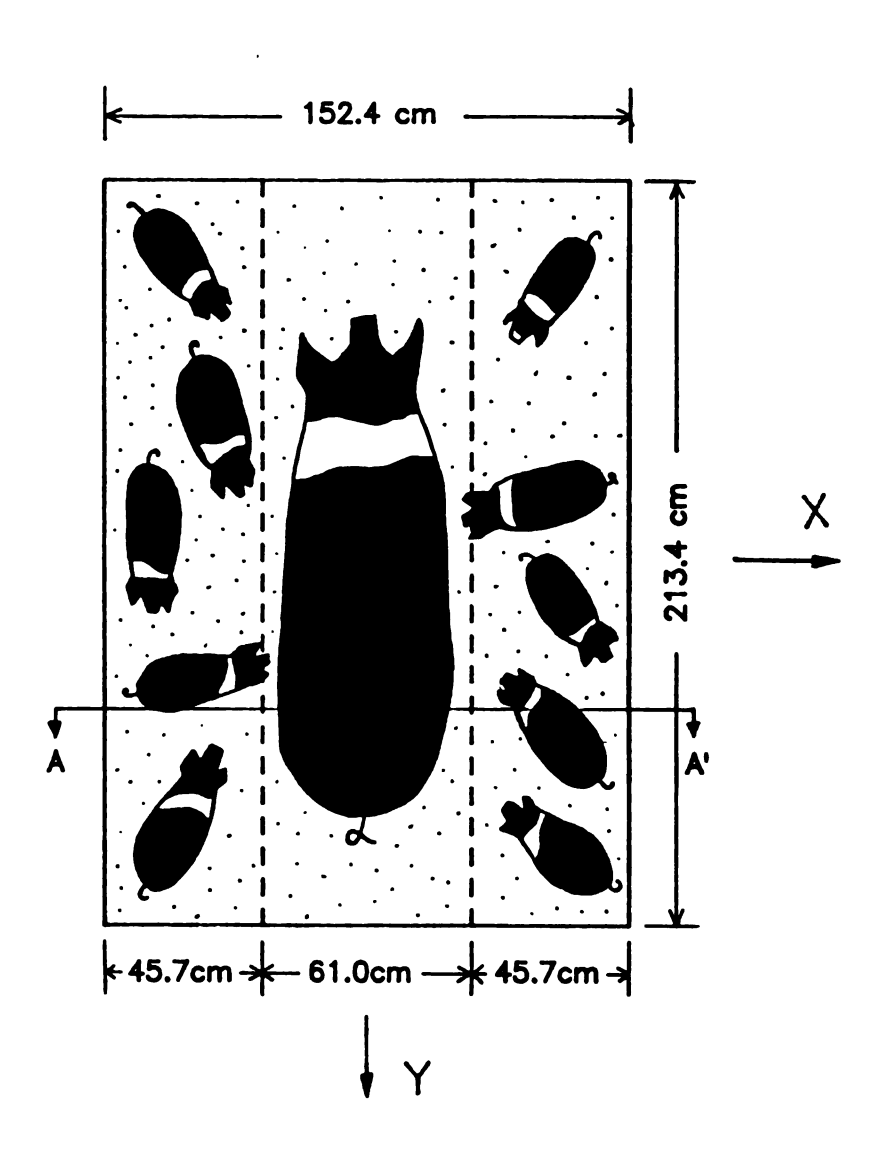


Figure 3.2 Typical crate dimensions.

symmetry. The shaded part shown in Figure 1.2 was the region analyzed.

Two simple models were introduced to decide the amount of floor depth to be analyzed. The rigid insulation used to insulate the concrete floor from the earth in the typical system of a concrete floor heated with hot water was located at the 10.2 cm (4 inches) depth as shown in Figure 3.1. The first model, therefore, had 10.2 cm depth, whose boundary was assumed to be totally insulated. Hart and Couvillion (1986) reported that water from wells deeper than 600 cm (20 feet) has a constant temperature year round of approximately 10°C (50°F). Therefore, the second model had 600 cm depth, whose boundary temperature was 10°C. That was a real situation even though the model had too many elements. The result showed the temperature on the floor did not change significantly with the model depth. The bottom of the concrete floor, therefore, was assumed to be a nonconducting insulated boundary; 10.2 cm (4 inches) was selected as the depth of the model. This simplification reduced the computer memory requirement and the running time. The boundaries with respect to the Z - axis were the floor and the top of the rigid insulation beneath the concrete.

The size of the model to be analyzed was 76.2 cm \times 167.6 cm \times 10.2 cm (30 inches \times 66 inches \times 4 inches). The boundary conditions on the surfaces were

$$T=60\,^{\circ}$$
 C on the surfaces of the pipes
$$k\frac{\partial T}{\partial n}=q+h(T-T_{\infty}) \qquad \text{on the floor surface}$$

$$\frac{\partial T}{\partial n}=0 \qquad \text{on the all of the other surfaces except the floor}$$

The temperature on the outside surface of the pipe was assumed as same as the hot water temperature 60°C (140°F) regardless of the thickness and the

material property of pipe. The values of input data, such as the surface conductance (h) of concrete and the thermal conductivity (k) of concrete, insulation, steel, and copper, came from the ASHRAE Handbook (1981), Meyer and Hansen (1980), and Kreith (1965).

The surface convection coefficient on concrete at zero air speed was 11.35 W/m² °K (0.0139 Btu/hr inch² °F). Since Muehling and Stanislaw (1979) recommended rigid insulation board for perimeter insulation and for insulation under concrete floor, particularly in heated floors, the wood or cane fiberboard was thermal conductivity selected and its 0.0577 W/m $^{\circ}$ K (0.00278)was Btu/hr inch 'F). The new plastic insulations, such as polystyrene and polyurethane, are also used for a rigid insulation. But, they were not considered in this study because of their low structural strength. The thermal conductivity of concrete was 1.8025 W/m 'K (0.08681 Btu/hr inch 'F).

Van Fossen and Overhults (1980) recommended 60°C (140°F) as the water temperature and Spillman and Murphy (1976) found that most of the farrowing houses were operated with a room temperature from 16°C to 24°C (60°F to 75°F). Therefore, I assumed the water temperature to be 60°C and the room temperature to be 15.6°C (60°F), the coolest condition.

3.2 Calculated Temperature Values

The temperature distribution on the cross section A - A' in the Figure 3.2 is shown in Figure 3.3. The shape of temperature distribution shown in Figure

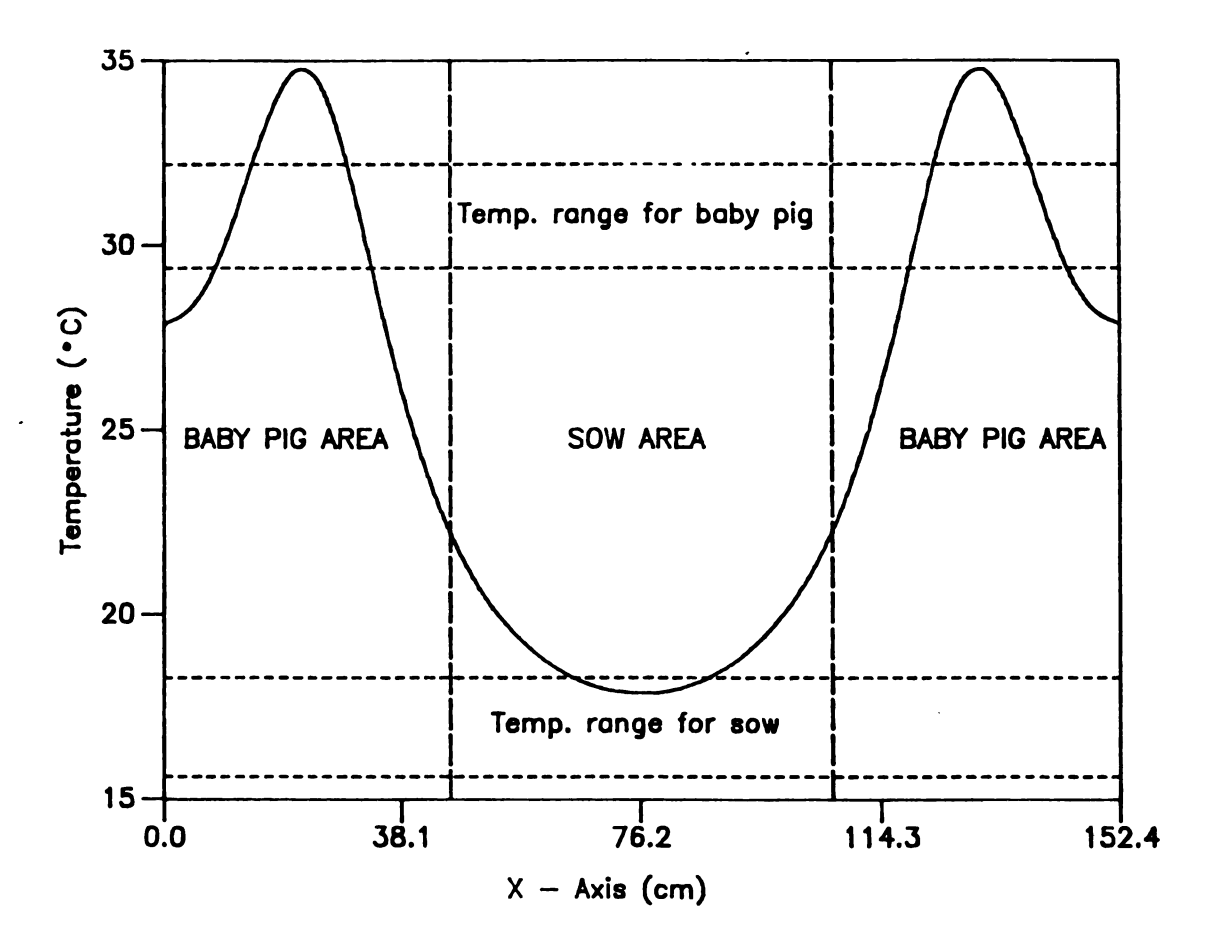


Figure 3.3 Temperature distribution on the floor of the typical farrowing house heated with hot water.

3.3 was the same shape of floor temperature measured by Karhnak and Aldrich (1971). The 34 % of the baby pig area had a temperature higher than the recommended temperature range of 29.4°C to 32.2°C (85°F to 90°F). The overheated area wastes energy and increases the operating costs. The 45 % area had a temperature below 29.4°C which is too cold for new-born pigs. Only 23 % area was in the optimal temperature range for baby pigs. In the sow area, the 34 % was in the desired temperature range of 15.6°C to 18.3°C (60°F to 65°F). The temperature contours are shown in Figure 3.4. The contours are straight line because of the assumption made about the pipes in the two-dimensional analysis.

Since the highest temperature in the creep area exceeded the desired values, the possibility of placing insulation over the pipes was analyzed. Applying the wood or fiber board insulation, 1.3 cm (0.5 inches) thick and 5.1 cm (2.0 inches) wide, above the pipe helps to remove the hot space in the baby pig area as shown in Figure 3.5, but it was not enough to provide the temperature distribution desired. The temperature distribution was not uniform within the comfortable temperature range for the baby pigs

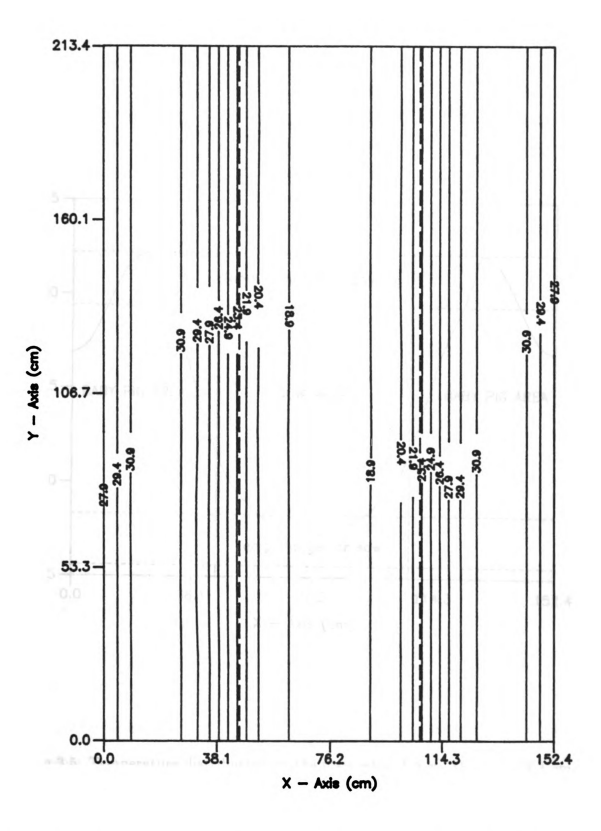


Figure 3.4 Temperature contour on the floor of the typical farrowing house heated with hot water.

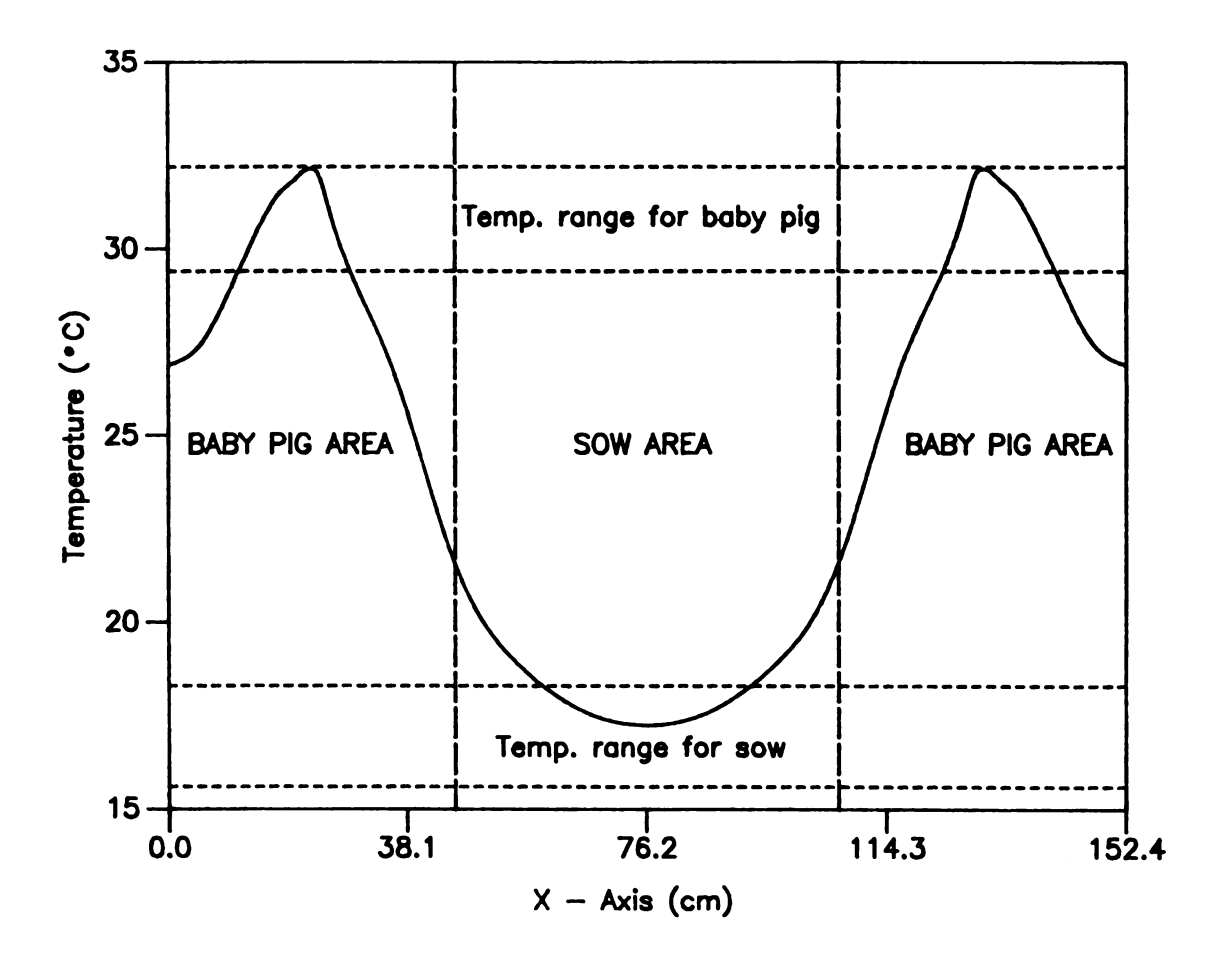


Figure 3.5 Temperature distribution on the floor when 1.3 cm thick and 5.1 cm wide flat insulation is applied over the hot water pipes.

IV. CALCULATIONS RELATED TO THE DESIGN OF A HOT WATER HEATING SYSTEM

The calculations in the previous chapter indicate that the typical hot water heating system does not produce the desired temperature distribution in either the baby pig creep area or the sow area. The number of elbows in this system also makes it undesirable because of the increased construction costs, increased pumping power required and the possibility of leaks.

The primary objective of the rest of this study was to obtain some prototype designs for hot water heating systems that use straight pipes and provide the desired temperature profiles by utilizing insulation at various locations in the floor.

The temperature distribution on the floor surface was calculated using a three-dimensional finite element computer program. The thermal properties, boundary conditions, room temperature, and the water temperature used in the previous chapter were also used in the three-dimensional study.

This chapter discusses the design parameters. Three prototype designs are presented and discussed in the next chapter.

4.1 Finite Element Grid Generation

The preparation of numerous input data for a three-dimensional finite element study is a time consuming task and a major source of errors. Programs that automatically generate the element input data are recommended. The advantages of generating the input data from a minimum amount of information are a) the ease of changing the few parameters for different problems, b) reduction of the hand labor involved, and c) avoidance of the human error. The necessary input data for generating a three-dimensional grid are as follows.:

- 1. Number of regions, number of boundary points and the minimum number of x, y, and z coordinates of boundary points that could describe the model.
- 2. Region connectivity data which show the connection to other regions.
- 3. Number of required subdivisions in ξ , η , and ζ directions that could be changed with the shape of region and significance for the region.
- 4. An integer node number that defines the region.

The procedure to reduce the matrix bandwidth is necessary for minimizing the memory size and the running time of the computer. The computer running time required to solve the matrix is proportional to the square of the bandwidth (Grooms, 1972). The node numbers from a grid generation program usually have large bandwidths because the numbering of nodes is sequential within a region, therefore, the elements on the boundary of the region have a big

difference between the largest and smallest node numbers.

The way to obtain a small bandwidth is to renumber the nodes so the nodes in each element are as close as possible. Since many algorithms for reducing the bandwidth are available (Grooms, 1972), the method considered herein was to number the element nodes in a sequence that starts at $\xi = -1$, $\zeta = +1$ and $\eta = -1$ and proceeds to $\xi = +1$, $\zeta = -1$ and $\eta = +1$ within a whole model. This simple renumbering system proved advantageous in analyzing the temperature distribution even though it did not give the minimum bandwidth.

The following basic procedures are performed in grid generation and bandwidth reduction for the three dimensional problem.

- 1. Minimum input data defining the model are read.
- 2. The nodes are numbered sequently from left to right $(\xi = -1 \text{ to } \xi = +1)$, from top to bottom $(\zeta = +1 \text{ to } \zeta = -1)$ and from front to rear $(\eta = -1 \text{ to } \eta = +1)$ skipping all previously numbered nodes within a region.
- 3. All nodes on the boundaries are stored for skipping when considering regions that are adjacent to the stored boundary.
- 4. The whole node numbers are stored and changed to the new ones renumbered for bandwidth reduction.

The grid generation program written in FORTRAN language is shown in Appendix A. One of the three-dimensional grid models used in this study is shown in Figure 4.1. The length in the vertical direction (z-axis) has been expanded for the sake of clarity.

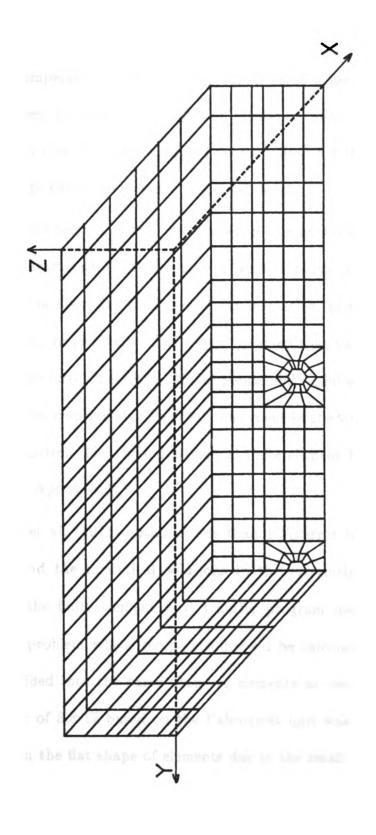


Figure 4.1 Element for the model of three heat pipes without fin and the location of coordinates (Dimension of x-axis is expanded).

4.2 Calculations Related to the Design of a Piping System

The temperature distribution on the floor of a farrowing house depends on the thickness, location, and width of insulation above the hot water pipe. Several cases for one pipe were analyzed to get a 'feel' for the temperature values as they related to the different insulation conditions.

The cross section of the model used in this analysis is shown in the Figure 4.2. The parameters W, D, tF, and tP are the width of insulation, the depth of insulation from floor, the thickness of flat insulation, and the thickness of perimeter insulation, respectively. The model assumed that two hot pipes were perpendicular to the farrowing crate. Nodal points and nodal elements of this model were 812 and 552, respectively. The CPU time spent in the VAX/VMS computer system was 17 minutes. The three-dimensional finite element heat transfer program used is given in Appendix B.

Laura et al. (1974) obtained less than 1 % error between the finite element results and the analytical solutions in the extremely complicated model. The error for the finite element heat transfer program used in this study was tested using a problem whose temperature could be calculated analytically. The model was divided into the same shape of elements as used in this study. The maximum error of 5.8 % based on the Fahrenheit unit was obtained. The main error came from the flat shape of elements due to the small thickness of model as shown in Figure 4.1.

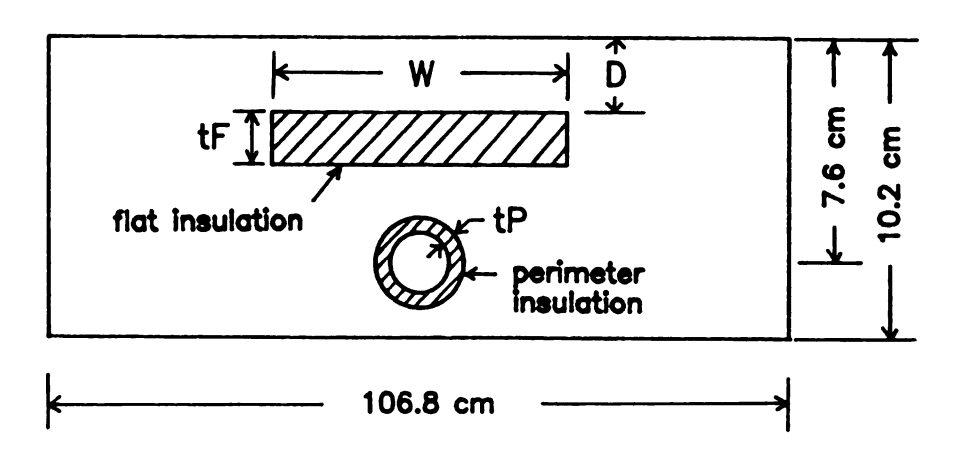


Figure 4.2 Variables for the test model.

4.2.1 Placement depth of flat insulation (D)

The temperature distribution as a function of the placement depth of an flat insulation, 1.3 cm (0.5 inches) thick and 15.2 cm (6.0 inches) wide, over the not-insulated pipe is shown in Figure 4.3. The only effect was that the deeper insulation placement leveled out the high temperature zone. A greater depth may be desirable when structural integrity of the floor is considered. It is impractical to place the insulation only 1.3 cm below the surface.

4.2.2 Thickness of flat insulation (tF)

Figure 4.4 shows the temperature distribution obtained by varying the thickness of the flat insulation whose width is 15.2 cm (6.0 inches), placed at a depth of 2.5 cm (1.0 inches), and without perimeter insulation on the pipe. A large temperature difference occurred just above the pipe but no significant change occurred in the region 17.6 cm from the pipe. The temperature on the floor just above the pipe was decreased 5 °C when compared with the 0.6 cm (0.25 inches) thickness of insulation. The temperature drop just above the pipe increased with the thickness of insulation nonlinearly as shown in Figure 4.5. The straight line was forced using only data exclude zero point in order to get the rate of a temperature drop with respect to the insulation thickness. The 1.94 °C / cm (8.89 °F / inch) rate was obtained. This information would be used to decide the thickness of insulation in the new models.

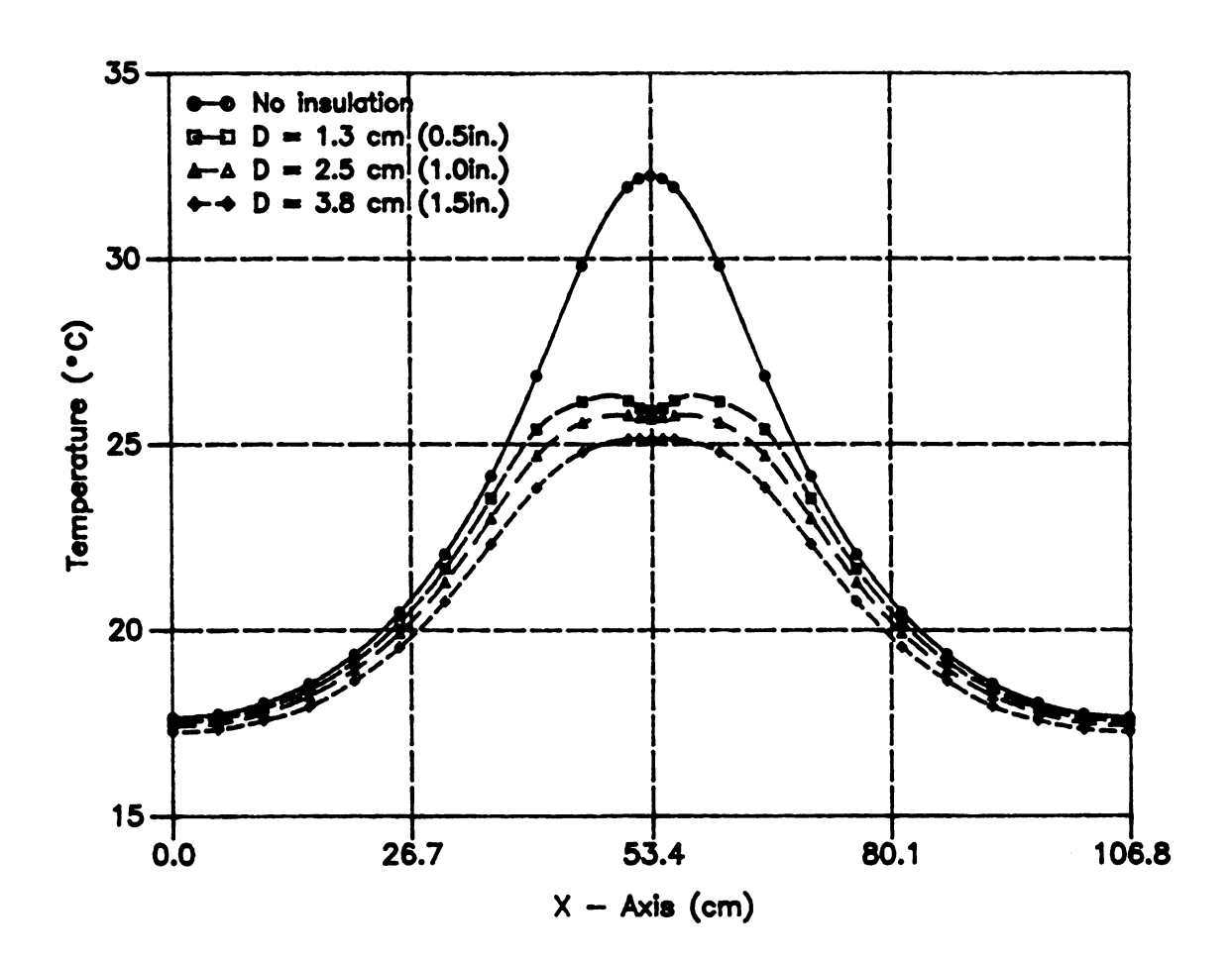


Figure 4.3 Effect of D, the placement depth of flat insulation (tF = 1.3 cm, W = 15.2 cm).

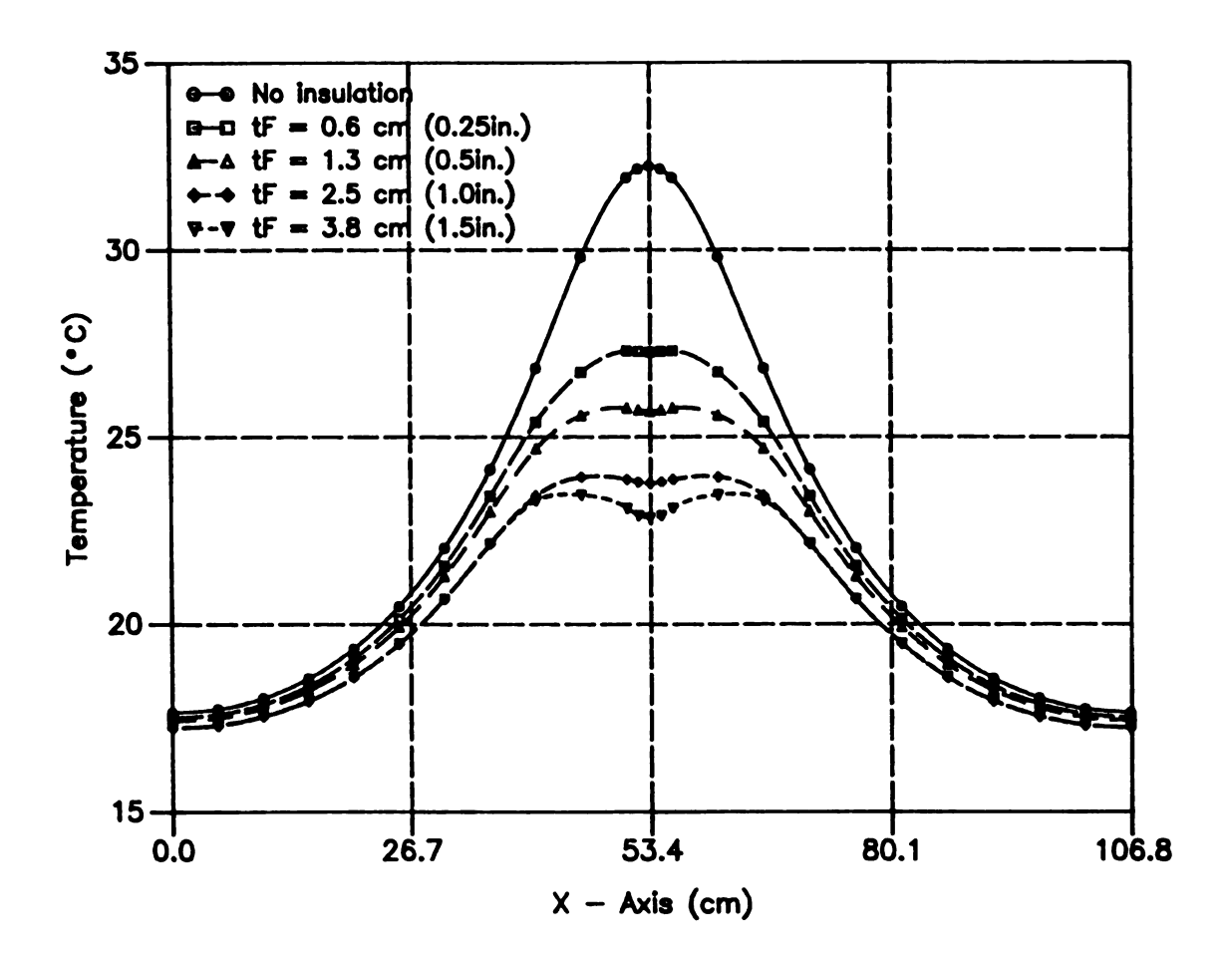


Figure 4.4 Effect of tF, the thickness of flat insulation (D = 2.5 cm, W = 15.2 cm).

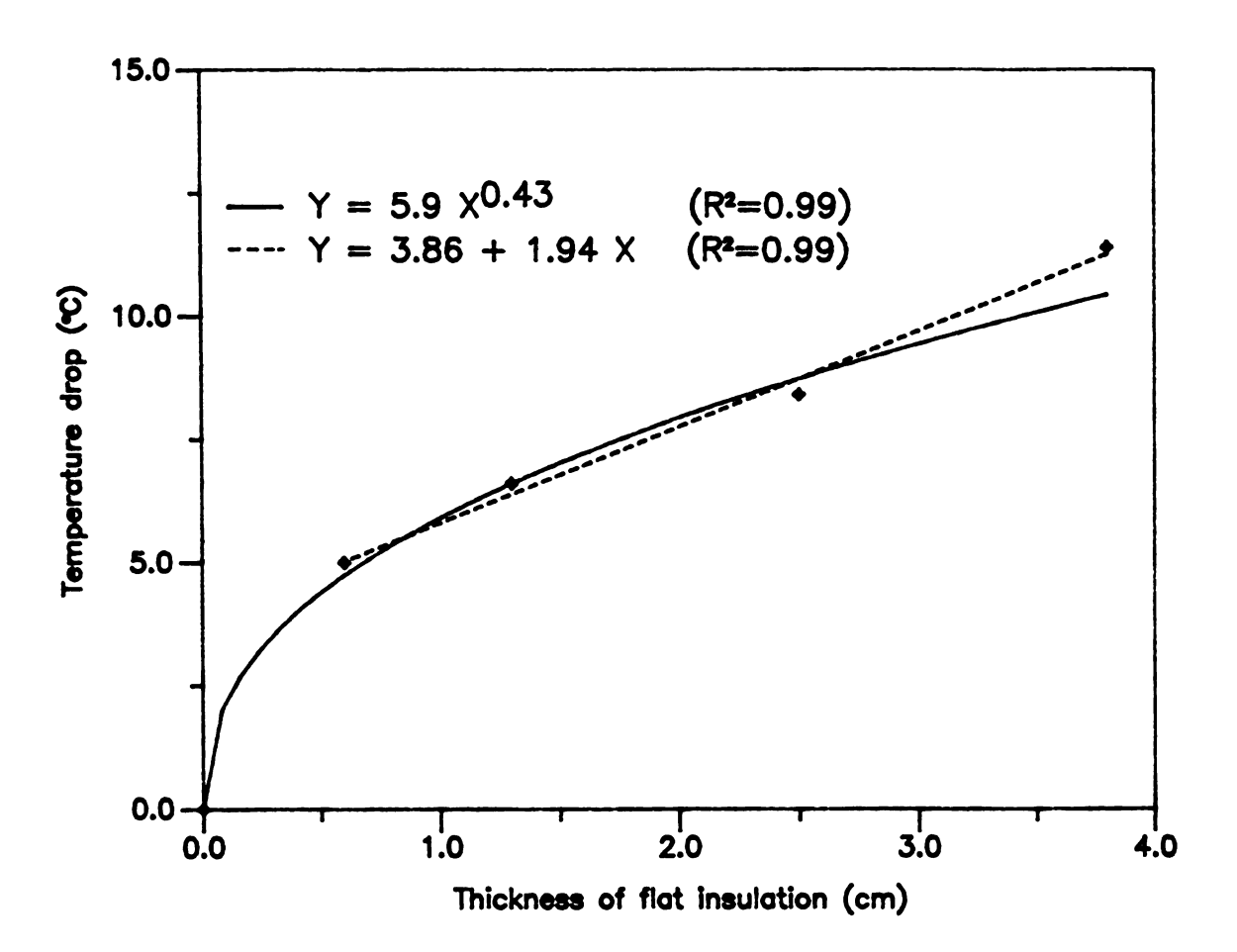


Figure 4.5 Temperature drop according to the thickness of flat insulation.

4.2.3 Width of flat insulation (W)

The changes in the maximum temperature with the width of flat insulation were analyzed in the case of two different thickness of a insulation, tF = 1.3 cm (0.5 inches) and tF = 2.5 cm (1.0 inches). The placement depth of the insulation was kept as D = 2.5 cm. No insulation was around the pipe. Significant temperature drops occurred with changes in the width of insulation as shown in Figure 4.6 and 4.7. The temperature drop just above the pipe increased linearly as shown in Figure 4.8 and 4.9 for each different thickness of insulation. When the linear regression was applied to each case, the rate of a temperature drop for 1.3 cm and 2.5 cm thickness of insulation was 0.36 °C / cm (1.64 °F / inch) and 0.43 °C / cm (1.96 °F /inch), respectively. The coefficient of determination (R²) in the linear regression was 0.98 and 0.96, respectively.

4.2.4 Thickness of perimeter insulation (tP)

The insulation wrapped around the pipe lowered the temperature significantly as shown in Figure 4.10. There was no flat insulation above the pipe. A thickness the 0.5 cm (0.2 inches) resulted in a 11.4°C decrease. The round insulation reduced the temperature through the whole region as well as leveled the temperature distribution. There was not a big temperature difference among the thickness of perimeter insulation. The maximum temperature difference between the various thickness of insulation was 2°C (3.6°F).

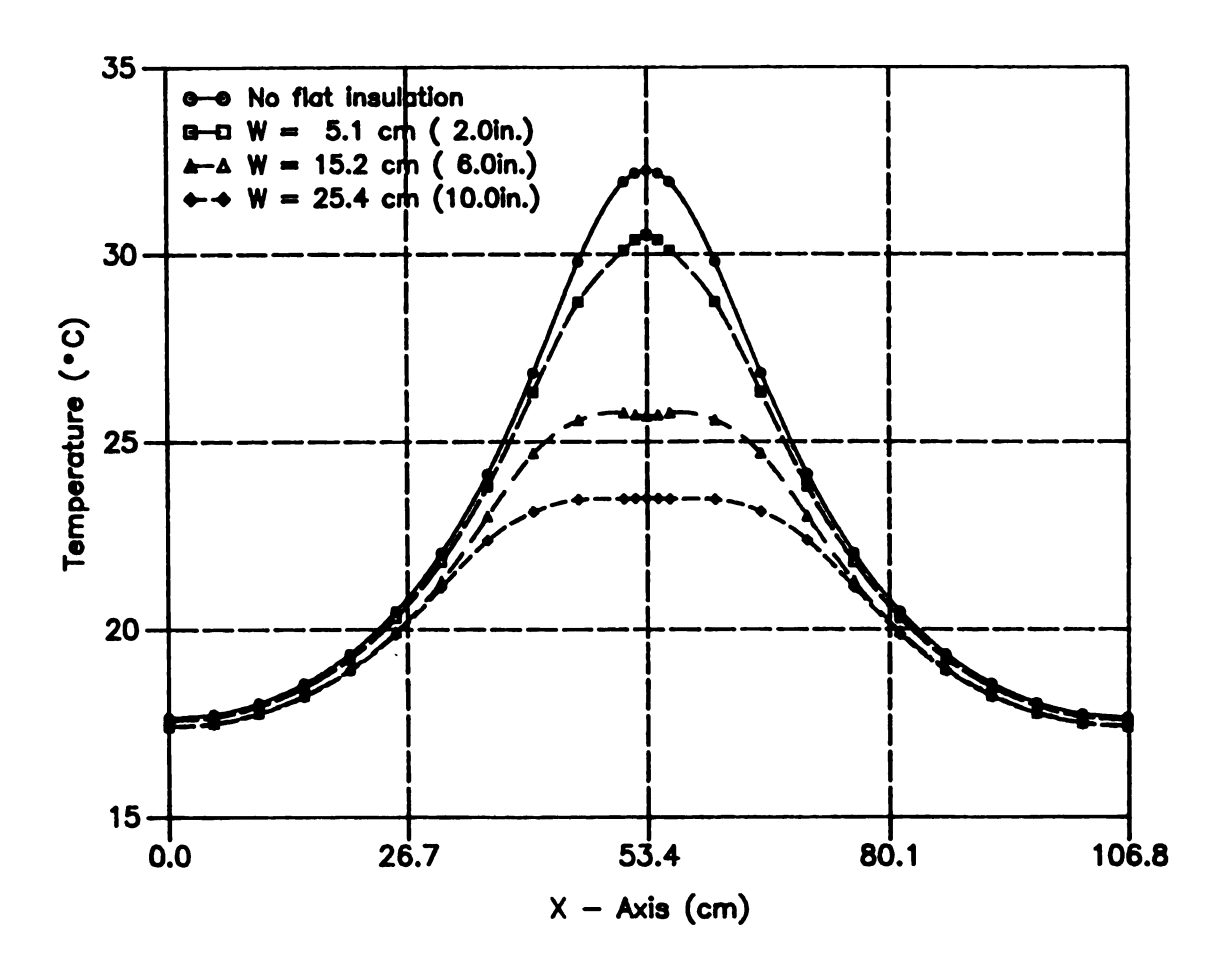


Figure 4.6 Effect of W, the width of flat insulation (tF = 1.3 cm, D = 2.5 cm).

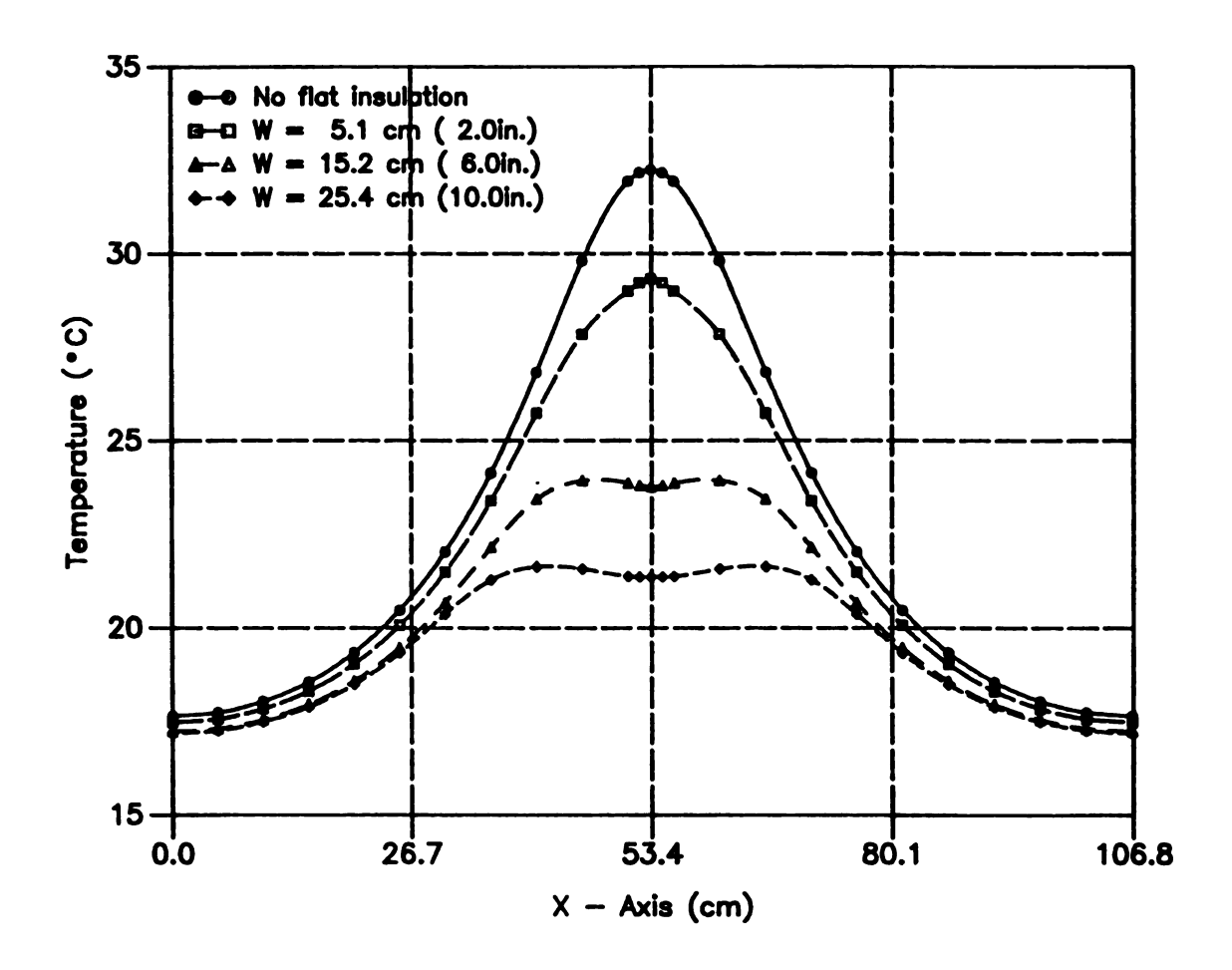


Figure 4.7 Effect of W, the width of flat insulation (tF = 2.5 cm, D = 2.5 cm).

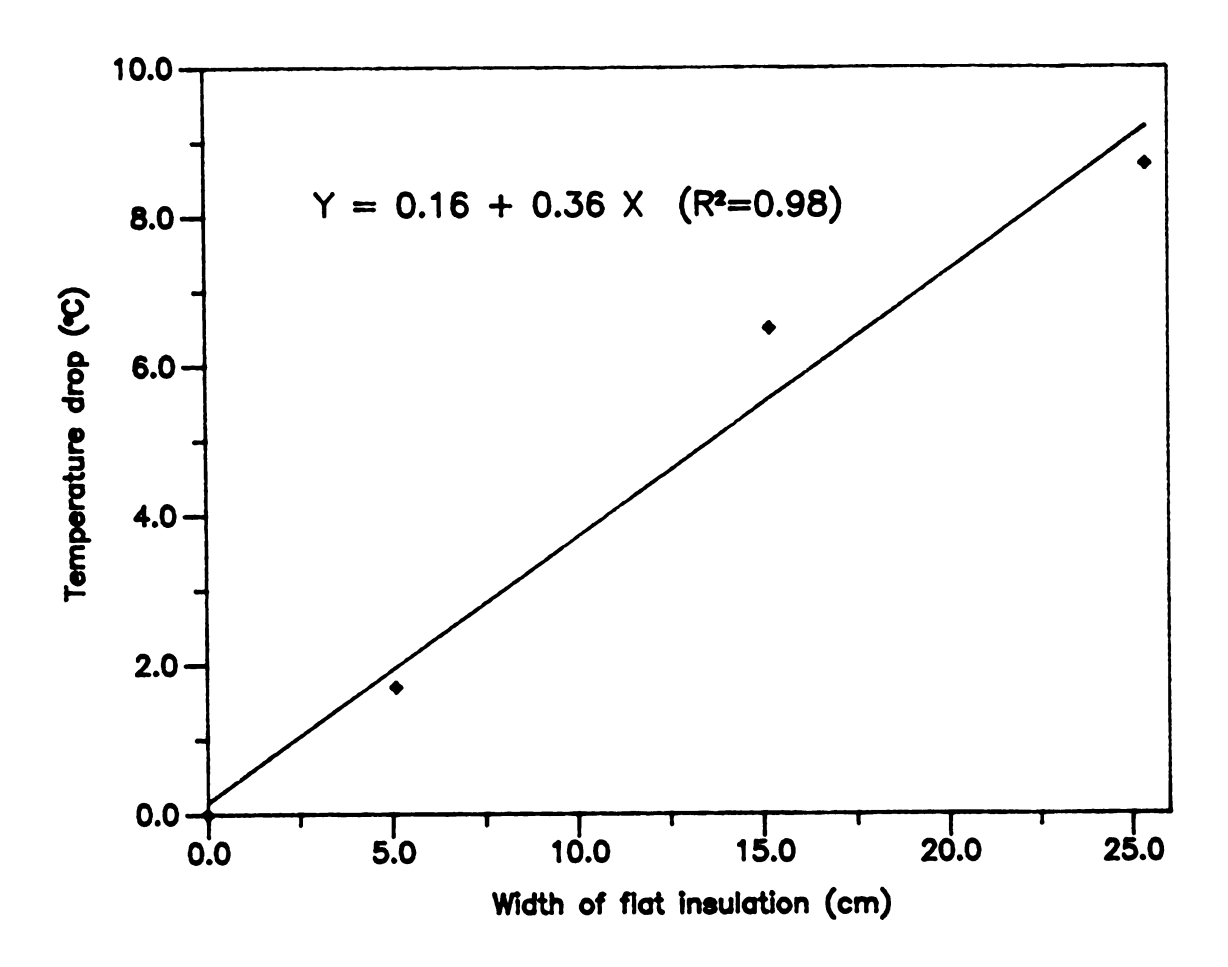


Figure 4.8 Temperature drop according to the width of flat insulation (tF = 1.3 cm, D = 2.5 cm).

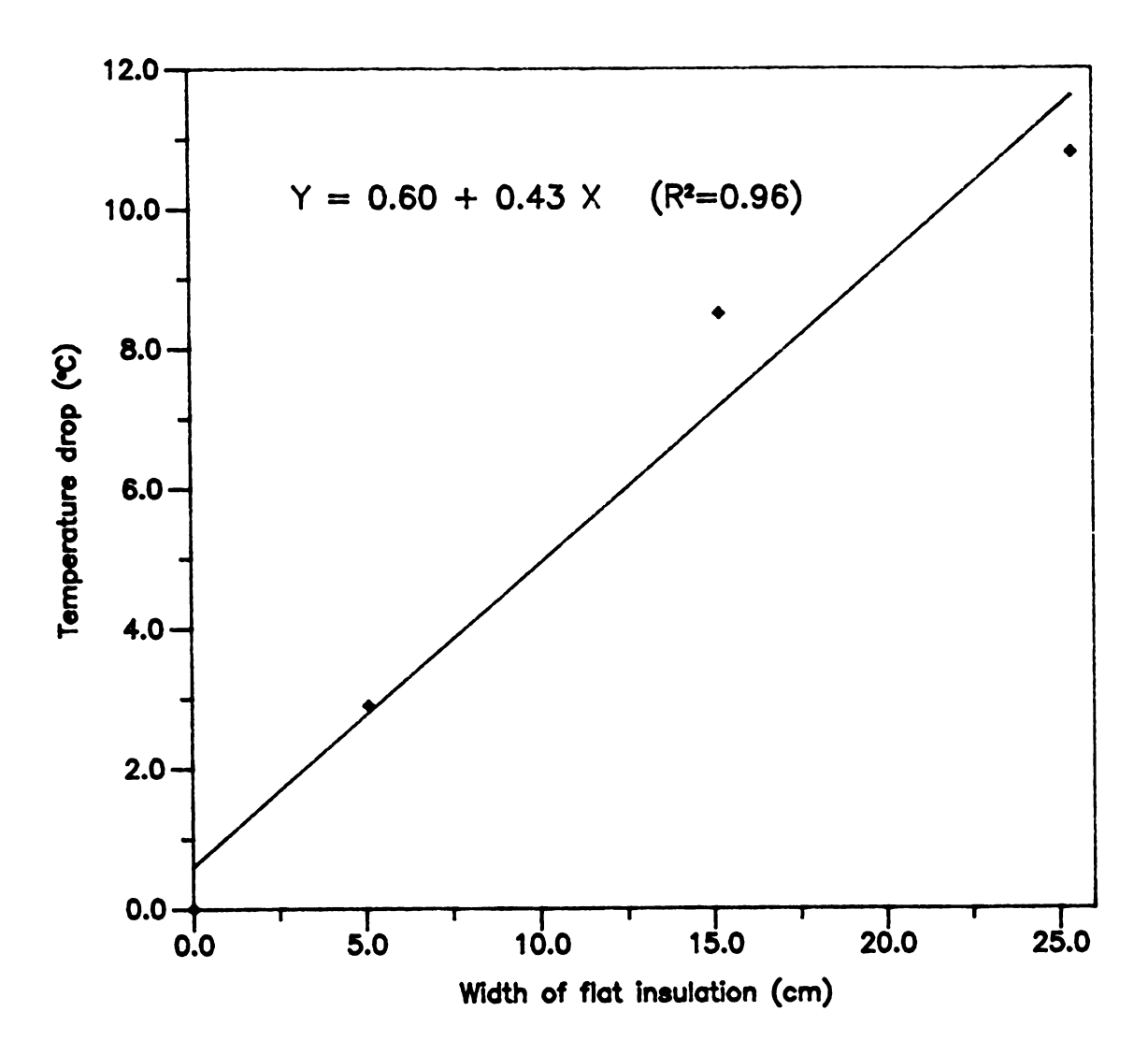


Figure 4.9 Temperature drop according to the width of flat insulation (tF = 2.5 cm, D = 2.5 cm).

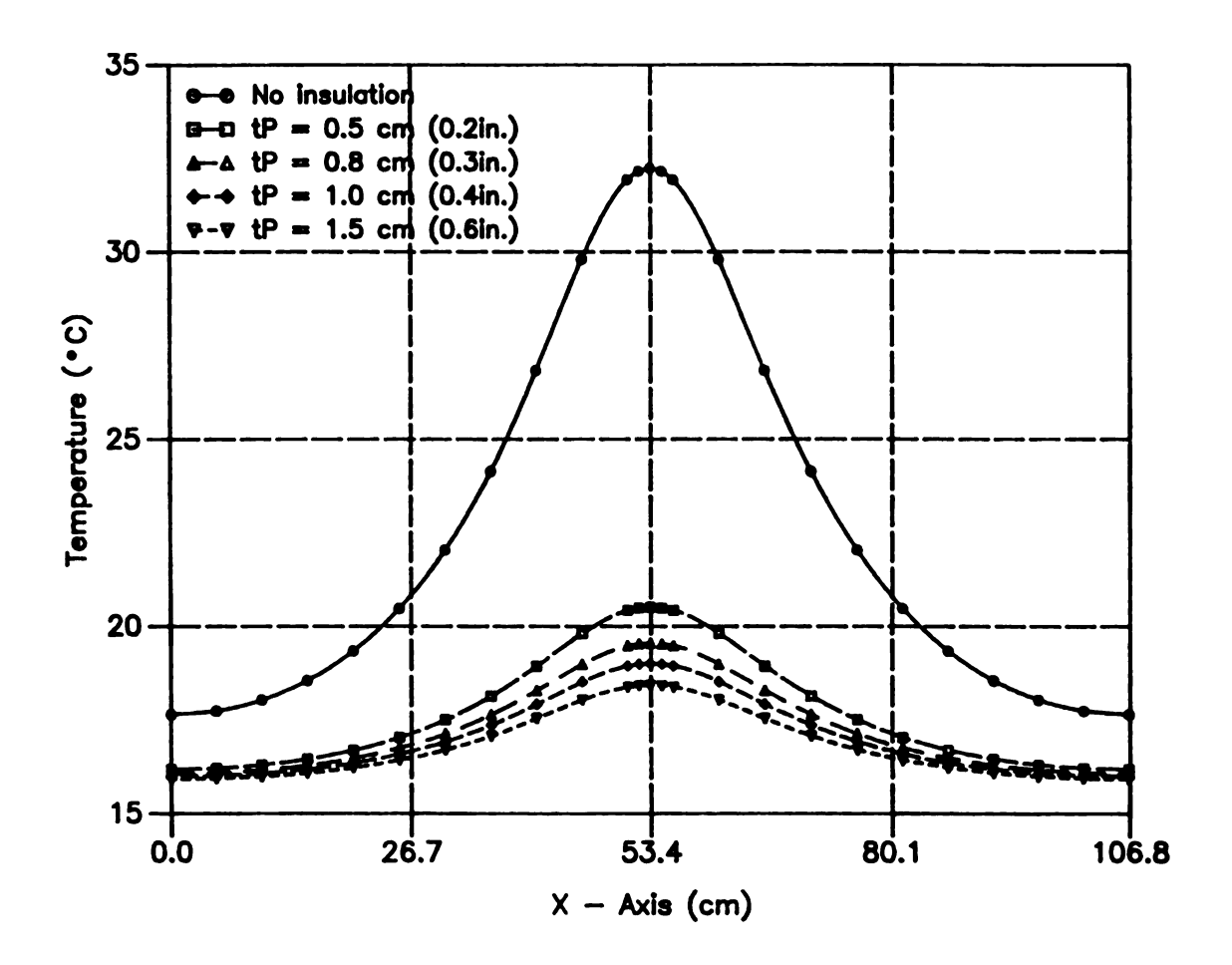


Figure 4.10 Effect of the thickness of perimeter insulation (No flat insulation).

4.2.5 Thickness of flat insulation above the perimeter insulated pipe

A thickness of 1.3 cm (0.5 inches) of flat insulation over the round pipe insulation whose thickness was 1.0 cm lowered the top temperature 0.9°C as shown in Figure 4.11. No significant difference was shown between the thickness of the flat insulation through the whole area. To level the top temperature, 1.3 cm thickness of flat insulation over the insulated pipe was desirable.

4.2.6 Width of flat insulation above the perimeter insulated pipe

The Figure 4.12 shows the change in the maximum temperature with width of the flat insulation on the perimeter insulated pipe. The thickness and placement depth of flat insulation were 1.3 cm and 2.5 cm, respectively. The thickness of perimeter insulation was 1.0 cm (0.4 inches). The wide insulation increased the area of maximum temperature, but lowered that temperature. No significant temperature difference was shown in the area 22.9 cm away from pipe.

4.2.7 Summary

The influence of the flat insulation and the pipe perimeter insulation on the floor temperature is now understood. Some design ideas could be deduced from that understanding.

The reasonable location of the flat insulation is 2.5 cm (1.0 inches) below the floor level. The 0.6 cm or 1.3 cm thick flat insulation is necessary to remove the hot space in the baby pig area. The 15.2 cm (6.0 inches) wide flat insulation

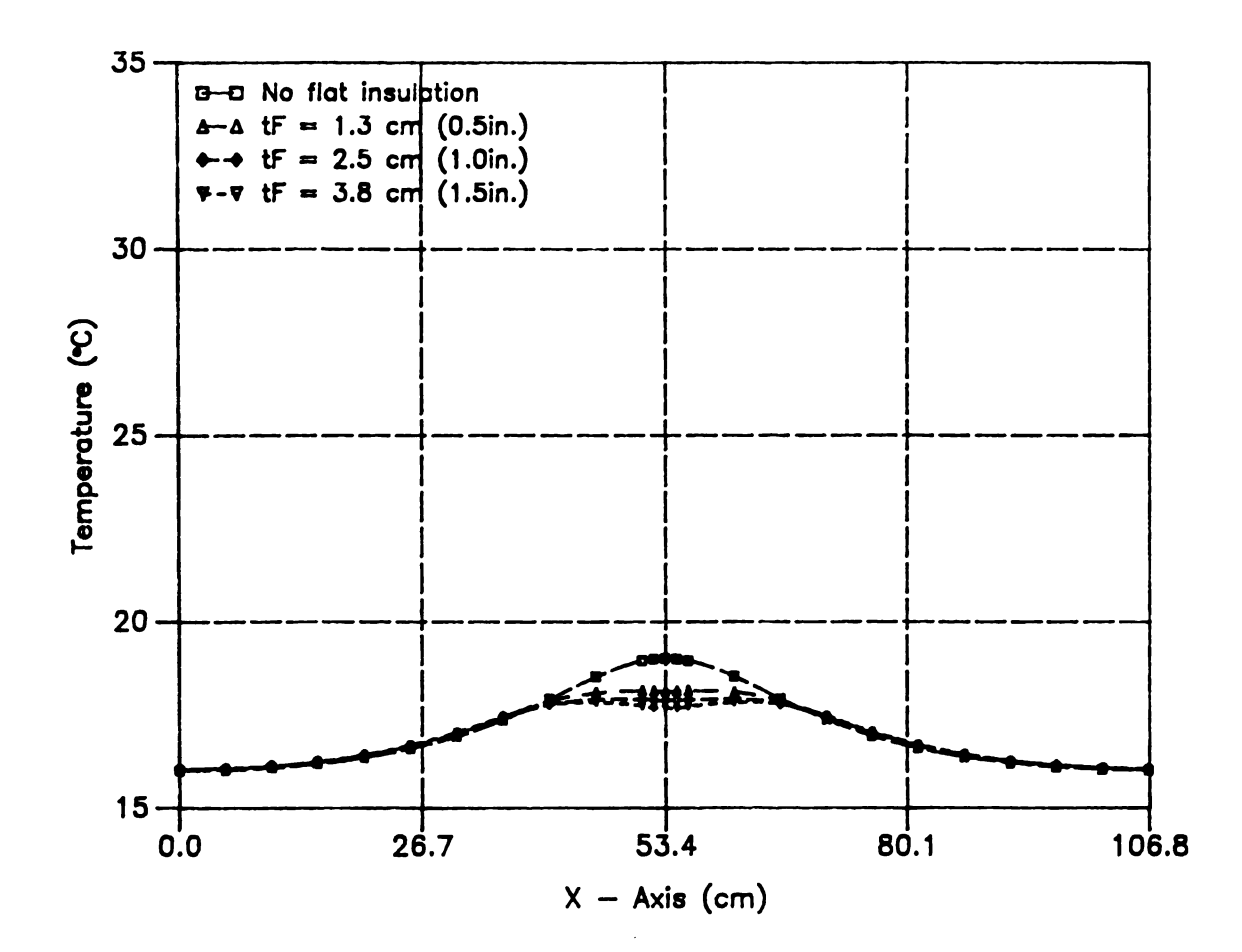


Figure 4.11 Effect of the thickness of flat insulation on the perimeter insulated pipe (D = 2.5 cm, W = 15.2 cm, tP = 1.0 cm).

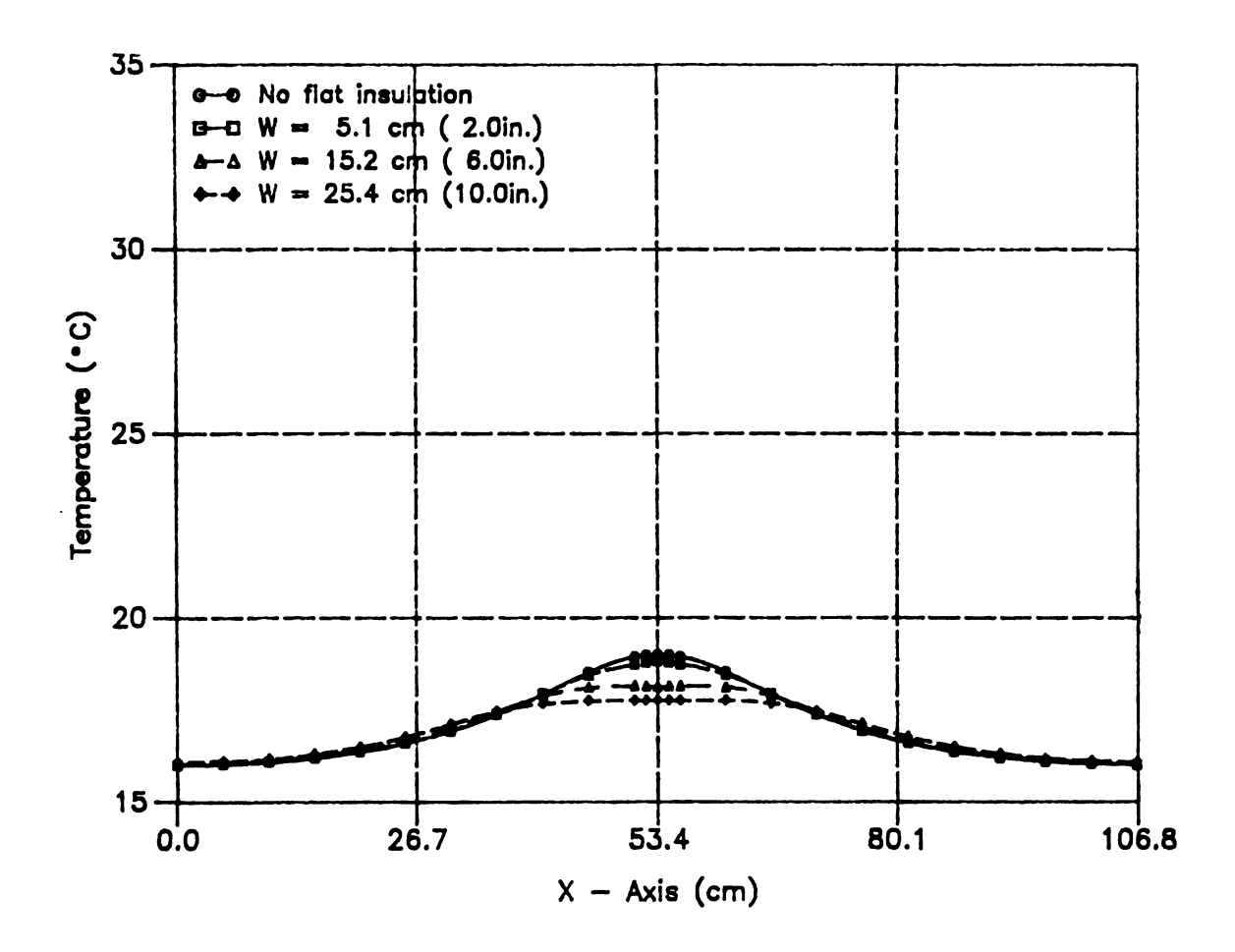


Figure 4.12 Effect of the width of flat insulation on the perimeter insulated pipe (tF = 1.3 cm, D = 2.5 cm, tP = 1.0 cm).

could level out the high temperature zone in the creep area.

The perimeter insulation around the pipe is necessary when the pipe goes beneath the sow area, and the 1.0 cm (0.4 inches) thickness of perimeter insulation is appropriate. Additionally, thin flat insulation could be insulated over the insulated pipe in the sow area to level out the high temperature and to drop a highest temperature a little. The two - pipe system failed to keep the creep area in the 29.4°C to 32.2°C (85°F to 90°F) temperature range; only one-third part of the creep area had a temperature over 25°C (77°F) in the case of no insulation. Therefore a three - pipe system is needed.

V. PROTOTYPE MODELS FOR HOT WATER HEATING SYSTEMS IN A FARROWING HOUSE

5.1 Three Heating Pipes without Fins

The temperature distribution on the floor of a farrowing house heated with three hot water pipes was analyzed using the model shown in Figure 5.1.

This model contains a quarter of a farrowing crate.

The variables used to find the optimum temperature distribution on the farrowing floor were the length (L₁), width (W₁, W₂) and the thickness (TI) of the flat insulation over the pipes and the length (L₂) of the perimeter insulation around the pipes. The thickness of a perimeter insulation on the pipes and the space between pipes were selected as 1.0 cm (0.4 inches) and 53.3 cm (21.0 inches), respectively. The depth of the flat insulation was 2.5 cm (1.0 inches) below the floor surface. The model consisted of 1694 nodes and 1194 elements. It took 27 minutes of CPU time on the VAX/VMS computer system to solve the system of equations.

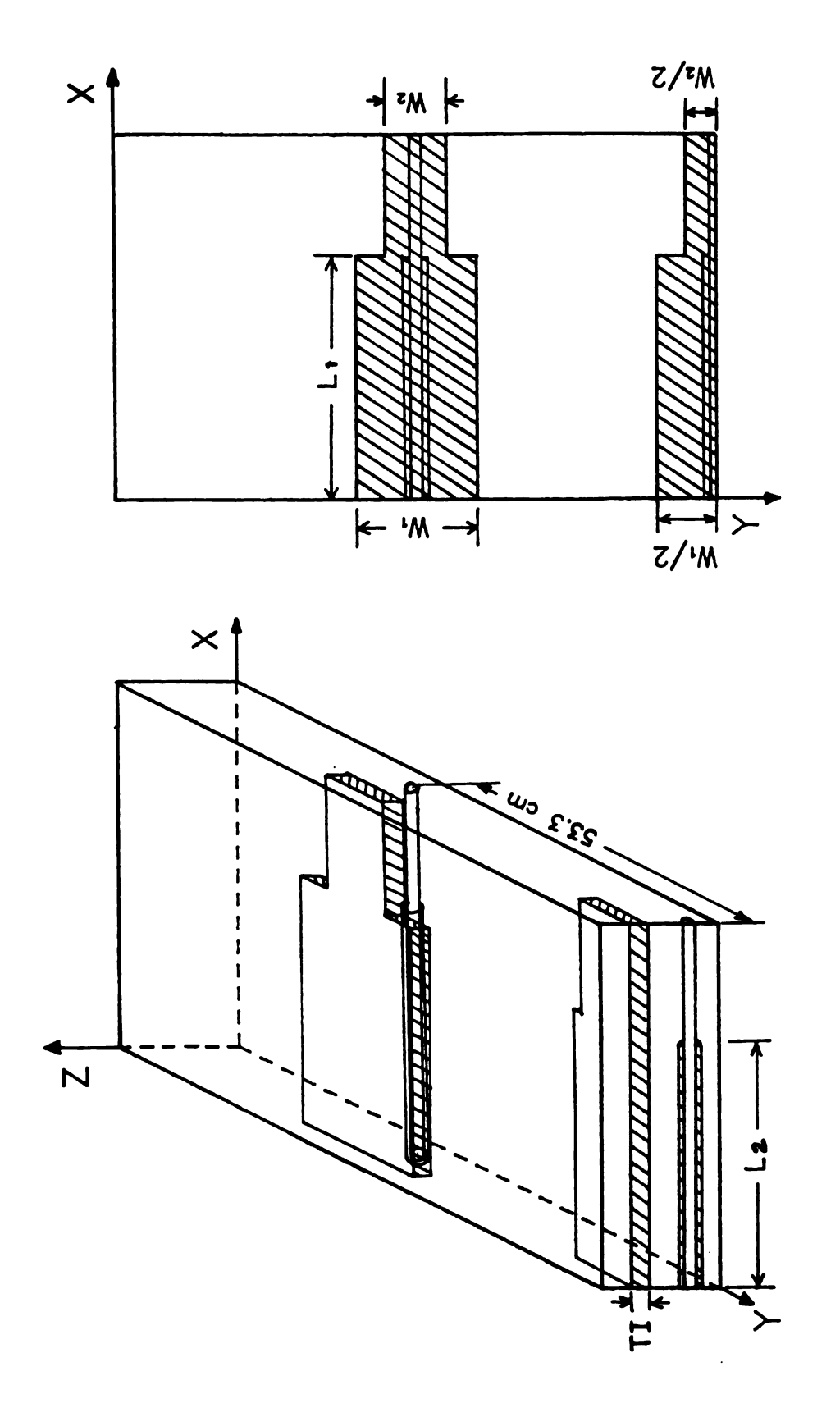


Figure 5.1 Variables for the model of three pipes without fin.

5.1.1 Thickness of flat insulation

Temperature distributions for an insulation thicknesses of 0.64 cm (0.25 inches) and 1.3 cm (0.5 inches) were calculated under the condition of $L_1 = 50.8$ cm (20.0 inches), $W_1 = W_2 = 15.2$ cm (6.0 inches), and $L_2 = 76.2$ cm (30.0 inches). See Figure 5.1 for an explanation of symbols.

The left drawing of the Figure 5.2 shows the temperature distribution along the X - axis when Y = 106.7 cm. This location is just above the pipe. The left side of the vertical dotted line in the left drawing is the sow area, and the right side the litter area. The high and low horizontal dotted lines show the temperature range appropriate for the sow and litter, respectively. The right drawing of the Figure 5.2 represents the temperature distribution along the Y - axis when X = 76.2 cm. The two horizontal dotted lines define the range of suitable temperatures for the litter. The temperature distributions shown in Figure 5.2 are the highest temperature values with respect to the X and Y - axis in the entire farrowing area.

The flat insulation made the temperature in the baby pig area produced a lower temperature than desired, but provided a temperature approaching the desired temperature range in the sow area. The maximum 1.5°C difference was obtained between the 0.6 cm and 1.3 cm thicknesses of a flat insulation in the baby pig area. Without the flat insulation, there was a hot spot higher than the maximum desirable temperature 32.2°C (90°F) in the baby pig area, and the minimum temperature in the sow area was 1.6°C higher than the maximum desirable temperature 18.3°C (65°F).

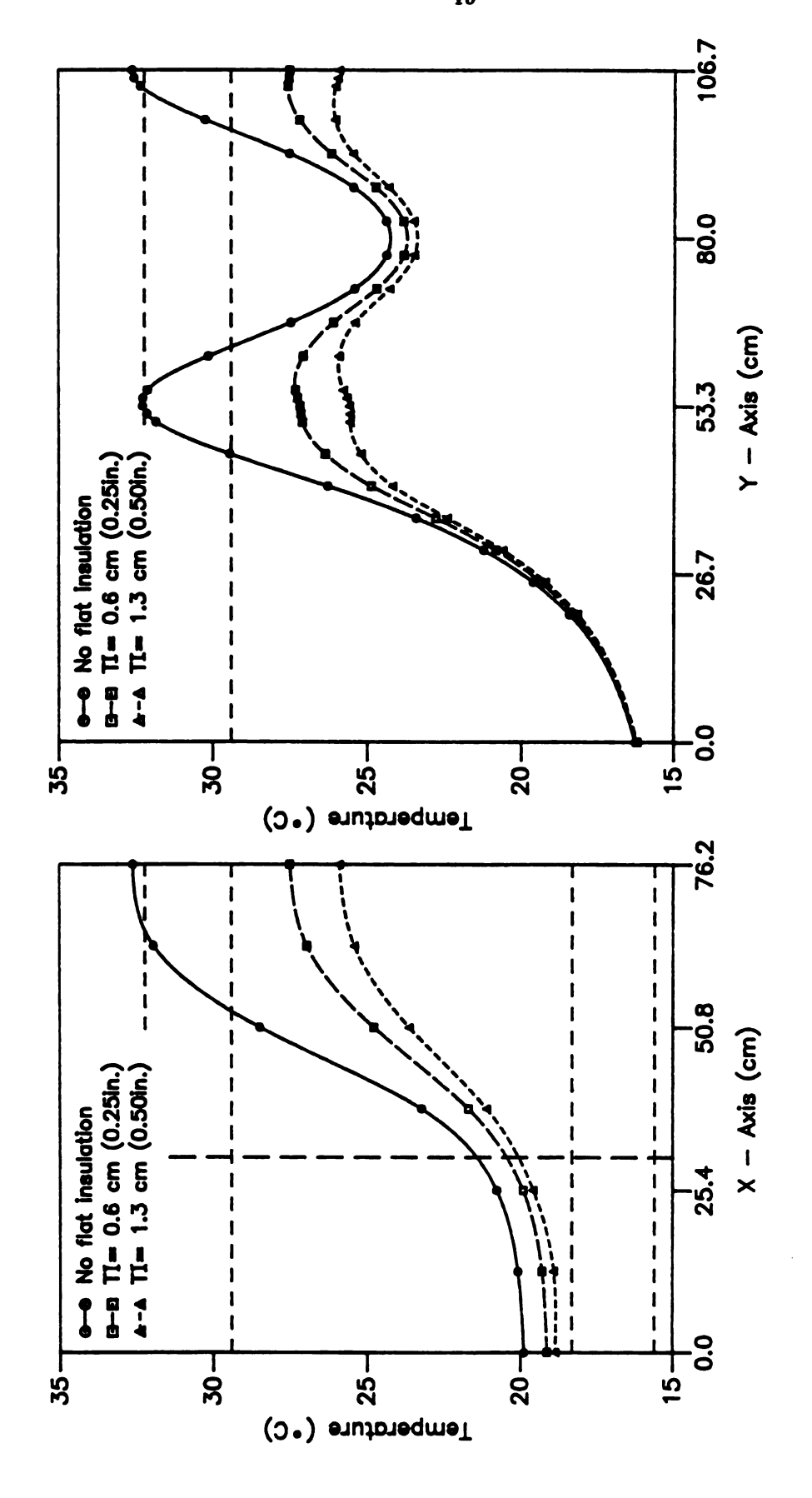


Figure 5.2 Effect of the thickness of flat insulation ($L_1 = 50.8$ cm, $W_1 = W_2 = 15.2$ cm, $L_2 = 76.2$ cm).

5.1.2 Width of flat insulation

The width of a flat insulation in the baby pig area (W_2) was changed from 0.0 cm to 15.2 cm (6.0 inches) to determine the effect of the width of the insulation. The sow area was insulated with $L_1 = L_2 = 50.8$ cm, $W_1 = 15.2$ cm size insulation in the all cases. The thickness of insulation (TI) was 1.3 cm (0.5 inches). The 5.1 cm (2.0 inches) insulation width was better than other widths even though a low temperature zone for the baby pig existed between the hot water pipes as shown in Figure 5.3. The highest temperature would be increased when the thinner insulation (TI = 0.64 cm) was applied.

5.1.3 The length of perimeter insulation

The 38.1 cm (15 inches) and 50.8 cm (20 inches) length of the perimeter insulation were compared in the flat insulation condition of TI = 0.64 cm, $W_1 = 15.2$ cm, $W_2 = 5.1$ cm, and $L_2 = 50.8$ cm. The 38.1 cm length of the perimeter insulation showed wider high temperature distribution than the 50.8 cm length of insulation in the sow area, since the 50.8 cm length of the perimeter insulation showed the wider low temperature distribution than the 38.1 cm length of insulation in the litter area as shown in the left side drawing of Figure 5.4. The 50.8 cm length of perimeter insulation was more desirable than 38.1 cm length.

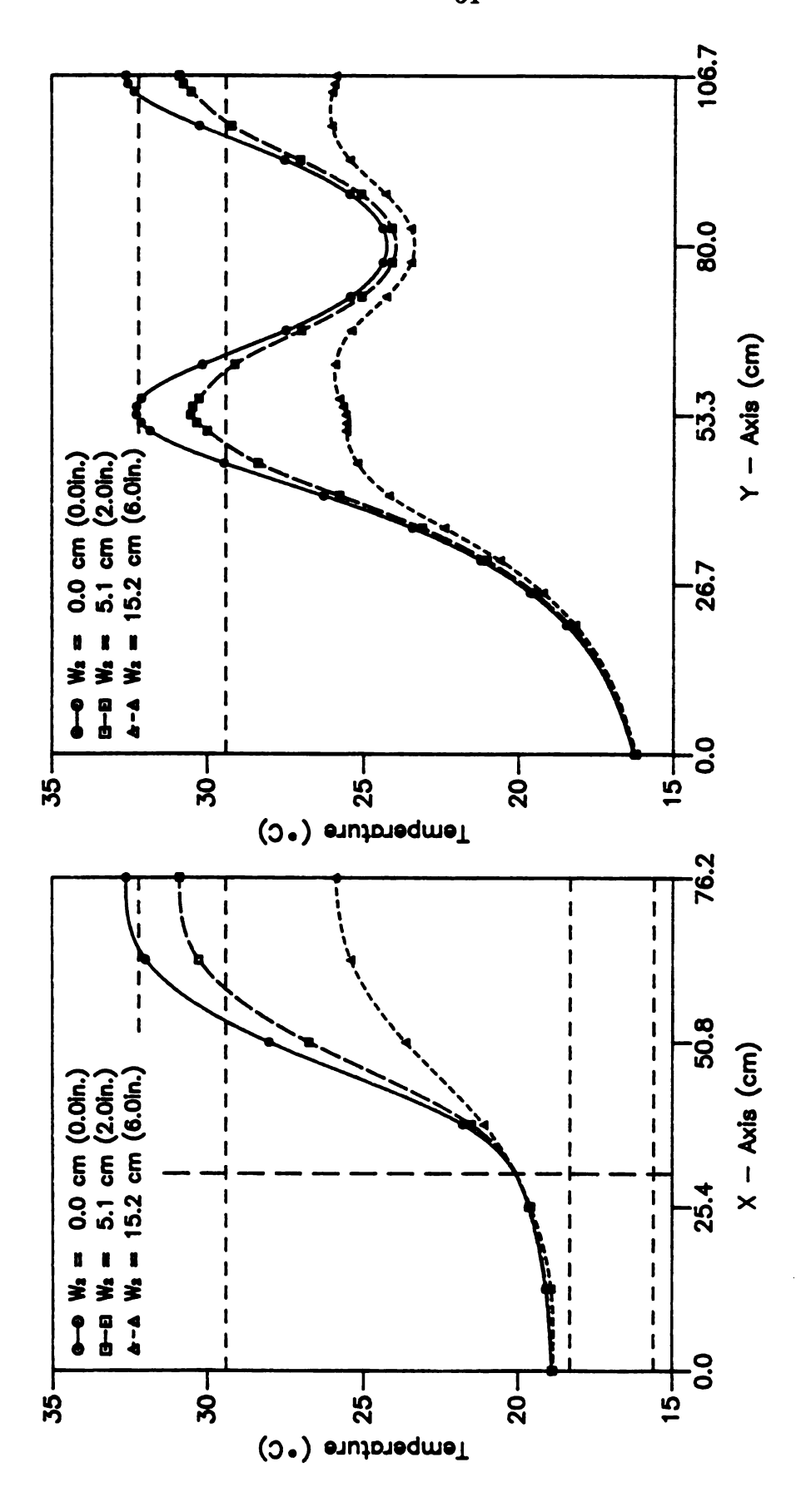


Figure 5.3 Effect of the width of flat insulation ($L_1 = L_2 = 50.8$ cm, $W_1 = 15.2$ cm, TI = 1.3 cm).

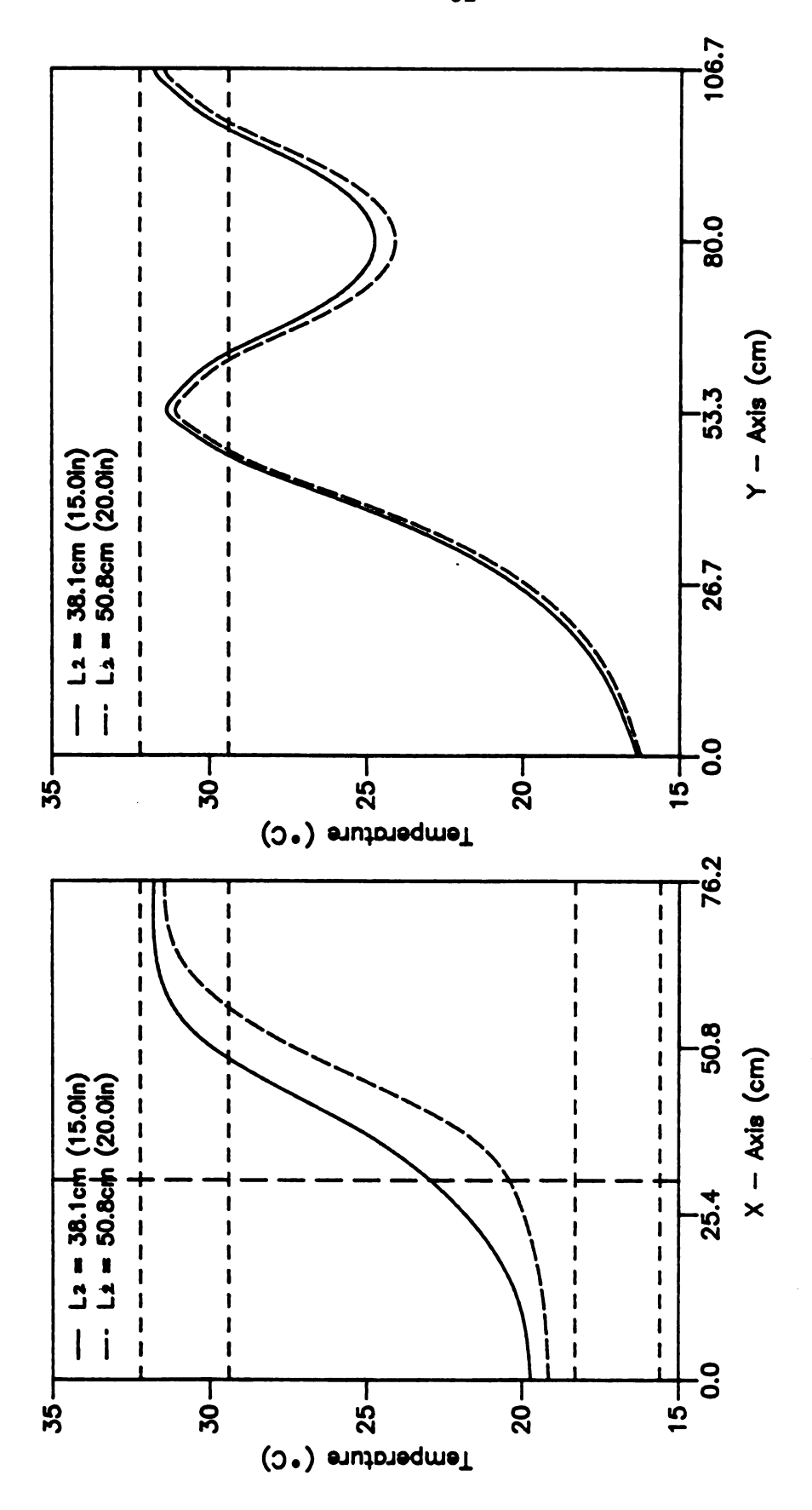


Figure 5.4 Effect of the length of perimeter (L₁ = 50.8 cm, W₁ = 15.2 cm, W₂ = 5.1 cm, TI = 0.64 cm).

5.1.4 Recommended model

Of the various combinations considered, the most desirable model when using three pipes is shown in Figure 5.5. All of the flat insulation had 0.64 cm (0.25 inches) of thickness. The space between the flat insulation in the litter area and the sow area was provided to permit heat flow to the litter area, and to widen the high temperature zone in the litter area. The two dotted lines shown in Figure 5.5 are the borders between sow and litter areas.

The temperature distribution on the quarter-floor is shown in Figure 5.6. The temperature was 0.6°C higher than suggested for the sow, but nearly constant across the whole sow area. If the thicker insulation is used throughout the sow area, the temperature would be decreased a little, but not significantly. A small portion of the litter area was in the desirable temperature zone. If the flat insulation in the litter area is removed, a higher temperature zone could be obtained. Figure 5.7 and Figure 5.8 show the temperature contour and the three-dimensional temperature distribution on the whole floor, respectively. As shown in Figure 5.7, six separate hot areas exist for litter while a nearly constant temperature distribution exists in the sow area. A cooler area for the litter occurs on the floor between the pipes.

It was difficult to get the desirable temperature distribution in the litter area when the only three hot water pipes were used for heating the floor. The possibility of attaching fins to the pipes to get an additional conduction effect was proposed. The idea is analyzed in the following sections because additional pipes in the heating system complicate the construction, and increase the operating

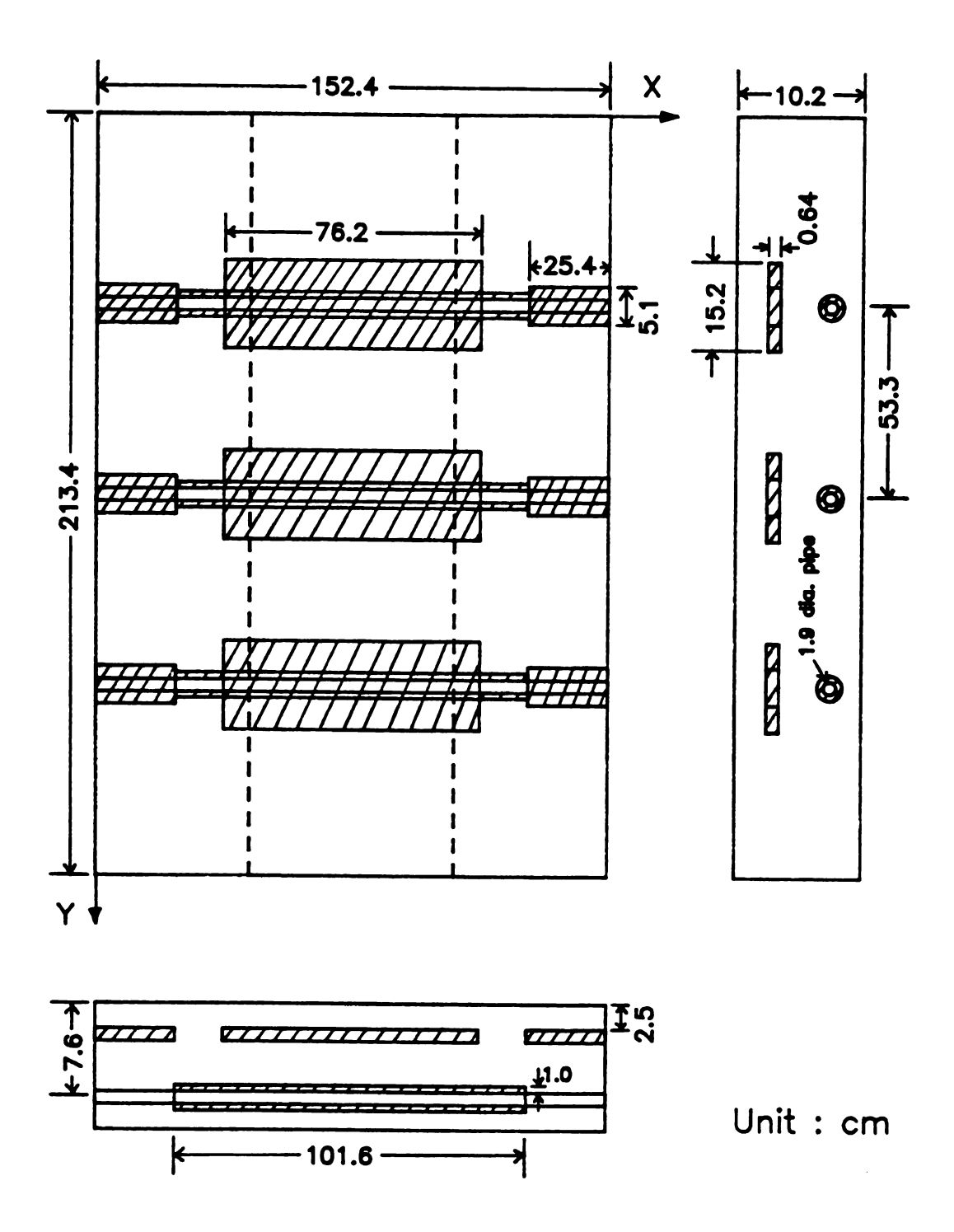


Figure 5.5 Recommended model for three pipes without fin.

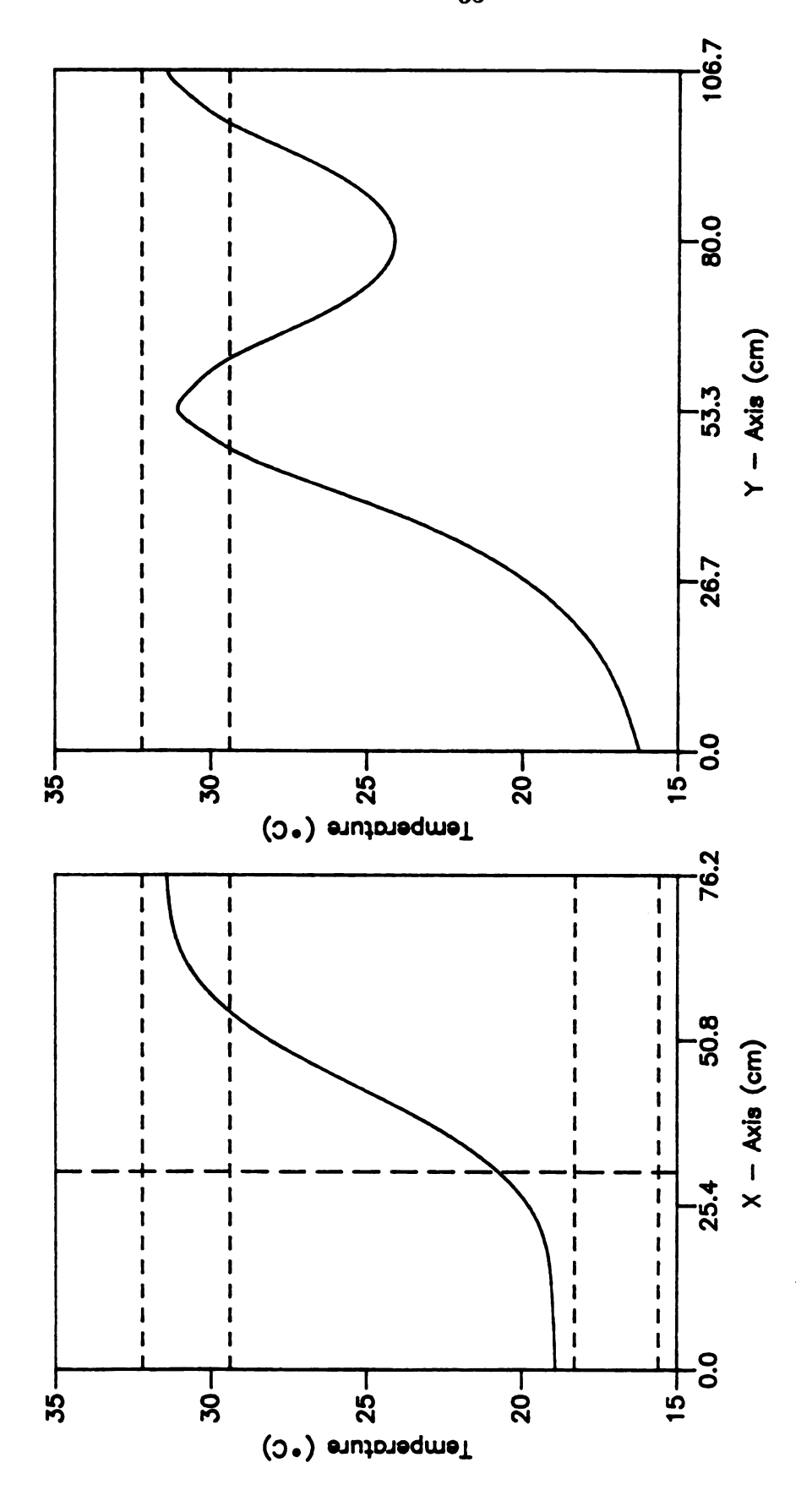


Figure 5.6 Temperature distribution on the floor of recommended model for three pipes without fin.

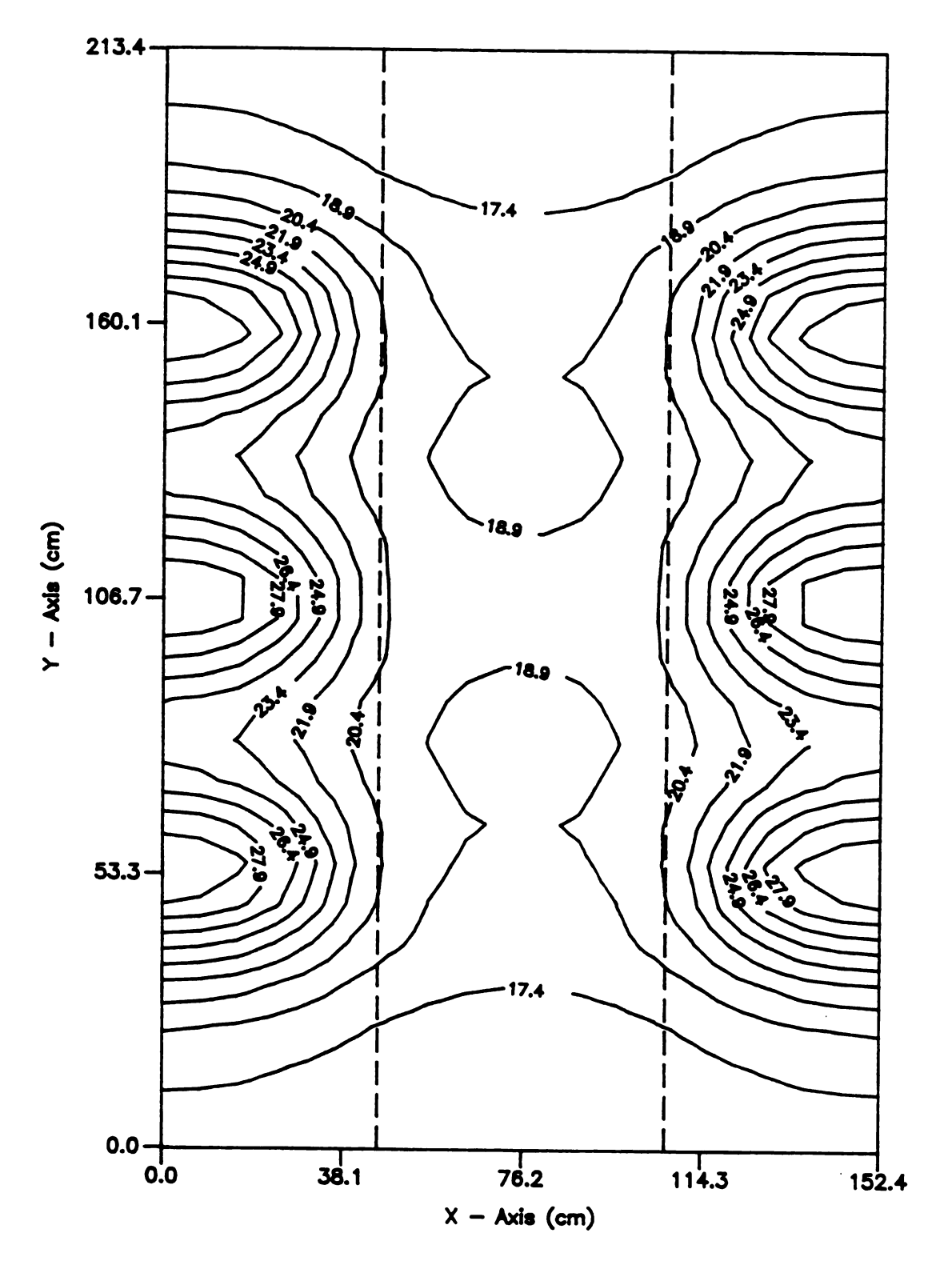


Figure 5.7 Temperature contour on the floor of the recommended model for three pipes without fin.

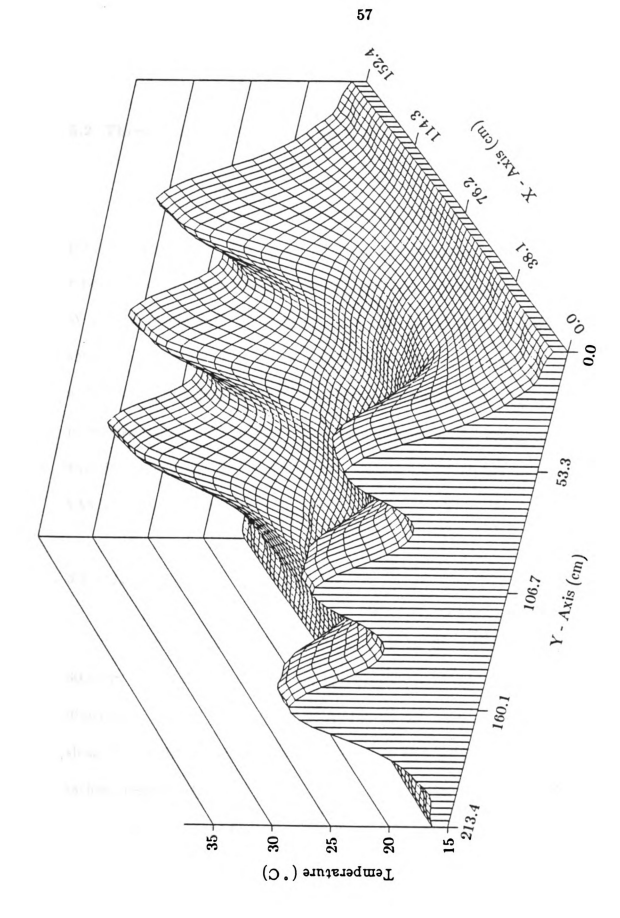


Figure 5.8 Three-dimensional temperature distribution of recommended model for three pipes without fin.

costs, with no significant improvement in temperature distribution.

5.2 Three Heating Pipes with Steel Fins

A steel fin would be attached to each of the pipes to widen the high temperature zone in the litter area. The fin would probably be welded under the pipes for ease of construction. The thermal conductivity of the steel fin was 37.49 W / m°K (1.805 Btu / hr inch°F). The dimensions of the fin and insulation are shown in Figure 5.9. The length and thickness of the perimeter insulation were set at 50.8 cm (20 inches) and 1.0 cm (0.4 inches), respectively. The spacing between pipes was 53.3 cm (21 inches). The finite element model consisted of 2100 nodes and 1566 elements and required 28 minutes of CPU time to solve using the VAX/VMS computer system.

5.2.1 Length of fin

Five different fin lengths, 0 cm, 15.2 cm (6 inches), 22.9 cm (9 inches), 30.5 cm (12 inches), and 53.3 cm (21 inches), were analyzed for flat insulation dimensions of 15.2 cm wide, 76.2 cm (30 inches) long, and 1.3 cm (0.5 inches) thick. The width and thickness of the fin were 25.4 cm (10 inches) and 0.5 cm (0.2 inches), respectively.

The curves in Figure 5.10 show that addition of the steel fin increases the litter area temperature more than 2.5 °C. This increase occurs through the whole

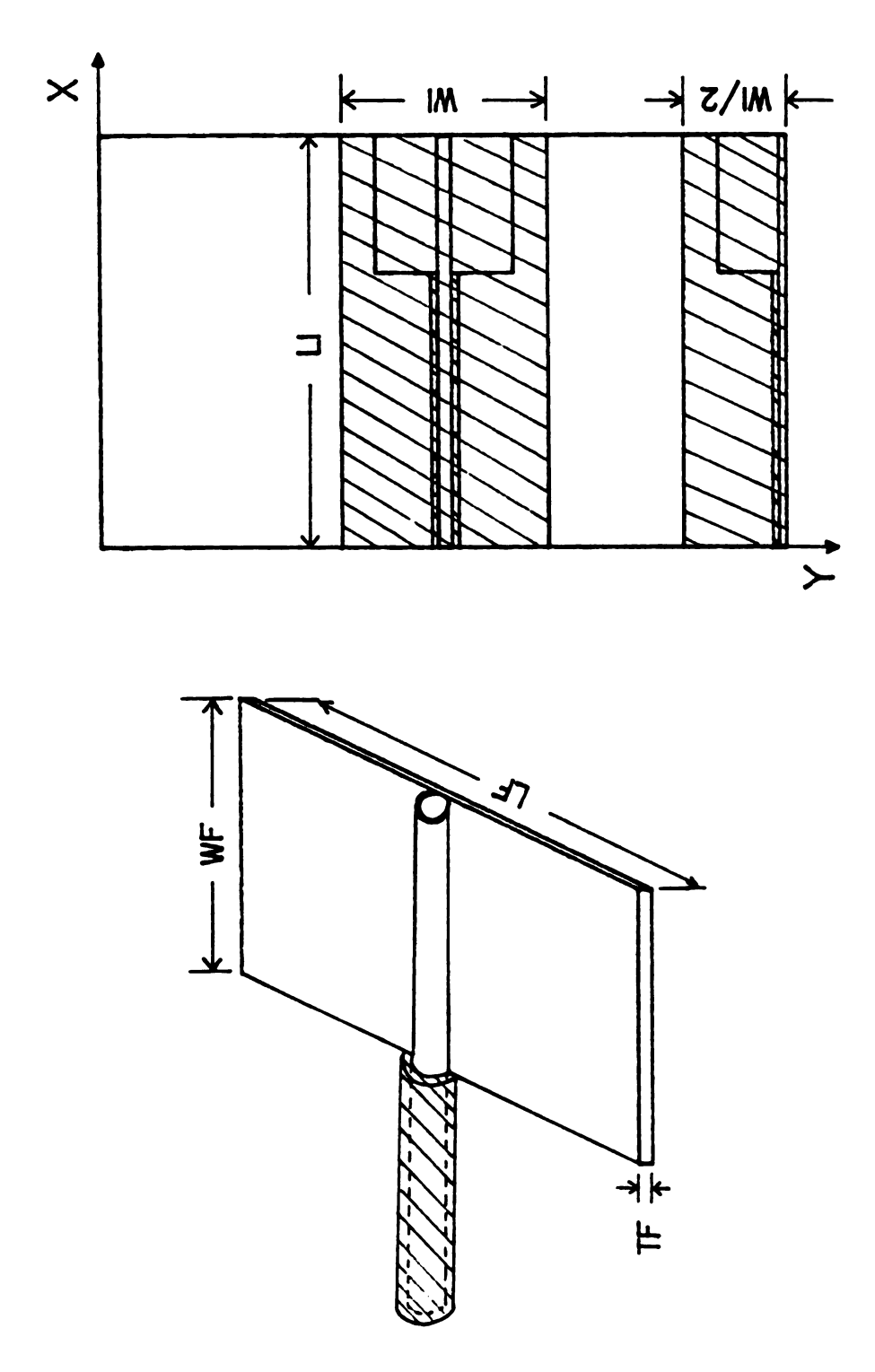


Figure 5.9 Variables of fin and insulation for model of three pipes with fin.

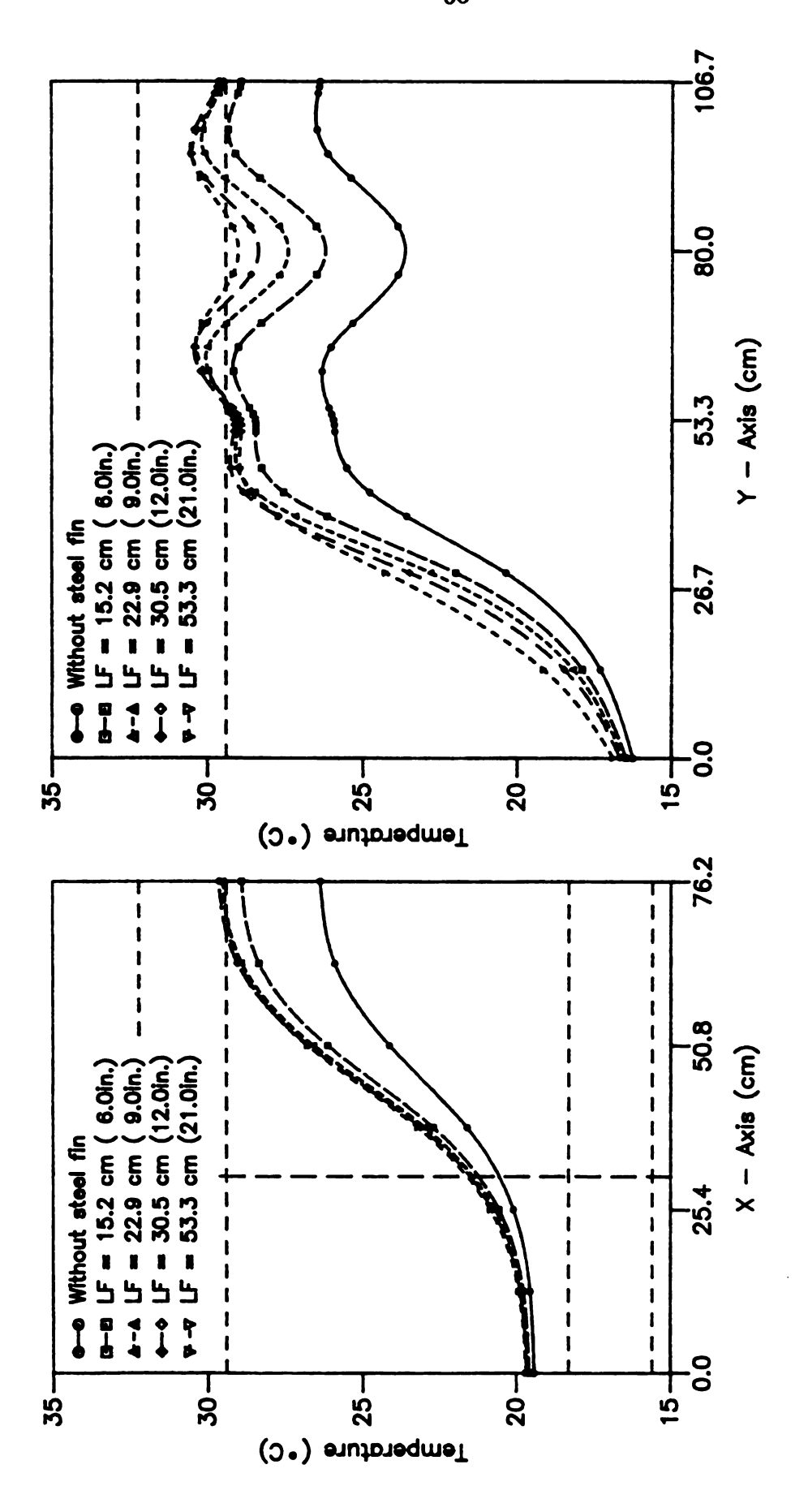


Figure 5.10 Effect of the length of steel fin (LI = 76.2 cm, WI = 15.2 cm, TI = 1.3 cm, WF = 25.4 cm, TF = 0.5 cm)

litter area. However, the length of the steel fin was not an important factor even though a longer fin raised the temperature between pipes. That was because the temperature on the steel fin dropped rapidly with respect to the fin length as demonstrated in Figure 5.11 which shows the temperature distribution at the same depth as the fin. The 22.4 cm (9 inches) length of steel fin was the most desirable when the thickness of flat insulation was reduced to 0.64 cm (0.25 inches) as shown in Figure 5.12.

5.2.2 Thickness of fin

Two fin thickness values, 0.5 cm (0.2 inches) and 0.25 cm (0.1 inches) were analyzed using a length of 22.9 cm (9 inches) and a width of 15.2 cm (6 inches). The flat insulation was 0.64 cm (0.25 inches) thick. Because the thinner fin produced a 1.1 °C lower maximum temperature than the thicker fin shown in Figure 5.13, the 0.5 cm thick fin was more desirable.

5.2.3 Recommended model

The most desirable model of using three hot water pipes with steel fins is presented in Figure 5.14 based on the insulation information obtained in the previous section, and fin information in this section. Most of the sow area was insulated with 1.3 cm (0.5 inches) thick flat insulation to decrease the temperature in this area. On the other hand, the litter area was insulated with 0.64 cm (0.25 inches) thick to enhance the temperature. The space between the flat insulation

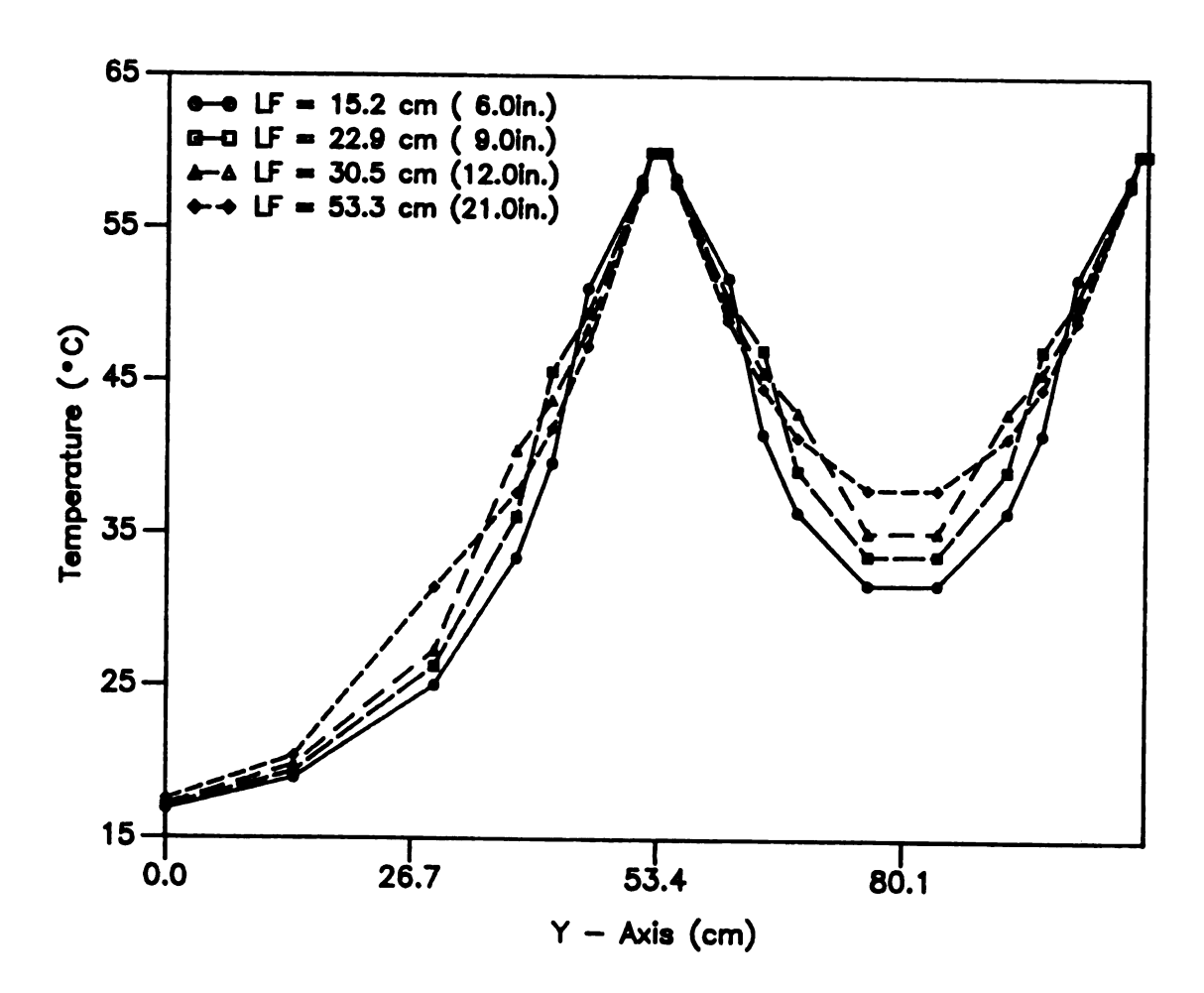


Figure 5.11 Temperature change on the steel fin.

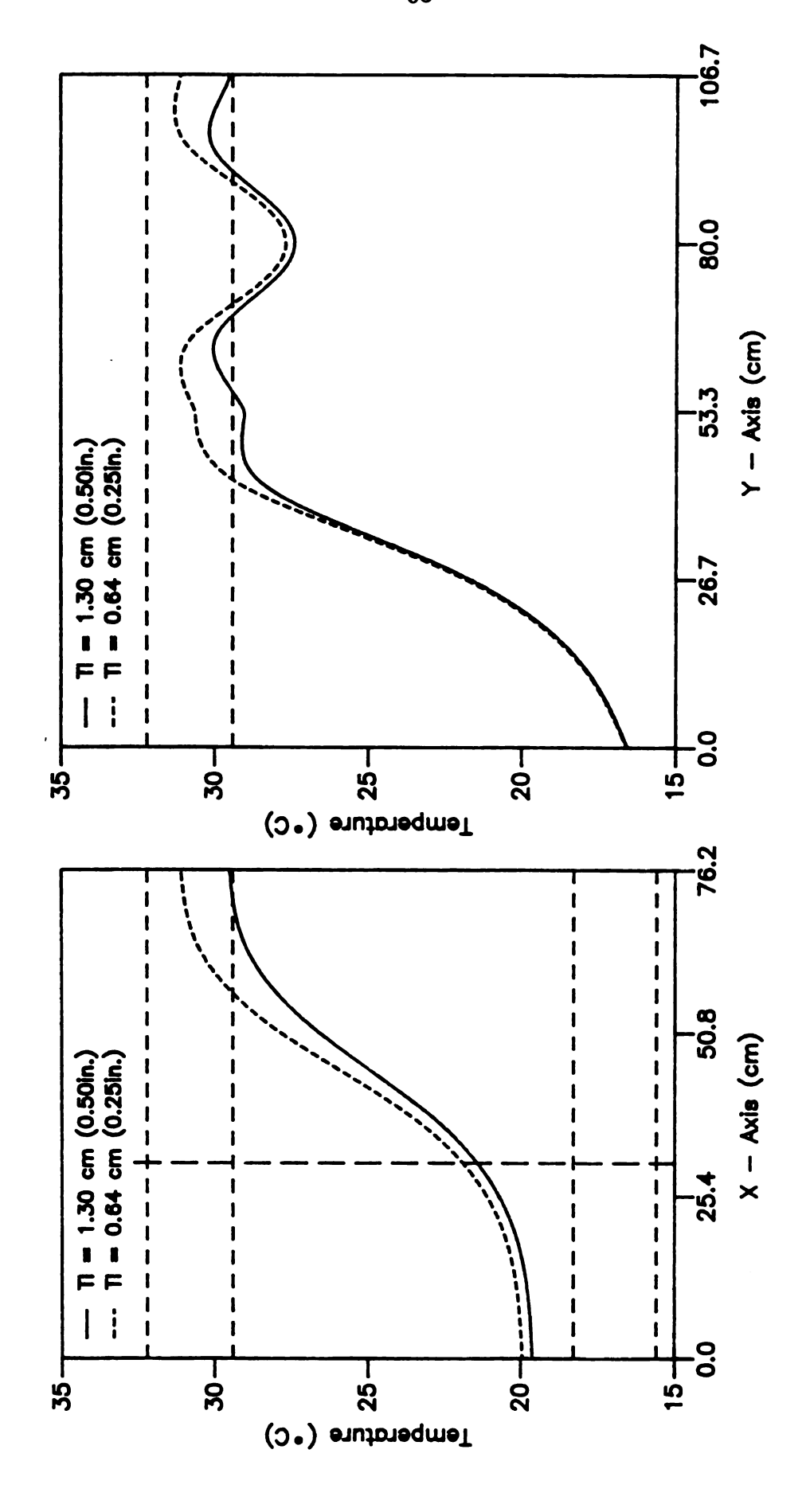


Figure 5.12 Effect of the thickness of flat insulation on 22.9 cm long steel fin.

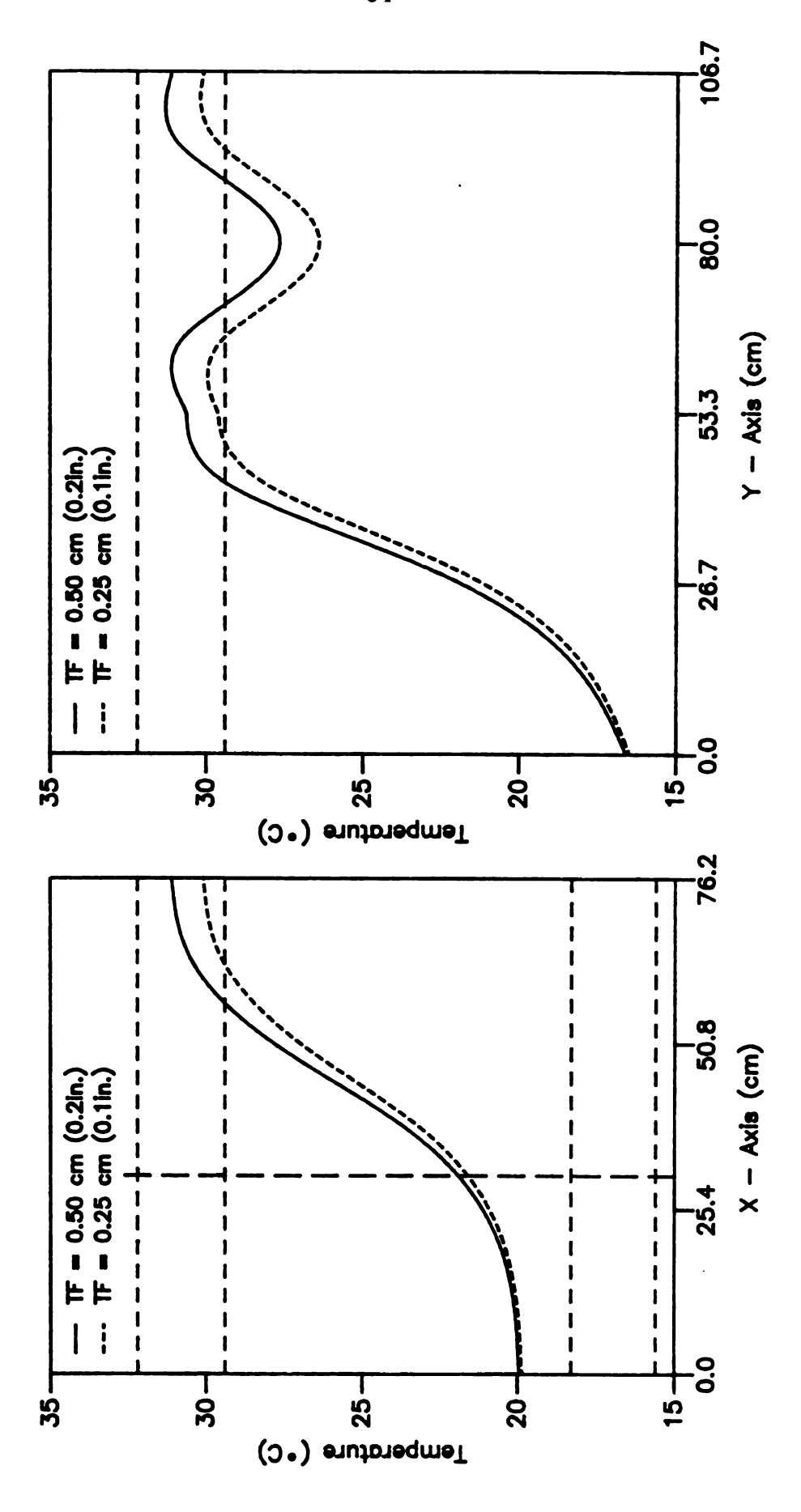


Figure 5.13 Effect of the thickness of steel fins.

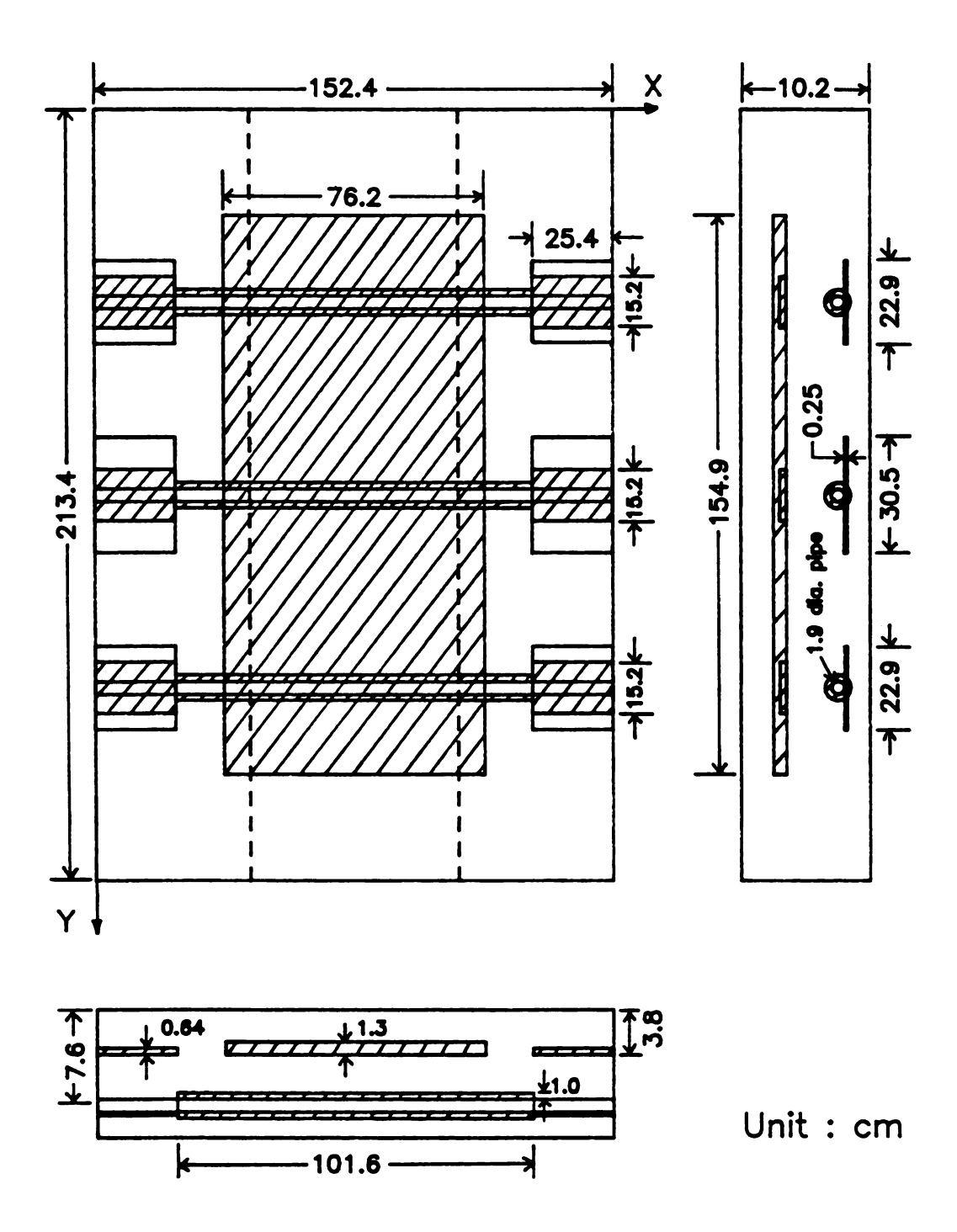


Figure 5.14 Recommended model for three pipes with steel fins.

of the litter area and the sow area was same as in the case of pipes without fins. The 30.5 cm (12 inches) long fin was attached to the center pipe since shorter 22.9 cm (9 inches) long fin to the side two pipes. That could widen a comfortable temperature space for baby pigs and raise the temperature of cooler area between pipes in the litter area.

Figure 5.15 shows the temperature distribution for the quarter part of the floor and Figure 5.16 and Figure 5.17 present the temperature contour and the three-dimensional temperature distribution of the whole farrowing floor, respectively. The temperature distribution in sow area was even and within the adequate temperature range except for the small center portion of the sow area. A large part of the litter area was within the desirable temperature range. Widening the space between pipes along with extending the length of the fin would be helpful in removing the cold zone existing in the upper and lower litter areas. Using a fin which is high in the thermal conductivity such as a copper would be another approach.

5.3 Three Heating Pipes With Copper Fins

A copper fin that has a high thermal conductivity was introduced to widen the desirable temperature zone for the litter and to reduce the size of fin. The thermal conductivity of copper is 377.23 W / cm °K (18.17 Btu / hr inch °F) which is 10 times higher than steel. The variables for the copper fin are the same as those shown in Figure 5.9 for the steel fin. The insulation constants were same

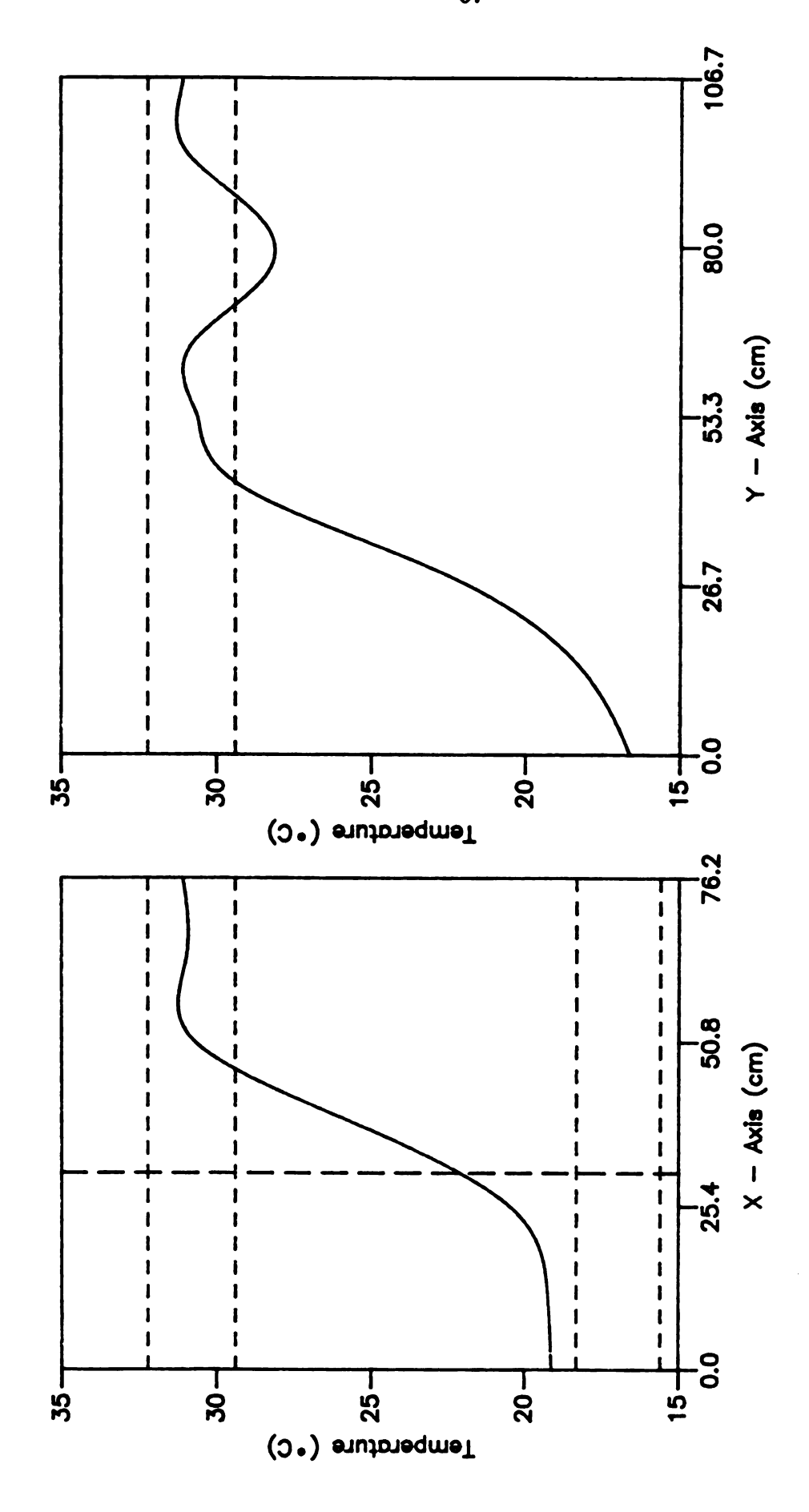


Figure 5.15 Temperature distribution on the floor of recommended model for three pipes with steel fins.

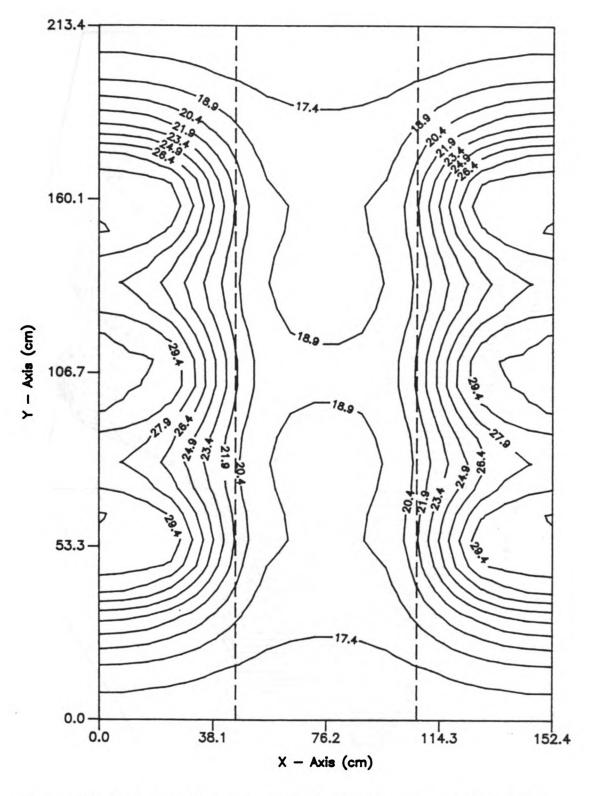


Figure 5.16 Temperature contour on the floor of the recommended model for three pipes with steel fins.

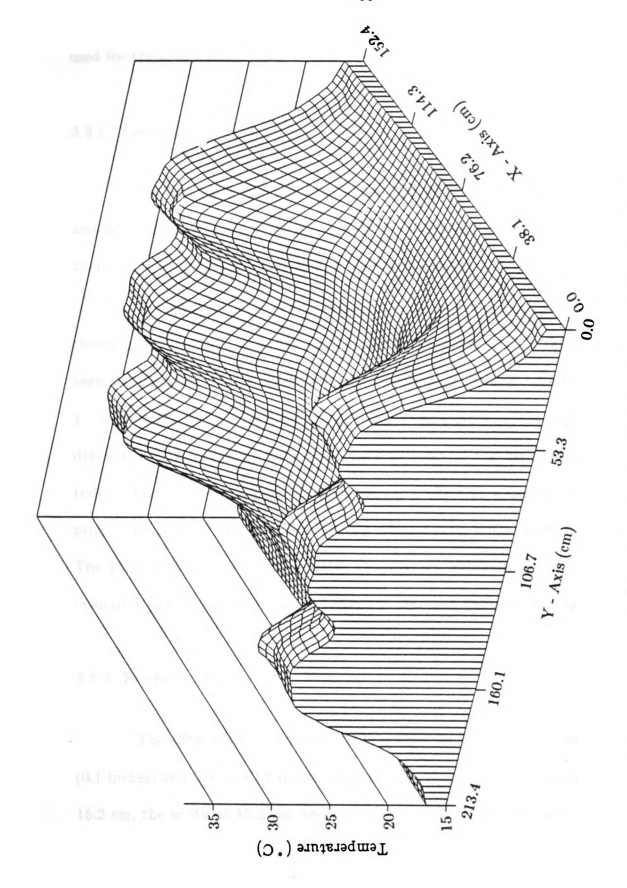


Figure 5.17 Three-dimensional temperature distribution of recommended model for three pipes with steel fins.

as in the case of the steel fin. The finite element model was also the same as that used for the steel fin.

5.3.1. Length of fin

The four cases of fin length, 0 cm, 15.2 cm (6 inches), 22.9 cm (9 inches), and 30.5 cm (12 inches), were analyzed. The width and thickness of the fin were 25.4 cm (10 inches) and 0.5 cm (0.2 inches), respectively.

The 15.2 cm long fin increased the highest temperature by 4.5°C as shown in Figure 5.18. The temperature distribution varied with the length of fin very significantly. Figure 5.19 shows the temperature changes with respect to the Y - axis at the buried depth of the fin. The temperature on the copper fin itself did not vary significantly with the length because of the high thermal conductivity. Therefore, the copper fin gave the same effect as widening the hot water pipe. The 15.2 cm and 22.9 cm long fin showed good temperature distributions. The 15.2 cm long fin showed a better temperature distribution when thinner flat insulation (TI = 0.64 cm) was used over the pipe and fin as shown Figure 5.20.

5.3.2 Thickness of fin

The effect of the thickness of the copper fin was analyzed using 0.25 cm (0.1 inches) and 0.5 cm (0.2 inches) thickness values under while keeping length at 15.2 cm, the width at 15.2 cm, and the thickness of the flat insulation at 0.64 cm. No significant difference attributable to the thicknesses of fins was found as shown

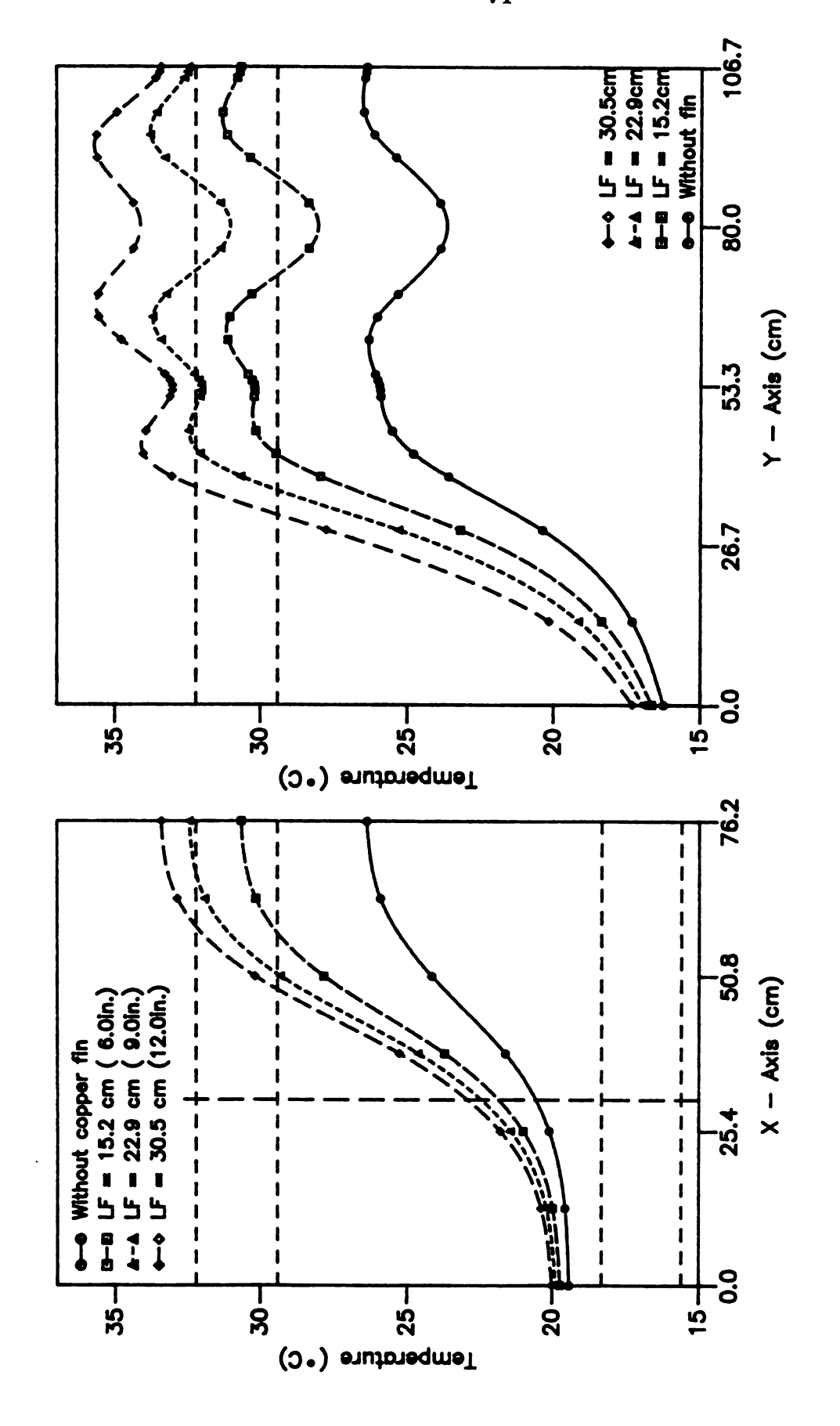


Figure 5.18 Effect of the length of copper fin (LI = 76.2 cm, WI = 15.2 cm, TI = 1.3 cm, WF = 25.4 cm, TF = 0.5 cm).

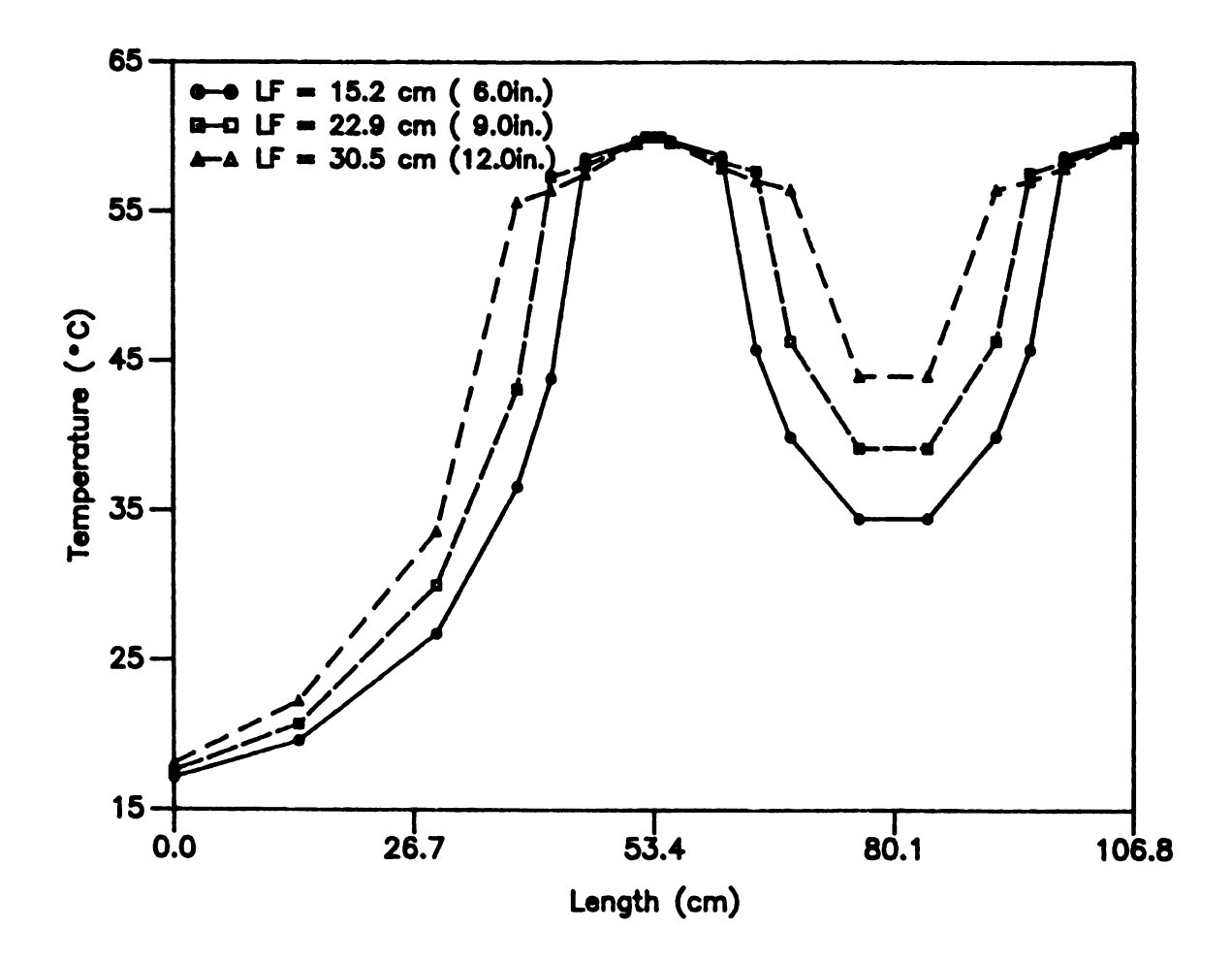


Figure 5.19 Temperature change on the copper fin.

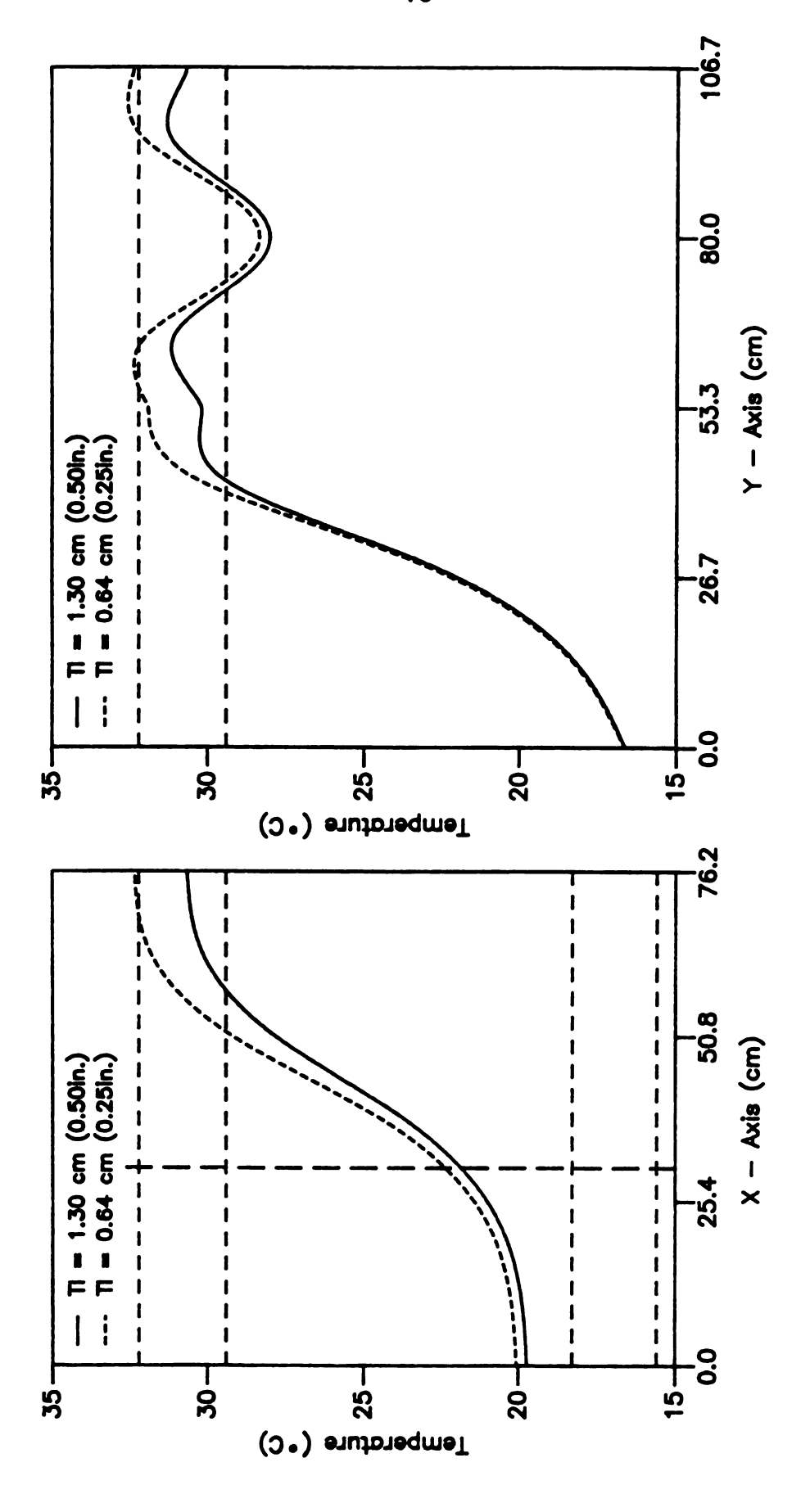


Figure 5.20 Effect of the thickness of flat insulation on 15.2 cm long copper fin.

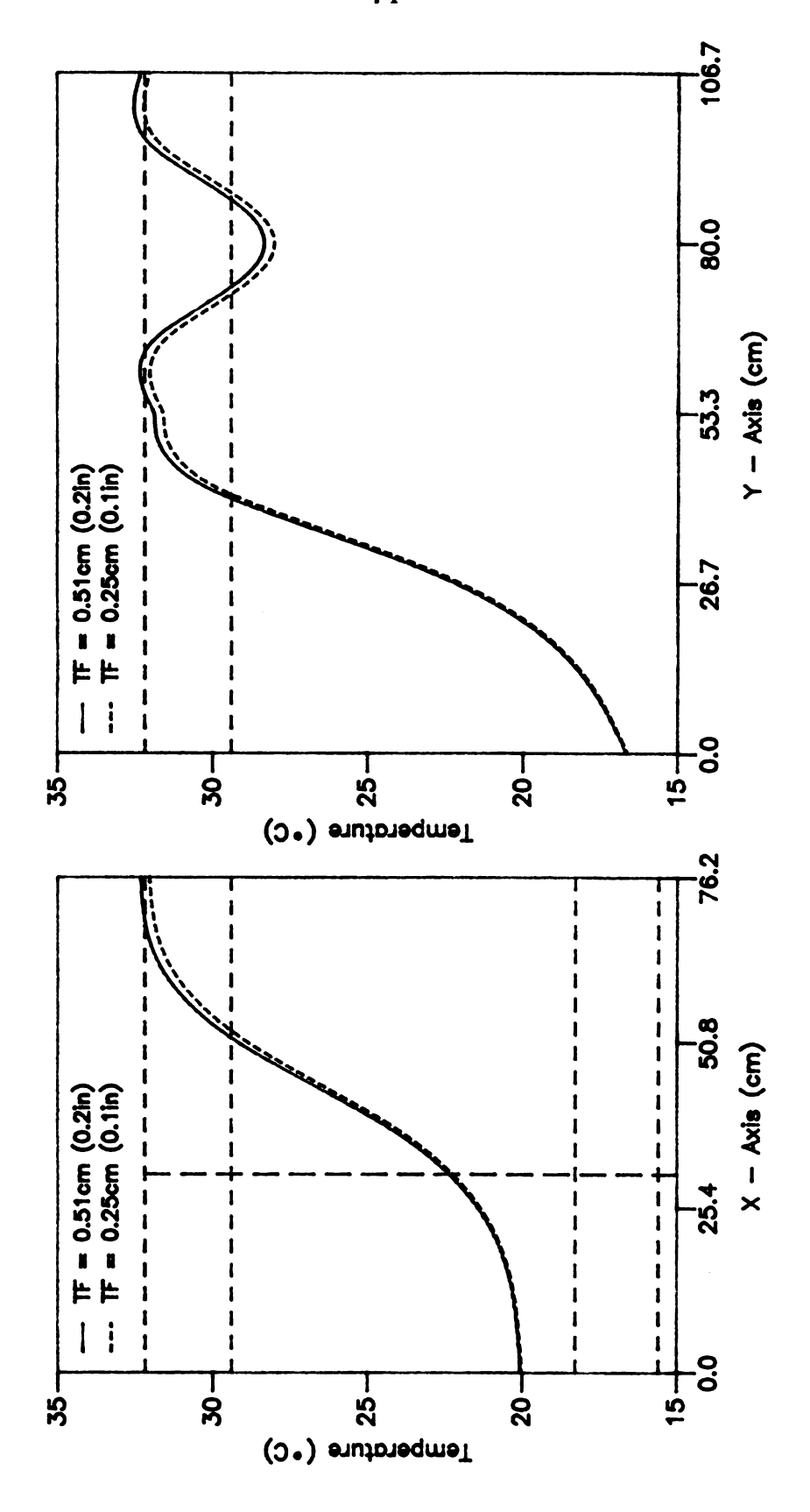


Figure 5.21 Effect of the thickness of copper fin.

in Figure 5.21. The 0.25 cm thickness fin is the most desirable from the economical viewpoint.

5.3.3 Width of flat insulation

The influence of the width of the flat insulation over the finned pipe was analyzed for the 22.9 cm (9 inches) long copper fin as shown in Figure 5.22. The widths of insulation were 15.2 cm (6 inches), 22.9 cm (9 inches), and 30.5 cm (12 inches) under the condition of 22.9 cm long fin and 1.3 cm thick insulation. The temperature distribution was influenced significantly by the width of the insulation. The same width of insulation and the length of fin, the 22.9 cm wide insulation and 22.9 cm long fin, showed the best temperature distribution in Figure 5.22.

5.3.4 Recommended model

Figure 5.23 shows the desirable farrowing unit heated using three hot water pipes with the copper fins attached. The 22.9 cm (9 inches) long fin was attached to the center pipe since 15.2 cm (6 inches) long fin to the side two pipes to widen a comfortable temperature zone in the baby pig area. The thickness of flat insulation in the sow area was 1.3 cm (0.5 inches) while the thickness in the litter area was 0.64 cm (0.25 inches). The width of insulation and the length of fin was set using the result determined in Figure 5.22. The model gave a good temperature distribution as shown in Figures 5.24, 5.25, and 5.26. The tempera-

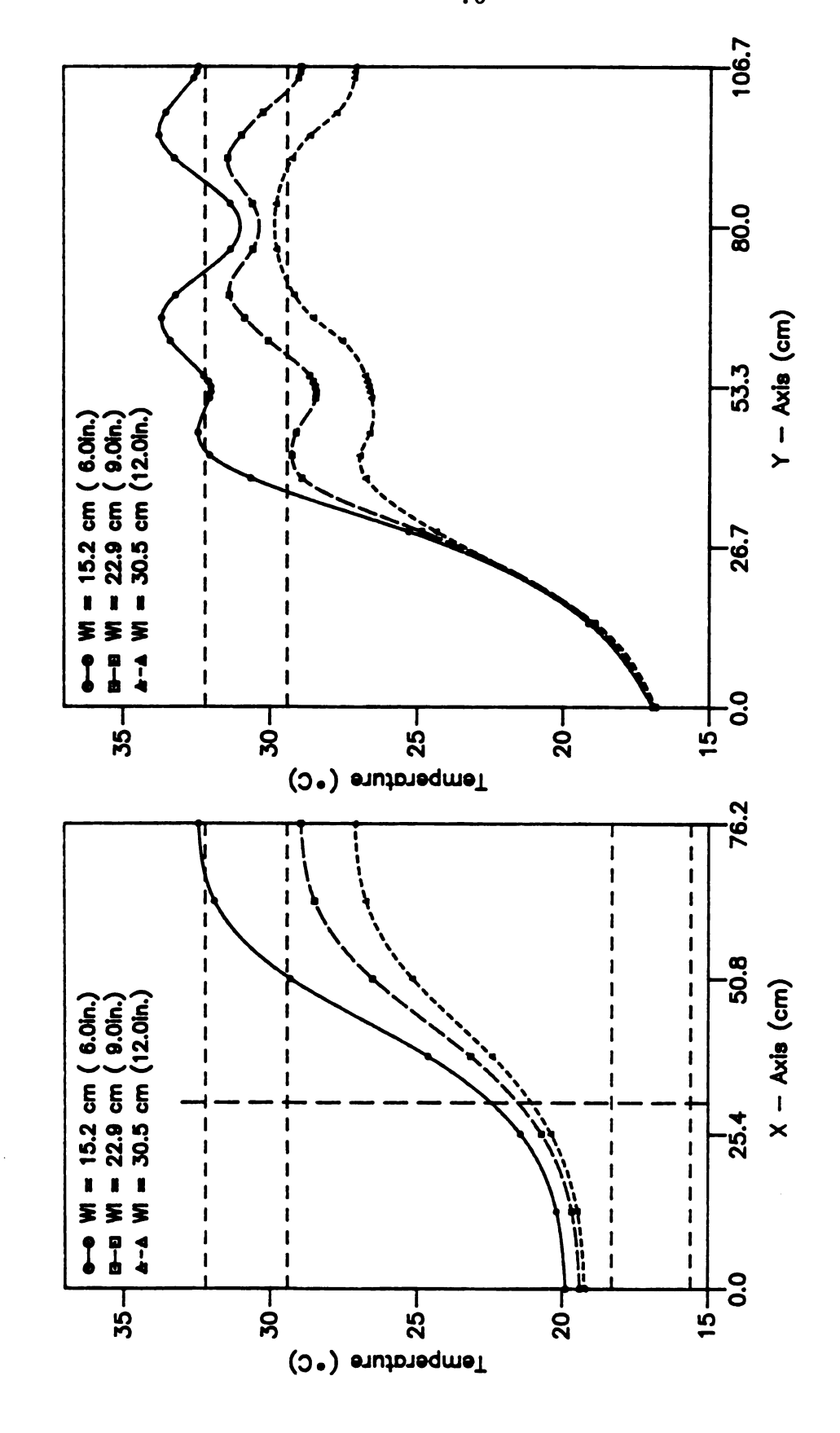


Figure 5.22 Effect of the width of flat insulation on 22.9 cm long copper fin.

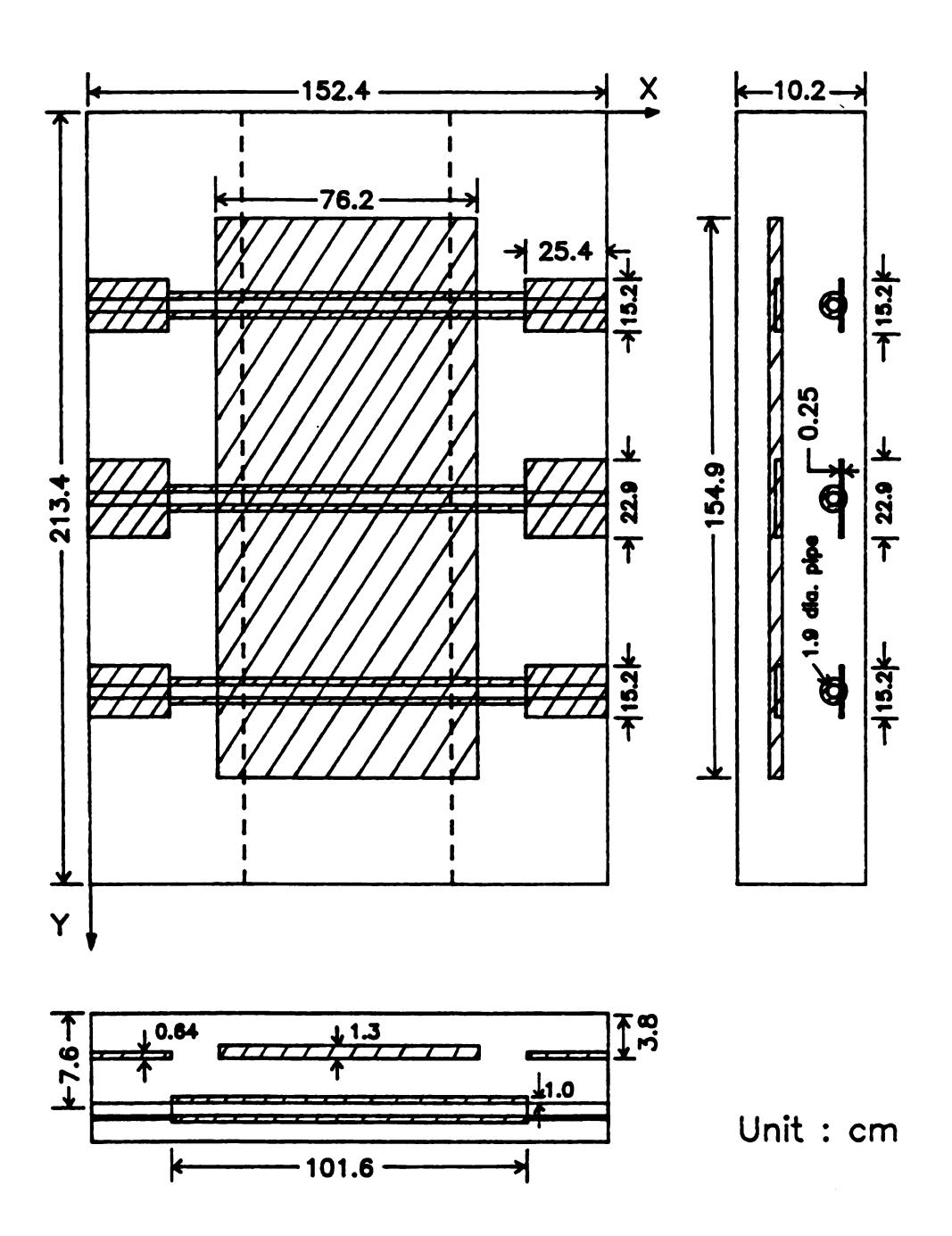


Figure 5.23 Recommended model for three pipes with copper fin.

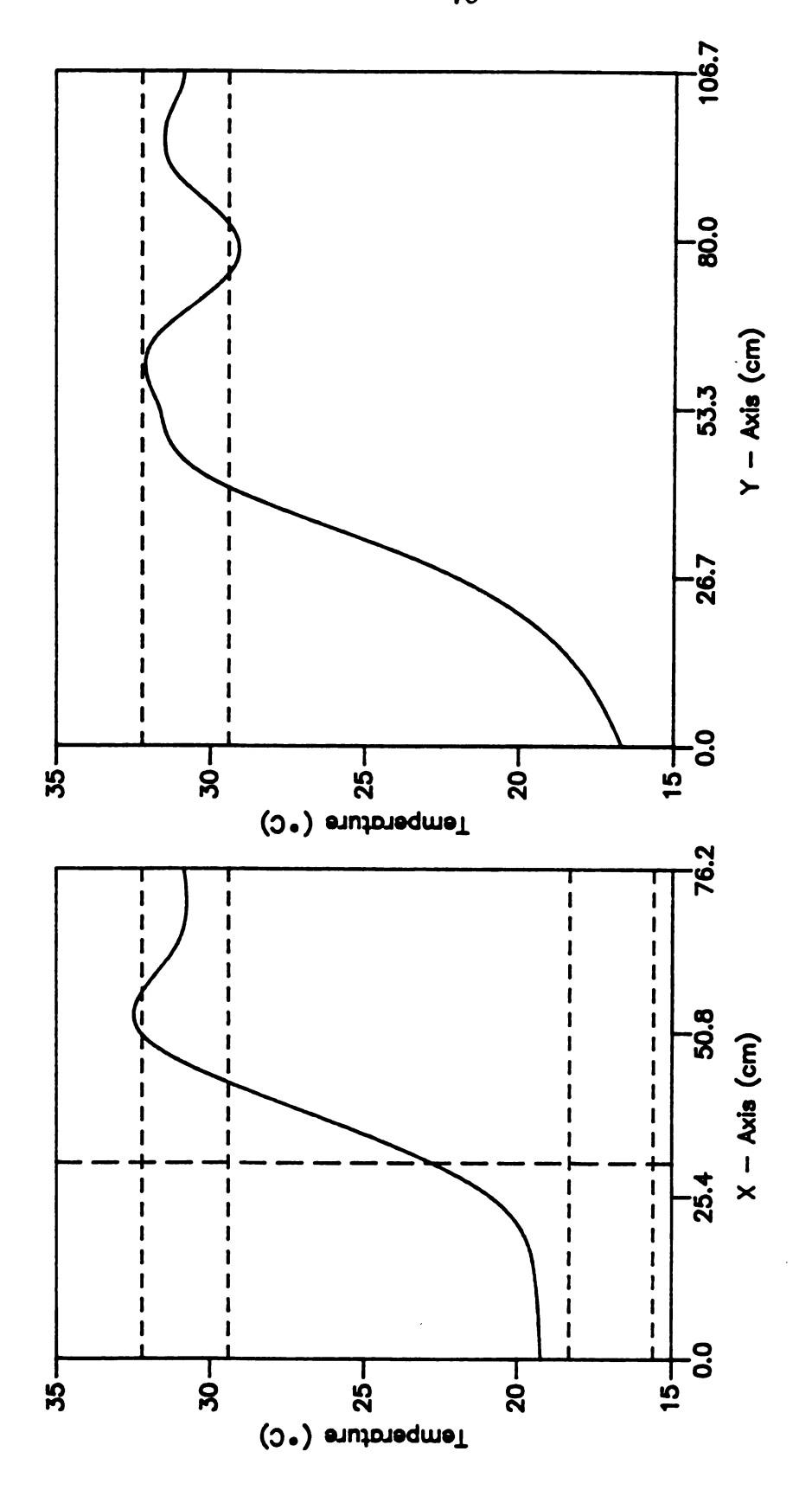


Figure 5.24 Temperature distribution on the floor of recommended model for three pipes with copper fins.

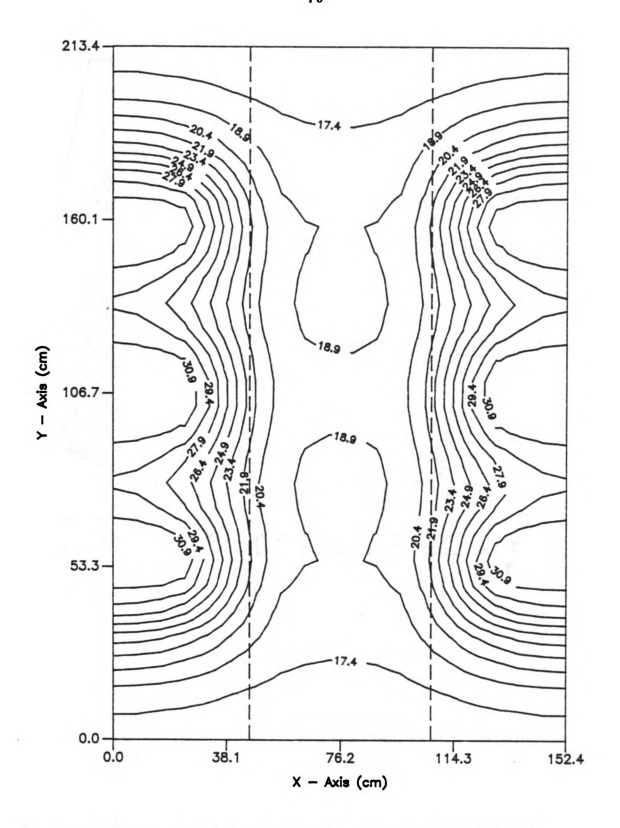


Figure 5.25 Temperature contour on the floor of the recommended model for three pipes with copper fins.

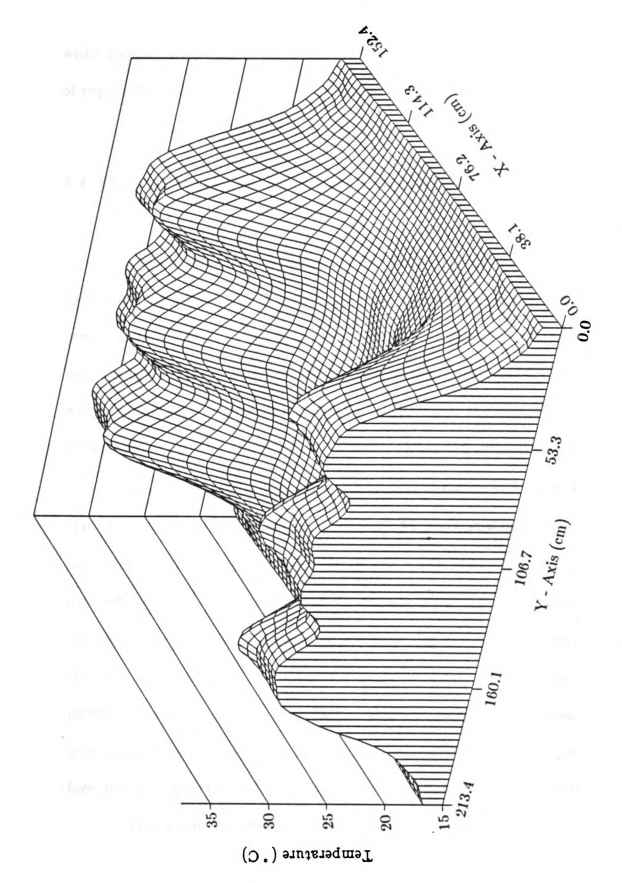


Figure 5.26 Three-dimensional temperature distribution of recommended model for three pipes with copper fins.

ture distribution in the sow area was very similar to the case of steel fins, but a wider comfort temperature zones for the litter was obtained even though the size of copper fins was smaller than the steel fins.

5.4 Effect of Room and Hot Water Temperature

The temperature distribution on the floor of a farrowing house is affected by the temperature of the hot water running through the pipes and by the room temperature. Generally, the floor temperature is controlled with the water temperature. Van Fossen and Overhults (1980) recommended 60°C (140°F) as the water temperature and not more than 5.6°C (10°F) as the temperature difference between the supply line and the return line to obtain a high thermal efficiency.

Heat loss for four different water temperatures, 62.8 °C (145 °F), 60.0 °C (140 °F), 57.2 °C (135 °F), and 54.4 °C (130 °F), were analyzed using the model consisting of three pipes and a steel fin (Figure 5.14). The water temperature had little effect on the floor temperature in the sow area, but did significantly affect the temperature in the litter area as shown in Figure 5.27. The temperature in the litter area was raised by 2.0 °C (3.6 °F) in the litter area when the water temperature rose 5.6 °C (10 °F). The highest temperature in the litter area was somewhat lower than the desirable temperature when the water was at 54.4 °C. Therefore, the crate near the end of the pipe system could be cool for the baby pigs.

The room temperature significantly influenced the floor temperature through the whole area as shown in Figure 5.28. The lowest temperature in the

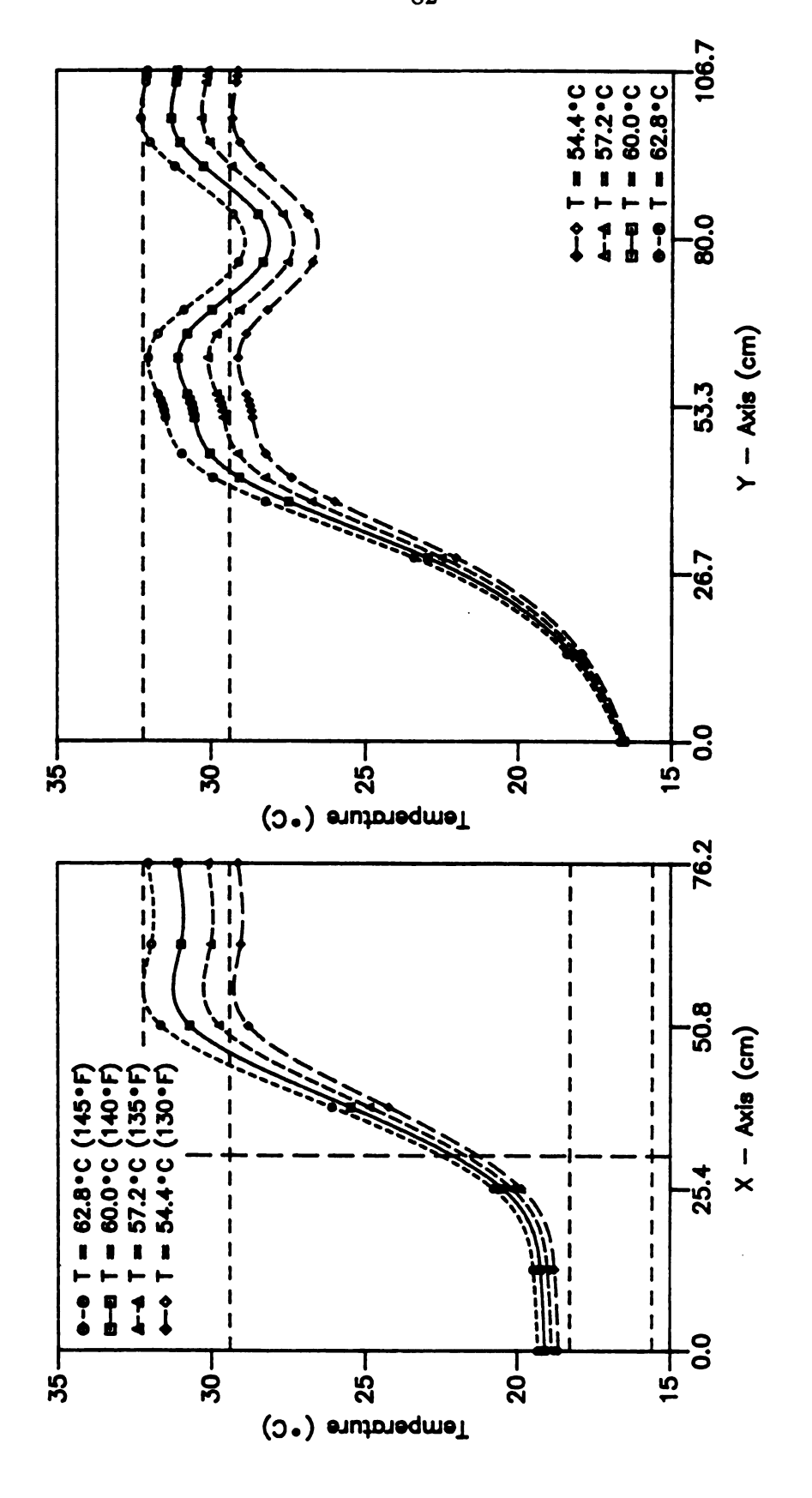


Figure 5.27 Effect of the hot water temperature at the room temperature 15.6°C.

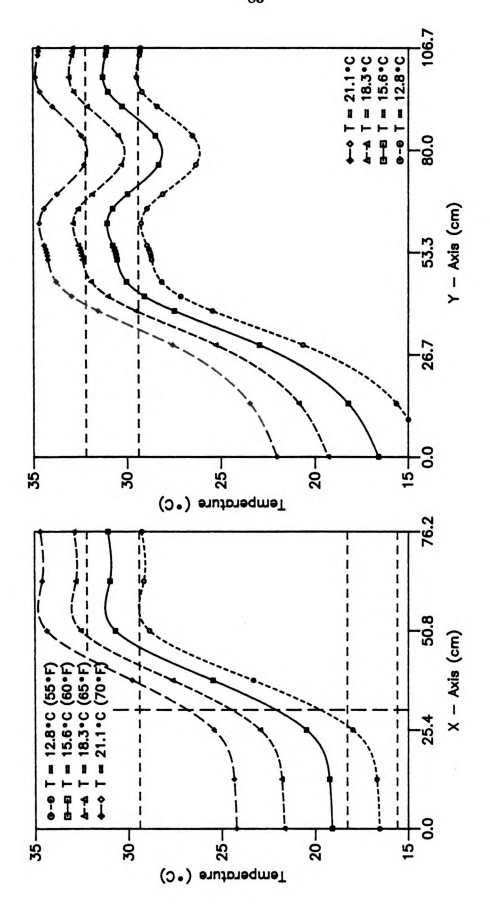


Figure 5.28 Effect of the room temperature at the water temperature 60 ° C.

sow area was 1.9°C to 3.4°C (3.4°F to 6.1°F) higher than the steady state room temperature. Raising the room temperature by 2.8°C (5°F) increased the temperature in the sow area by 2.5°C (4.5°F) which is around same as the room temperature change while the temperature in the litter area by 1.8°C (3.2°F). Spillman and Murphy (1976) surveyed most of the farrowing house operated with the room temperature from 16°C to 24°C (60°F to 75°F). Farrowing house with solid floor, typically concrete, tends to operate at somewhat lower temperature. Figure 5.28 shows the same result. A solid floor with hot pipe heating system could be operated at a lower room temperature.

Figure 5.29 gives the temperature distribution on the floor when the room temperature was 13.9 °C (57 °F) and the water temperature 62.8 °C (145 °F). A desirable temperature distribution is obtained throughout in both the sow and the litter area.

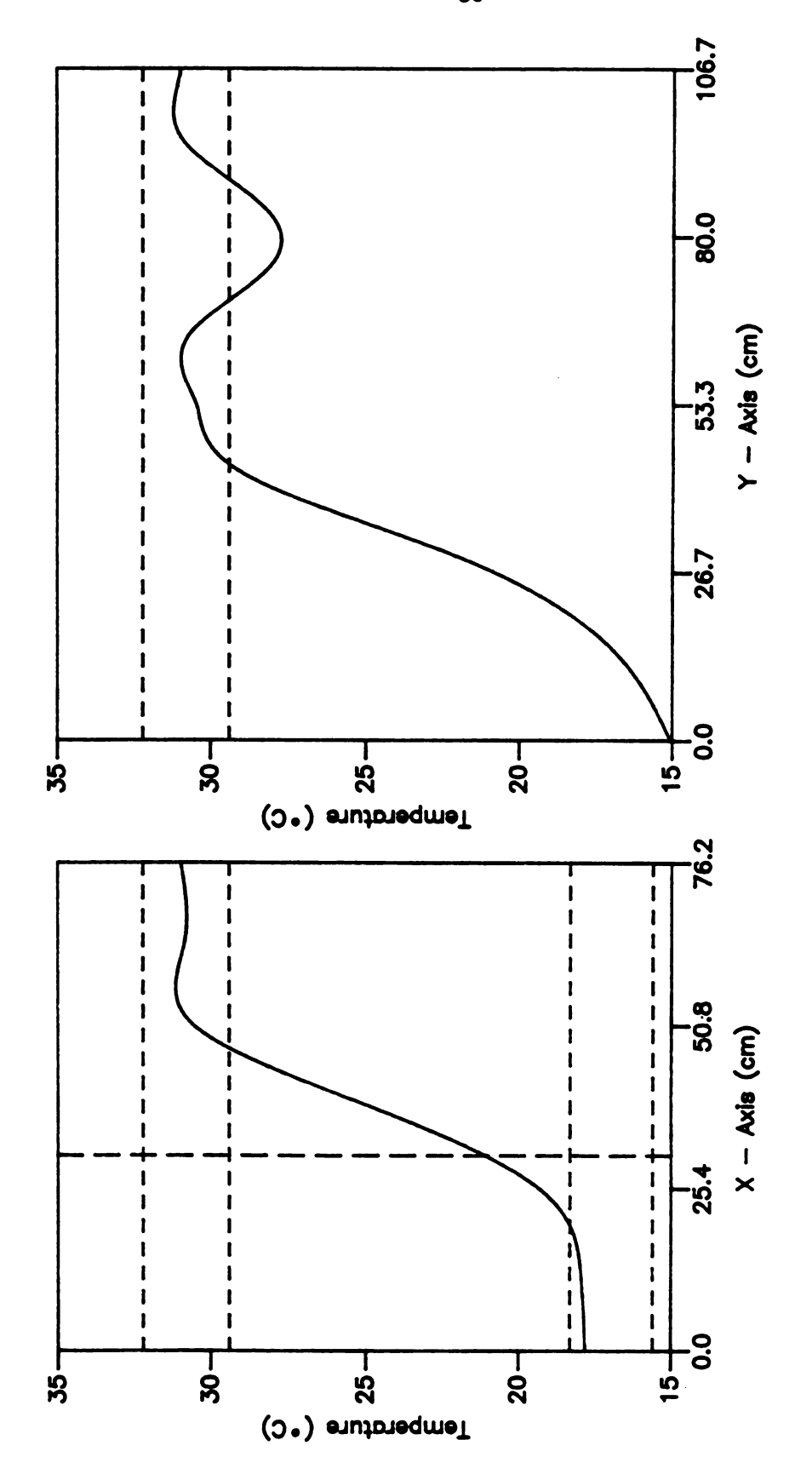


Figure 5.29 Temperature distribution in condition of 13.9 °C (57 °F) room temperature and 62.8 °C (145 °F) water temperature.

VI. DISCUSSION AND SUMMARY

The floor temperature values for three new layouts of hot water floor heating pipes were calculated. The three layouts consisted of (1) pipes only, (2) pipes with steel fins, and (3) pipes with copper fins. The temperature distributions on the floor for the three different layouts were similar. Each had six separate hot areas for the baby pigs per stall and a relatively uniform temperature distribution in the sow area. The six separate hot spaces in the litter area should encourage baby pigs to scatter, preventing piling up and crushing. Moreover, since the high temperature zones in the litter area were well out of the sow area, baby pigs might stay out of the sow area where there is the risk of being crushed by sow. These new models could reduce the baby pig loss because Liptrap et al. (1987) reported that one of the main causes of baby pig mortality was crushing and injury.

The lower temperature zones between the pipes in the baby pig area would be used by the baby pigs that prefer a lower temperature environment because individual baby pigs vary in their preferred temperature. Several groups of litters with substantially different heat requirements owing to their age or weight are in a farrowing room at the same time. Each crate in the typical farrowing house, however, has the same temperature environment since it has the same type of pipe circuit. Therefore, it is impossible to satisfy the needs each

litter in the typical farrowing house at the same time.

Controlling the fin size and insulation could solve the decrease in water temperature problem in the typical farrowing house. Van Fossen and Overhults (1980) recommended that the water temperature should not drop more than 5.6°C (10°F) from the supply line to the return line. Such a difference of water temperature between the supply pipe and the return pipe makes the temperature on the litter area near the return pipe to decrease by 2°C (3.6°F) compared with the area near the supply pipe as shown in Figure 5.27. If a larger fin and/or less insulation is used for the crate near the end of return line, the temperature drop in the litter area would be decreased and the temperature drop from inlet to outlet could be tolerated.

The new models have simple heating pipe circuits that reduce the pumping resistance by 36 % compared with the complicate heating pipe circuit of the typical layout shown in Figure 1.1. The comparison is given in Appendix C. The head loss due to the pipe fittings was significantly diminished in the new model. Therefore, that simple circuit would reduce the operation cost.

The room temperature in the new model can be somewhat lowered than that in the current model while still keeping a desirable temperature in the sow area as shown in Figure 5.29.

Some advantages of the new models are:

1. Preventing baby pigs from piling up on each other and being crushed by the sow owing to the desirable temperature distribution.

- 2. Baby pigs can select their comfortable temperature area because various temperature zones exist within the litter area.
- 3. Heating the only necessary area for baby pigs, not all of the baby pig area, can save the energy consumption.
- 4. New model could remove the effect to the floor temperature change by the water temperature difference between the supply line and return line.
- 5. Energy consumption and operation cost could be decreased by the lower room temperature and simple heating pipe circuit.

VII. CONCLUSIONS

The typical hot water floor heating system for a solid floor or partially slotted floor in the farrowing house has some problems in the pipe circuit and its thermal efficiency. To solve those problems, the new heating pipe circuit was introduced. To find the best model for the sow and her litter, the temperature distributions on the floors of various models were analyzed using the three-dimensional finite element method.

The basic information about the heating ability of hot water pipes with flat and perimeter insulations and steel and copper fins attached to the pipes were obtained. This information was used to decide the numbers of pipes, the insulation size and placement and the fin size in order to obtain a desirable temperature distribution on the floor. Even though several models that have new pipe circuits were analyzed for the case of solid-floor farrowing system, the basic information could be helpful in the design of the new hot water pipe circuits for partially slotted floor farrowing system, and a partially slotted floor swine finishing pen.

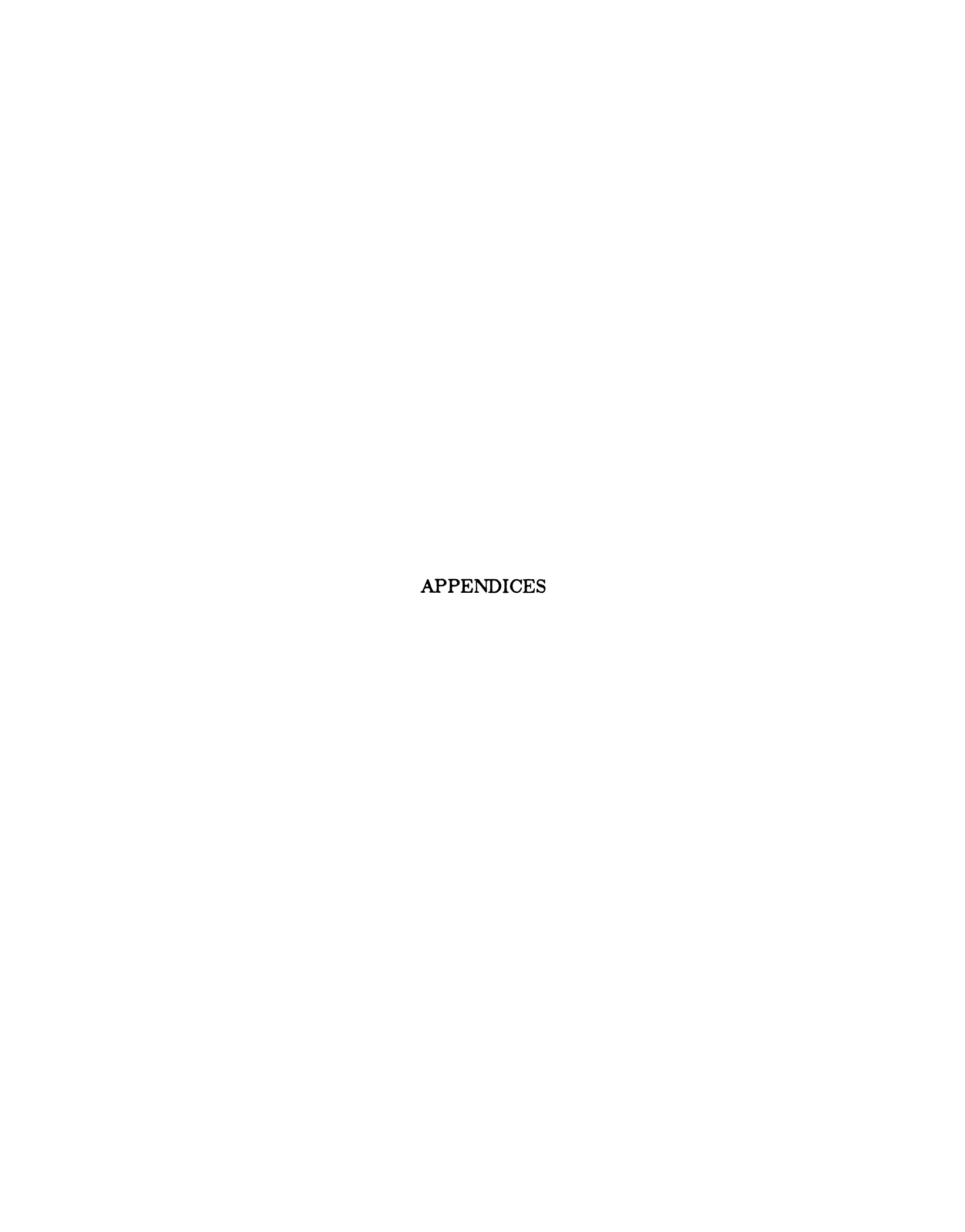
Three different cases, using only hot water pipes and using pipes with a steel fin or a copper fin attached were analyzed to determine the best model for each case. The three pipes across the crate were reasonable number of pipes and the fins attached to the pipes were necessary to widen the high temperature zone in the litter area. The perimeter insulation around the pipe running across the

sow area was essential. Three recommended models of each case showed adequate temperature distributions for the litter and the sow. The new models make it possible to build crates having different local floor temperature in the same farrowing house. Energy consumption and operation cost can be reduced in the new pipe circuit. There will be some difficulties to attach fins to pipes and lay insulation over the pipes. The proposed models can be modified for manufacture if they are hard to construct as is.

Future studies are suggested as follows:

- 1. All data showed in this study were derived from the simulated models.

 Measuring the actual temperature on the floor after constructing the recommended model is needed for validation of the simulation.
- 2. In the model, I was assumed there was no bedding on the floor and did not include heat produced by the sow. Further study is necessary to analyze the temperature distribution while including the effects of the sow.
- 3. The floor will be weakened compared with the typical floor when the wide flat insulation is laid over the pipes. A stress analysis for the floor should be performed to determine its durability and strength.



APPENDIX A

GRID GENERATION PROGRAM

APPENDIX A

PROGRAM GRID_3D C C**** This program generates the node numbers and element numbers in 3-D model and reoders the node numbers for minimizing the bandwidth \mathbf{C} C \mathbf{C} **VARIABLES** C ____ C C INBP : The number of boundary points Č **INGR** : The number of regions C NBP : Boundary points C NGR : Region number Č : Band width **NBW** Č : The shape function N C XC,YC,ZC : x, y and z coordinates of the region nodes č XP,YP,ZP : x, y and z coordinates of the boundary points Č JT : The region connectivity data CCC**NDN** : Node numbers consisting of one region NN : The region node number **NNRB** : The node numbers on the boundary of the region Č XE,YE,ZE : x, y and z coordinates of the elements : Node numbers of elements NE C C C Followings are modified for each different model C C č Č XP,YP,ZP: (NBP) ;(150) Č : (NRG,6); (60,6)JT NN,XC,TC,ZC: (ZETA MAX, ETA MAX, KSAI MAX); (10,10,10) Č : (NRG, 6, ZETA & ETA MAX, KSAI & ÉTA MÁX);(60,6,10,10) **NNRB** C XE,YE,ZE,NE: (KSAIMAX * ETAMAX * ZETAMAX) ;(500) C AXI : (3000,3) NAXI : (3000) CCC IELEOLD : (2000.8)**IELENEW** : (2000,8)

```
DIMENSION XP(150), YP(150), ZP(150), XRG(9), YRG(9), ZRG(9)
     DIMENSION N(8),NDN(8),NN(10,10,10)
     DIMENSION XC(10,10,10),YC(10,10,10),ZC(10,10,10),NNRB(60,6,10,10)
     DIMENSION XE(500), YE(500), ZE(500), NR(8), NE(500), JT(60,6)
      DIMENSION AXI(3000,3), NAXI(3000), IELEOLD(2000,8), IELENEW(2000,8)
      REAL N.KSAI
     DATA IN/5/,IO/6/,NBW/0/,NB/0/,NEL/0/,NODE/1/
\mathbf{C}
   Input of the global coordinate and connectivity data
      OPEN(UNIT=IN,FILE='GRIDIN.DAT',STATUS='OLD')
      OPEN(UNIT=IO,FILE='GRIDIO.DAT',STATUS='NEW')
      READ (IN,*) INRG,INBP
      DO 100 I=1,INBP
 100 READ(IN,*) NBP,XP(I),YP(I),ZP(I)
      DO 2 I=1,INRG
      READ(IN,*) NRG,(JT(NRG,J),J=1,6)
\mathbf{C}
C*** Loop of generating elements
C*
\mathbf{C}
      DO 16 KK=1,INRG
      READ(IN,*) NRG,NKSAI,NETA,NZETA,(NDN(I),I=1,8)
\mathbf{C}
   Generation of the region nodal coordinates
      DO 5 I = 1.8
         II = NDN(I)
         XRG(I) = XP(II)
         YRG(I)=YP(II)
         ZRG(I) = ZP(II)
      CONTINUE
      XRG(9)=XRG(1)
      YRG(9) = YRG(1)
      ZRG(9)=ZRG(1)
C
      TR=NKSAI-1
      DX=2./TR
      TR=NETA-1
      DY=2./TR
      TR=NZETA-1
      DZ=2./TR
\mathbf{C}
      DO 12 I=1,NZETA
         TR = I-1
         ZETA=1-TR*DZ
        DO 12 J=1.NETA
            TR = J-1
            ETA = -1 + TR*DY
          DO 12 K=1,NKSAI
              TR = K-1
              KSAI = -1 + TR*DX
```

```
C
          N(1)=0.125*(1.-KSAI)*(1.-ETA)*(1.-ZETA)
          N(2)=0.125*(1.+KSAÍ)*(1.-ETÁ)*(1.-ZETÁ)
N(3)=0.125*(1.+KSAI)*(1.+ETA)*(1.-ZETA)
          N(4)=0.125*(1.-KSAI)*(1.+ETA)*(1.-ZETA)
N(5)=0.125*(1.-KSAI)*(1.-ETA)*(1.+ZETA)
N(6)=0.125*(1.+KSAI)*(1.-ETA)*(1.+ZETA)
          N(7)=0.125*(1.+KSAI)*(1.+ETA)*(1.+ZETA)
          N(8)=0.125*(1.-KSAI)*(1.+ETA)*(1.+ZETA)
\mathbf{C}
          XC(I,J,K)=0.0
          YC(I,J,K)=0.0
          ZC(I,J,K)=0.0
       DO 12 L=1.8
          XC(I,J,K)=XC(I,J,K)+XRG(L)*N(L)
          YC(I,J,K)=YC(I,J,K)+YRG(L)*N(L)
          ZC(I,J,K)=ZC(I,J,K)+ZRG(L)*N(L)
      CONTINUE
  12
   Generation of the region node numbers
      KX1=1
      KY1=1
      KZ1=1
      KX2=NKSAI
      KY2=NETA
      KZ2=NZETA
\mathbf{C}
      DO 51 I=1.6
       NRT = JT(NRG,I)
        IF(NRT.EQ. 0 .OR. NRT.GT. NRG) GO TO 51
       DO 56 J=1.6
      IF(JT(NRT,J).EQ.NRG) NRTS=J
  56
        IF(I.EQ.1 .OR. I.EQ.6) THEN
             L=NETA
             M=NKSAI
          ELSE IF(I.EQ.2 .OR. I.EQ.4) THEN
                L=NZETA
                M=NETA
             ELSE IF(I.EQ.3 .OR. I.EQ.5) THEN
                  L=NZETA
                  M=NKSAI
       END IF
\mathbf{C}
       DO 60 KL=1,L
       DO 60 KM=1,M
       GO TO (45,46,47,48,49,50),I
       NN(NZETA,KL,KM)=NNRB(NRT,NRTS,KL,KM)
  45
          KZ2=NZETA-1
          GO TO 60
       NN(KL,KM,1)=NNRB(NRT,NRTS,KL,KM)
   46
          KX1=2
          GO TO 60
```

```
NN(KL,1,KM) = NNRB(NRT,NRTS,KL,KM)
 47
       KY1=2
       GO TO 60
 48
     NN(KL,KM,NKSAI)=NNRB(NRT,NRTS,KL,KM)
       KX2=NKSAI-1
       GO TO 60
     NN(KL, NETA, KM) = NNRB(NRT, NRTS, KL, KM)
 49
       KY2=NETA-1
        GO TO 60
     NN(1,KL,KM) = NNRB(NRT,NRTS,KL,KM)
        KZ1=2
     CONTINUE
 60
     CONTINUE
 51
C
     IF(KX1.GT.KX2) GO TO 105
     IF(KY1.GT.KY2) GO TO 105
     IF(KZ1.GT.KZ2) GO TO 105
C
     DO 10 I=KZ1,KZ2
        DO 10 J=KY1,KY2
          DO 10 K=KX1,KX2
             NB = NB + 1
             NN(I,J,K)=NB
     CONTINUE
 10
  Storage of the boundary node numbers
 105 DO 42 I=1,NETA
        DO 42 J=1,NKSAI
           NNRB(NRG,1,I,J)=NN(NZETA,I,J)
           NNRB(NRG,6,I,J)=NN(1,I,J)
  42
     CONTINUE
     DO 43 I=1, NZETA
        DO 43 J=1, NETA
           NNRB(NRG,2,I,J)=NN(I,J,1)
           NNRB(NRG,4,I,J)=NN(I,J,NKSAI)
     CONTINUE
     DO 44 I=1, NZETA
        DO 44 J=1,NKSAI
           NNRB(NRG,3,I,J)=NN(I,1,J)
           NNRB(NRG,5,I,J)=NN(I,NETA,J)
     CONTINUE
C
  Output of the region node numbers & x, y, z to AXI(NODE,3)
     DO 63 I=1,NZETA
       DO 63 J=1, NETA
        DO 63 K=1,NKSAI
           IF(NN(I,J,K).LT.NODE) GO TO 63
           AXI(NODE,1)=XC(I,J,K)
           AXI(NODE,2)=YC(I,J,K)
           AXI(NODE,3)=ZC(I,J,K)
           NAXI(NODE)=NODE
           NODE=NODE+1
```

```
63
     CONTINUE
C Saving the elements and node numbers into ELEOLD(NEL,8)
     DO 64 I=1,NZETA
      DO 64 J=1,NETA
        DO 64 K=1,NKSAI
           XE(L)=XC(I,J,K)
           YE(L)=YC(I,J,K)
           ZE(L)=ZC(l,J,K)
           NE(L)=NN(I,J,K)
           L=L+1
     CONTINUE
  64
     DO 15 I=1,(NZETA-1)
       DO 15 J=2, NETA
        DO 15 K=2.NKSAI
           NR(1)=NKSAI*NETA*I+NKSAI*(J-2)+(K-1)
           NR(2)=NKSAI*NETA*I+NKSAI*(J-2)+K
           NR(3)=NKSAI*NETA*I+NKSAI*(J-1)+K
           NR(4) = NKSAI*NETA*I + NKSAI*(J-1) + (K-1)
           NR(5)=NKSAI*NETA*(I-1)+NKSAI*(J-2)+(K-1)
           NR(6) = NKSAI*NETA*(I-1) + NKSAI*(J-2) + K
           NR(7) = NKSAI*NETA*(I-1) + NKSAI*(J-1) + K
           NR(8)=NKSAI*NETA*(I-1)+NKSAI*(J-1)+(K-1)
           NEL=NEL+1
        DO 66 M=1,8
  66
          IELEOLD(NEL,M)=NE(NR(M))
      CONTINUE
  15
C Output of last number of elements in each region
      WRITE(IO,300) NRG,NEL
     FORMAT(3X,'LAST NO. OF ELEMENTS IN ',I3,' REGION IS',I5)
      CONTINUE
  16
\mathbf{C}
C
C
C*** Reodering the node numbers for minimizing the band width
C*************************
C
Č
       Y:MAX->MIN
         Z:MAX->MIN
Č
            X:MIN->MAX
      NODE—NODE-1
      LAST=NODE-1
      DO 200 J=1,LAST
  Finding MIN X, MAX Y and MAX Z
\mathbf{C}
      L=J
```

```
JFIRST=J+1
     DO 210 I=JFIRST, NODE
     IF((AXI(L,2)-AXI(I,2)).GT.0.0001) THEN
        GO TO 210
      ELSE IF((AXI(L,2)-AXI(I,2)).LT.-0.0001) THEN
       ELSE IF((AXI(L,3)-AXI(I,3)).GT.0.0001) THEN
            GO TO 210
         ELSE IF((AXI(L,3)-AXI(I,3)).LT.-0.0001) THEN
           ELSE IF((AXI(L,1)-AXI(I,1)).LT.0.0001) THEN
              GO TO 210
            ELSE
              L=I
     END IF
210 CONTINUE
     DO 220 M=1,3
        TEMP = AXI(L,M)
        AXI(L,M)=AXI(J,M)
        AXI(J,M)=TEMP
220 CONTINUE
      NTEMP = NAXI(L)
      NAXI(L)=NAXI(J)
      NAXI(J)=NTEMP
 200 CONTINUE
C Exchanging the node numbers
     DO 230 I=1,NEL
      DO 230 J=1,8
        IELENEW(I,J)=0
 230 CONTINUE
C CHANGE THE NODE NUMBER
     DO 240 I=1,NODE
           M=NAXI(I)
      DO 250 J=1,NEL
        DO 250 K=1,8
           IF( IELEOLD(J,K) .NE. M) GO TO 250
           IELENEW(J,K)=I
 250 CONTINUE
 240 CONTINUE
C***
     Calculating the band width
C*****
C
     DO 280 I=1.NEL
      DO 280 L=1.7
        DO 280 M=L+1,8
           LB = LABS(IELENEW(I,L)-IELENEW(I,M))+1
           IF(LB.LE.NBW) GO TO 280
```

```
NBW=LB
             NELBW=I
 280 CONTINUE
\mathbf{C}
       Output of x,y,z coordinates of nodes and node numbers
C*****
\mathbf{C}
      DO 260 I=1,NODE
        WRITE(IO,261) I,(AXI(I,J),J=1,3)
        FORMAT(4X,I4,5X,3F10.5)
 261
 260 CONTINUE
\mathbf{C}
      DO 270 I=1,NEL
        WRITE(IO,271) I,(IELENEW(I,J),J=1,8)
       FORMAT(1X,915)
 271
 270 CONTINUE
  WRITE(IO,71) NBW,NELBW
71 FORMAT(///,1X,23H BAND WIDTH QUANTITY IS,14,
1 'CALCULATED IN ELEMENT',14)
      CLOSE(UNIT=IN,STATUS='SAVE')
      CLOSE(UNIT=IO,STATUS='SAVE')
       STOP
      END
```

APPENDIX B

FINITE ELEMENT HEAT TRANSFER PROGRAM

APPENDIX B

```
PROGRAM HEAT_3D
\mathbf{C}
C*
C***
          This program determines the temperature distribution
C***
         on the floor of farrowing house by F. E. M. Input data
          for this program comes from grid_generating program.
C
C
C
    VARIABLES
C
C
C
       NP
                     : Total number of nodes
C
                     : Total number of elements
       NE
C
       NBW
                     : Band width
C
       XE,YE,ZE
                     : Coordinates of elements
C
                     : Coordinates of global elements
       XG,YG,ZG
č
       PX,PY,PZ
X, Y, Z
                     : Partial derivatives of shape function
00000000
                            : Another expressions of Ksai, Eta and Zeta
       NS
                     : Element node numbers
                            : Element stiffness matrix
       ESM
       EF
                     : Element force vector
       Α
                     : Column vector containg {T}, {F} and [K]
       В
                     : Derivatives of the shape functions
                            : Last pointer indicating the last storage for {T}
       JGF
       JGSM
CCC
       JEND
                     : Thermal conductivity of concrete
       K1
       K2
                     : Thermal conductivity of insulation
C
       Η
                     : Convection coefficient
\mathbf{C}
                            : Thermal conductivity
       TCON
\mathbf{C}
        TINF
                            : Ambient temperature
Č
        TEMP
                            : Initial steady state temperature
\mathbf{C}
C
C
    SUBROUTINES
C
C
C
                      : Assigning the thermal conductivity to the each element
       BNDRYK
                     : Determination of the calculating points in 2-D
C
       NAT2D
\mathbf{C}
       NAT3D
                                                      in 3-D
                     : Calculation of the derivative matrix of shape function ([B])
\mathbf{C}
       DERSHP
```

```
C
      ASMBL
                   : Direct stiffness procedure
Č
      SHAPE
                   : Calculation of partial derivatives of shape function
C
      MODIFY
                   : Input of the prescribed nodal values
                   : Decomposition of the grobal stiffness matrix
      DCMPBD
Č
                   : Soving the system of equations by backward substitution
      SLVBD
č
Ċ
   Followings are modified for each different model
\mathbf{C}
Č
C
      1. XG,YG,ZG
                         : (NP)
                   : (JEND = NP + NP + BDW*NP)
      2. A
3. NS
CCC
      3. NS
                  : (NE)
      4. SUBROUTINE BNDRYK & MODIFY
      5. OPEN FILE
Č
      6. CONVECTIVE SURFACE BOUNDARY CONDITION
         *******************
      IMPLICIT REAL (A-H,O-Z)
      DIMENSION XG(1470), YG(1470), ZG(1470)
        COMMON /XYZ/ XE(8),YE(8),ZE(8)
COMMON /NATU/KSAI(8),ETA(8),ZETA(8),WC
COMMON /AV/ A(119070),JGF,JGSM,NP,NBW
        COMMON /ELEM/ESM(8,8),EF(8),NS(1068,8)
      COMMON /SHA/ X,Y,Z,N(8),PX(8),PY(8),PZ(8),B(3,8)
REAL N,KSAI,K1,K2,K3
        OPEN(UNIT=IN,FILE='HEATIN.DAT',STATUS='OLD')
      OPEN(UNIT=IO,FILE='HEATIO.DAT',STATUS='NEW')
DATA IN/5/,IO/6/
      DATA K1/0.0868055/,K2/0.0013888/,H/0.013889/,TINF/60./,TEMP/140./
      DATA K3/1.80544/
        READ(IN,*) NP,NE,NBW
        WRITE(IO,*) NP,NE,NBW,K1,K2,K3,H,TINF,TEMP
\mathbf{C}
   Calculation of pointers and initialization of the column vector [A]
C
       JGF = NP
       JGSM = JGF + NP
       JEND=JGSM+NP*NBW
       DO 10 I=1,JEND
  10
        A(I) = 0.0
  Input of the node and element data (X,Y,Z & Node numbers)
       DO 11 I=1,NP
        READ(IN,*)II,XG(I),YG(I),ZG(I)
  11
       DO 12 I=1,NE
        READ(IN,*) II,(NS(I,J),J=1,8)
   12
 C*** Generation of system of equations
 C
```

```
DO 30 KK=1,NE
\mathbf{C}
C Initialization of the element stiffness matrix and element force vector
     DO 13 I=1.8
           EF(I)=0.0
       DO 13 J=1.8
            ESM(I,J)=0.0
     CONTINUE
  13
  Retrieval of element nodal coordinates and node numbers
      DO 14 I=1,8
            J = NS(KK,I)
            XE(I)=XG(J)
            YE(I)=YG(J)
            ZE(I)=ZG(J)
      CONTINUÉ
  14
  Check whether element has boundary convective surface or not
      ICON=0
      DO 15 I=1.8
            IF(ABS(ZE(I)-4.0) .GT. 0.00001) GO TO 15
            ICON=1
      CONTINUE
      CALL BNDRYK(KK,K1,K2,K3,TCON)
  Calculation of [B]T[D][B]
      WC=1.0
      CALL NAT3D
      DO 17 K=1.8
            X = KSAI(K)
            Y = ETA(K)
              =ZETA(K)
            CALL DERSHP(DET,ICON)
       DO 16 I=1.8
        DO 16 J=1.8
          DO 16 L=1,3
            ESM(I,J) = ESM(I,J) + TCON*DET*WC*B(L,I)*B(L,J)
      CONTINUE
      CONTINUE
  17
   Check of the boundary condition
      IF(ICON .NE. 1) GO TO 25
      CALL NAT2D
      DO 20 K=1.4
            X = KSAI(K)
            Y = ETA(K)
            Z = 1.0
            CALL DERSHP(DET,ICON)
        DO 19 I=1.8
```

```
DO 18 J=1.8
           ESM(I,J)=ESM(I,J)+H*WC*DET*N(I)*N(J)
 18
       EF(I)=EF(I)+H*WC*DET*TINF*N(I)
 19
 20 CONTÍNUE
 25
     CALL ASMBL(KK)
 30
    CONTINUE
C
C**********************************
C*** End of the loop of generating the system of equations
\mathbf{C}
     CALL MODIFY(TEMP)
     CALL DCMPBD
     CALL SLVBD
C Output of surface temperature
      WRITE(IO.40)
 40 FORMAT(//,3X,'XE(I)',5X,'YE(I)',5X,'ZX(I)',5X,'TEMP',//)
DO 60 I=1,NP
           IF(ABS(ZG(I)-4.0).GT.0.00001) GO TO 60
           \overrightarrow{W}RITE(IO,50) XG(I),YG(I),ZG(I),A(I)
  50
           FORMAT(3X,4F10.4)
     CONTINUE
     DO 70 I=1,NP
           IF(ABS(ZG(I)-0.7348).GT.0.00001) GO TO 70
           WRITE(IO,50) XG(I),YG(I),ZG(I),A(I)
     CONTINUE
  70
      CLOSE(UNIT=IN,STATUS='SAVE')
      CLOSE(UNIT=IO,STATUS='SAVE')
      STOP
     END
```

```
SUBROUTINE BNDRYK(KK,K1,K2,K3,TCON)
      IMPLICIT REAL (A-H,O-Z)
      COMMON /XYZ/XE(8),YE(8),ZE(8)
      REAL K1,K2,K3
C
C**
       Subroutine of assigning the K to each element
C
       X = (XE(1) + XE(2))/2.
       Y = (YE(1) + YE(4))/2.
       Z=(ZE(1)+ZE(5))/2.
IF(((ABS(X).GT.0.0) .AND. (ABS(X).LT.15.0) .AND.
    2
          ABS(Y).GT.25.95).AND. (ABS(Y).LT.66.0) .AND.
          ABS(Z).GT.2.2).\acute{A}ND. (\acute{A}BS(Z).\acute{L}T.2.5)).\acute{O}R.
    2
    2
         ((ABS(X).GT.15.0).AND. (ABS(X).LT.20.0) .AND.
    2
          (ABS(Y).GT.30.28).AND. (ABS(Y).LT.48.62) .AND.
    rac{2}{2}
          (ABS(Z).GT.2.2) (ABS(Z).LT.2.5) OR.
         ((ABS(X).GT.15.0).AND. (ABS(X).LT.20.0).AND.
    2
          ABS(Y).GT.56.98).AND. (ABS(Y).LT.66.0) .AND.
         (ABS(Z).GT.2.2) .ÁND. (ABS(Z).LT.2.5)) .ÓR. ((ABS(X).GT.20.0).AND. (ABS(X).LT.30.0) .AND.
    rac{2}{2}
    2
          ABS(Y).GT.34.60).AND. (ABS(Y).LT.44.45) .AND.
    ABS(Z).GT.2.2) AND. (ABS(Z).LT.2.5)) OR.
         ((ABS(X).GT.20.0).AND. (ABS(X).LT.30.0) .AND.
          'ABS(Y).GT.61.15).AND. (ABS(Y).LT.66.0) .AND.
          (ABS(Z).GT.2.2) .ÁND. (ABS(Z).L´T.2.5)) .ÓR. (KK.GE.25) .AND. (KK.LE.27)) .OR.
           KK.GE.55) .AND. (KK.LE.57)
                                                 .OR.
           KK.GE.61) .AND. (KK.LE.63)
                                                 .OR.
           KK.GE.73) .AND. (KK.LE.75)
                                                 .OR.
           KK.GE.79) .AND. (KK.LE.81)
                                                 .OR.
           KK.GE.67) .AND. (KK.LE.69)
                                                 .OR.
           KK.GE.91) .AND. (KK.LE.93)
                                                 .OR.
           KK.GE.451) .AND. (KK.LE.453))
                                                  .OR.
           KK.GE.457) .AND. (KK.LE.459)
                                                  .OR.
           KK.GE.463) .AND. (KK.LE.465)
                                                  .OR.
           KK.GE.469) .AND. (KK.LE.471)
                                                  .OR.
           KK.GE.505) .AND. (KK.LE.507)
                                                  .OR.
           KK.GE.535) .AND. (KK.LE.537)
                                                  .OR.
    2
           KK.GE.541) .AND. (KK.LE.543)
                                                  .OR.
    2
           KK.GE.553) .AND. (KK.LE.555)
                                                  .OR.
    \frac{2}{2}
           KK.GE.559) .AND. (KK.LE.561)
                                                  .OR.
         (( KK.GE.547) .AND. (KK.LE.549))
(( KK.GE.571) .AND. (KK.LE.573)))
                                                  .OR.
                                                   THEN
              TCON=K2
       ELSE IF((( KK.GE.76 ) .AND. (KK.LE.78 )) .OR.
                                                   .OR.
           KK.GE.70 ) .AND. (KK.LE.72 ))
                                                   .OR.
           KK.GE.322) .AND. (KK.LE.324))
    3
    3
           KK.GE.352) .AND. (KK.LE.354))
                                                   .OR.
    3
                                                   .OR.
           KK.GE.466) .AND. (KK.LE.468)
           KK.GE.556) .AND. (KK.LE.558)
KK.GE.550) .AND. (KK.LE.552)
    3
                                                   .OR.
    3
                                                   .OR.
         (( KK.GE.910) .AND. (KK.LE.912)))
                                                   THEN
```

```
TCON=K3
      ELSE
            TCON=K1
      ENDIF
      RETURN
      END
C
      SUBROUTINE ASMBL(KK)
      IMPLICIT REAL (A-H,Ò-Z)
COMMON /AV/A(119070),JGF,JGSM,NP,NBW
      COMMON /ELEM/ESM(8,8),EF(8),NS(1068,8)
       Subroutine of direct stiffness procedure
C*
C
      DO 20 I=1,8
            II=NS(KK,I)
            A(JGF+II)=A(JGF+II)+EF(I)
       DO 10 J=1.8
            JJ=NS(KK,J)+1-II
            IF(JJ.LE.0) GO TO 10
            J1 = JGSM + (JJ-1)*NP + II - (JJ-1)*(JJ-2)/2
            A(J1)=A(J1)+ESM(I,J)
  10
       CONTINUE
  20
      CONTINUE
      RETURN
      END
\mathbf{C}
\mathbf{C}
      SUBROUTINE NAT2D
      IMPLICIT REAL (A-H,O-Z)
      DIMENSION G(2)
      COMMON /NATU/KSAI(8),ETA(8),ZETA(8),WC
      REAL KSAI
      DATA (G(I),I=1,2)/0.577350,-0.577350/
       Subroutine of determining the Ksai and Eta in Gauss-Legendre method
C
      M=0
      DO 10 I=1,2
       DO 10 J=1,2
            M=M+1
            KSAI(M)=G(J)
            ETA(M)=G(I)
  10 CONTINUE
      RETURN
      END
CCC
```

```
SUBROUTINE NAT3D
      IMPLICIT REAL (A-H,O-Z)
      DIMENSION G(2)
      COMMON /NATU/KSAI(8),ETA(8),ZETA(8),WC
      REAL KSAI
      DATA (G(I),I=1,2)/0.577350,-0.577350/
C
        Subroutine of determining the Ksai, Eta and Zeta in Gauss-Legendre method
C<sup>*</sup>
C
      M=0
      DO 10 I=1,2
        DO 10 J=1,2
         DO 10 K=1,2
             M=M+1
             KSAI(M)=G(K)
             ETA(M)=G(J)
              ZETA(M)=G(I)
  10 CONTINUE
       RETURN
       END
\mathbf{C}
       SUBROUTINE SHAPE
       IMPLICIT REAL (A-H,O-Z)
       COMMON /SHA/X,Y,Z,N(8),PX(8),PY(8),PZ(8),B(3,8)
       REAL N
C
C***
        Subroutine of calculating shape function ([N]) and partial derivatives
C***
        of shape fuctions ([PX],[PY],[PZ]) in the natural coordinates X: KSAI Y: ETA Z: ZETA
C***
C
       N(1)=(1./8.)*(1-X)*(1-Y)*(1-Z)
       N(2) = (1./8.)*(1+X)*(1-Y)*(1-Z)
       N(3) = (1./8.)*(1+X)*(1+Y)*(1-Z)
       N(4) = (1./8.)*(1-X)*(1+Y)*(1-Z)
       N(5)=(1./8.)*(1-X)*(1-Y)*(1+Z)
       N(6) = (1./8.)*(1+X)*(1-Y)*(1+Z)

N(7) = (1./8.)*(1+X)*(1+Y)*(1+Z)
       N(8) = (1./8.)*(1-X)*(1+Y)*(1+Z)
\mathbf{C}
       PX(1)=(-1./8.)*(1-Y)*(1-Z)
       PX(2) = (1./8.)*(1-Y)*(1-Z)
       PX(3) = (1./8.)*(1+Y)*(1-Z)
       PX(4) = (-1./8.)*(1+Y)*(1-Z)
       PX(5) = (-1./8.)*(1-Y)*(1+Z)
       PX(6) = (1./8.)*(1-Y)*(1+Z)

PX(7) = (1./8.)*(1+Y)*(1+Z)
       PX(8) = (-1./8.)*(1+Y)*(1+Z)
C
       PY(1) = (-1./8.)*(1-X)*(1-Z)
```

```
PY(2) = (-1./8.)*(1+X)*(1-Z)

PY(3) = (1./8.)*(1+X)*(1-Z)
      PY(4)=(1./8.)*(1-X)*(1-Z)
      PY(5)=(-1./8.)*(1-X)*(1+Z)
      PY(6) = (-1./8.)*(1+X)*(1+Z)
      PY(7) = (1./8.)*(1+X)*(1+Z)
      PY(8)=(1./8.)*(1-X)*(1+Z)
\mathbf{C}
      PZ(1) = (-1./8.)*(1-X)*(1-Y)
      PZ(2)=(-1./8.)*(1+X)*(1-Y)
      PZ(3)=(-1./8.)*(1+X)*(1+Y)
      PZ(4)=(-1./8.)*(1-X)*(1+Y)
      PZ(5)=(1./8.)*(1-X)*(1-Y)
      PZ(6) = (1./8.)*(1+X)*(1-Y)
              =(`1.′/8.)*(1+X)*(1+Ý)
      PZ(7)=
      PZ(8) = (1./8.)*(1-X)*(1+Y)
\mathbf{C}
      RETURN
      END
\mathbf{C}
C
       SUBROUTINE DERSHP(DET,ICON)
       IMPLICIT REAL (A-H,O-Z)
       REAL JA, INJ, N
      DIMENSION JA(3,3),INJ(3,3)
COMMON /SHA/X,Y,Z,N(8),PX(8),PY(8),PZ(8),B(3,8)
       COMMON /XYZ/XE(8),YE(8),ZE(8)
C
C***
        Subroutine of calculating the derivative of shape function [B]
C*
C
       CALL SHAPE
C
C Calculating the Jacobian matrix
       DO 10 I=1,3
         DO 10 J=1,3
              JA(I,J)=0.0
      CONTINÙE
       DO 20 I=1.8
              JA(1,1)=JA(1,1)+PX(I)*XE(I)
              JA(1,2)=JA(1,2)+PX(I)*YE(I)
              JA(1,3)=JA(1,3)+PX(I)*ZE(I)
              JA(2,1)=JA(2,1)+PY(I)*XE(I)
              JA(2,2)=JA(2,2)+PY(I)*YE
              JA(2,3) = JA(2,3) + PY(I) * ZE(I)
              JA(3,1)=JA(3,1)+PZ(I)*XE(I)
              JA(3,2)=JA(3,2)+PZ(I)*YE(I)
              JA(3,3) = JA(3,3) + PZ(I)*ZE(I)
   20
       CONTINUE
       IF(ICON.NE.1) GO TO 30
       JA(1,3)=0.0
```

```
JA(2,3)=0.0
      JA(3,1)=0.0
      JA(3,2)=0.0
      JA(3,3)=1.0
C
\mathbf{C}
  Calculating of the inverse of Jacobian matrix
  30
     DELTA = JA(1,1)*JA(2,2)*JA(3,3)-JA(1,1)*JA(2,3)*JA(3,2)
          -JA(1,2)*JA(2,1)*JA(3,3)+JA(1,2)*JA(2,3)*JA(3,1)
   1
          +JA(1,3)*JA(2,1)*JA(3,2)-JA(1,3)*JA(3,1)*JA(2,2)
      DET=ABS(DELTA)
      D=1./DELTA
      INJ(1,1) = D*(JA(2,2)*JA(3,3)-JA(2,3)*JA(3,2)
      INJ(1,2)=D*(JA(1,3)*JA(3,2)-JA(1,2)*JA(3,3))
      INJ(1,3)=D*(JA(1,2)*JA(2,3)-JA(2,2)*JA(1,3))
      INJ(2,1) = D*(JA(3,1)*JA(2,3)-JA(2,1)*JA(3,3)
      INJ(2,2) = D*(JA(1,1)*JA(3,3)-JA(1,3)*JA(3,1)
      INJ(2,3) = D*(JA(2,1)*JA(1,3)-JA(1,1)*JA(2,3)
      INJ(3,1)=D*(JA(2,1)*JA(3,2)-JA(2,2)*JA(3,1))
      INJ(3,2)=D*(JA(1,2)*JA(3,1)-JA(1,1)*JA(3,2))
      INJ(3,3)=D*(JA(1,1)*JA(2,2)-JA(2,1)*JA(1,2))
C
   Calculating of the [B] matrix
      DO 40 I=1,3
       DO 40 J = 1.8
             B(I,J)=INJ(I,1)*PX(J)+INJ(I,2)*PY(J)+INJ(I,3)*PZ(J)
      CONTINUE
      RETURN
      END
С
\mathbf{C}
      SUBROUTINE MODIFY(TEMP)
      IMPLICIT REAL (A-H,O-Z)
      COMMON/AV/A(119070), JGF, JGSM, NP, NBW
\mathbf{C}
C***
        Subroutine of input of the known nodal temperature values
\mathbf{C}
      DO 30 I=1,NP
      IF(((I.GE.36) .AND.(I.LE.49)) .OR.((I.Ge.106) .AND. (I.LE.119)).OR.
      ((I.GE.666).AND.(I.LE.679)).OR.((I.GE.736).AND.(I.LE.749))) THEN
             IB=I
             BV = TEMP
             K=IB-1
         DO 20 J=2, NBW
             M=IB+J-1
             IF(M.GT.NP) GO TO 10
             IJ = JGSM + (J-1)*NP + IB - (J-1)*(J-2)/2
             A(JGF+M)=A(JGF+M)-A(IJ)*BV
             A(IJ)=0.0
           IF(K .LE. 0) GO TO 20
  10
             KJ = JGSM + (J-1)*NP + K - (J-1)*(J-2)/2
```

```
A(JGF+K)=A(JGF+K)-A(KJ)*BV
            A(KJ)=0.0
            K=K-1
 20
        CONTINUE
       A(JGF+IB)=A(JGSM+IB)*BV
     ELSE
      GO TO 30
     ENDIF
 30
     CONTINUE
     RETURN
     END
\mathbf{C}
\mathbf{C}
      SUBROUTINE DCMPBD
      IMPLICIT REAL (A-H,O-Z)
      COMMON /AV/A(119070), JGF, JGSM, NP, NBW
\mathbf{C}
C***
       Subroutine of decomposition of a banded matrix into upper
C***
       triangular form using Gauss elimination
C****
      NP1=NP-1
      DO 20 I=1,NP1
            MJ=I+NBW-1
            IF(MJ.GT.NP) MJ=NP
            NJ=I+1
            MK=NBW
            IF((NP-I+1) LT. NBW) MK=NP-I+1
            ND=0
       DO 10 J=NJ,MJ
            MK=MK-1
            ND = ND + 1
            NL=ND+1
         DO 10 K=1,MK
            NK = ND + K
            JK = JGSM + (K - 1)*NP + J - (K - 1)*(K - 2)/2
            INL=JGSM+(NL-1)*NP+I-(NL-1)*(NL-2)/2
            INK = JGSM + (NK-1)*NP + I - (NK-1)*(NK-2)/2
            II=JGSM+I
            A(JK)=A(JK)-A(INL)*A(INK)/A(II)
       CONTINUE
  10
      CONTINUE
      RETURN
      END
\mathbf{C}
\mathbf{C}
      SUBROUTINE SLVBD
      IMPLICIT REAL (A-H,O-Z)
      COMMON /AV/A(119070), JGF, JGSM, NP, NBW
C
       Subroutine of decomposition of the global force vector
C
```

```
NP1=NP-1
    DO 10 I=1,NP1
          MJ=I+NBW-1
          IF(MJ.GT.NP) MJ=NP
          NJ=I+1
          L=1
       DO 10 J=NJ,MJ
          L=L+1
          IL=JGSM+(L-1)*NP+I-(L-1)*(L-2)/2
          A(JGF+J)=A(JGF+J)-A(IL)*A(JGF+I)/A(JGSM+I)
 10
     CONTINUE
Č
  Backward substitution for solving the system of equations
     A(NP)=A(JGF+NP)/A(JGSM+NP)
     DO 20 K=1,NP1
          I=NP-K
          MJ=NBW
          IF((I+NBW-1).GT.NP) MJ=NP-I+1
          SU\dot{M}=0.0
       DO 30 J=2,MJ
          N=I+J-1
          IJ=JGSM+(J-1)*NP+I-(J-1)*(J-2)/2
          SUM = SUM + A(IJ) * A(N)
 30
       CONTINUE
     20
     RETURN
```

END

APPENDIX C

PIPE HEAD LOSS

APPENDIX C

The pumping resistance of typical pipe circuit (Figure 1.1) and the new pipe circuit (Figure 1.2) were calculated in the hot water floor systems. The farrowing house was assumed to have the 20 crates. The length of pipe and the bending points were 109.7 m (360 feet) and 80 for the typical pipe circuit and 91.4 m (300 feet) and 10 for the new pipe circuit, respectively. The pumping capacity was assumed as 15.1 l/min. (4 gallon/min.).

1) Losses due to wall friction

The water velocity in the circular tube is

$$\overline{V} = \frac{252.33 \text{ cm}^3/\text{s}}{(\pi/4) (1.905)^2 \text{ cm}^2} = 88.53 \text{ cm/s} = 0.8853 \text{ m/s}$$

At 60 °C (140 °F), kinematic viscosity, $\nu = 0.478 \times 10^{-6} \text{ m}^2/\text{s}$, so that

Re =
$$\frac{\overline{VD}}{\nu}$$
 = $\frac{0.8853 \text{ m/s} \times 0.01905 \text{ m}}{0.478 \times 10^{-6} \text{ m}^2/\text{s}}$ = 3.5282×10^4

The relative roughness is

$$\frac{\epsilon}{D} = \frac{0.045 \text{ mm}}{19.05 \text{ mm}} = 0.00236$$

for the wrought iron pipe.

From the Moody diagram, the friction factor is f = 0.028. From the modified Bernoulli equation,

$$\Delta P = -\frac{1}{2} \rho \overline{V}^2 \frac{fL}{D}$$

$$= -\frac{1}{2} (983.2 \text{ kg/m}^3) (0.8853)^2 \text{ m}^2/\text{s}^2 \frac{(0.028) \text{ (L) m}}{0.01905 \text{ m}}$$

$$= - (0.575 \text{ L) KPa}$$

For the typical pipe circuit,

$$\Delta P_{w1} = -(0.575) \times 109.7 \text{ KPa} = -63.1 \text{ KPa}$$

$$\Delta H_{w1} = -\frac{\Delta P_{w1}}{\rho g} = -\frac{63100 \text{ kg/m} \cdot \text{s}^2}{983.2 \text{ kg/m}^3 9.8 \text{ m/s}^2} = -6.55 \text{ m}$$

where ΔH_{w1} is head loss.

For the new pipe circuit,

$$\Delta P_{w2} = -(0.575) \times 91.4 \text{ KPa} = -52.6 \text{ KPa}$$

$$\Delta H_{w2} = -\frac{52600 \text{ kg/m} \cdot \text{s}^2}{983.2 \text{ kg/m}^3 9.8 \text{ m/s}^2} = -5.45 \text{ m}$$

2) Losses in pipe bending

The loss coefficient of standard 90° elbow (K) is 0.75. The pressure drop for one bending is

$$\Delta P = - K \frac{1}{2} \rho \overline{V}^2$$

$$= - (0.75) (\frac{1}{2}) (983.2 \text{ kg/m}^3) (0.8853)^2 \text{ m}^2/\text{s}^2$$

$$= - 0.289 \text{ KPa}$$

For the typical pipe circuit,

$$\Delta P_{b1} = -(0.289) (80) = -23.1 \text{ KPa}$$

$$\Delta H_{b1} = -\frac{23100 \text{ kg/m} \cdot \text{s}^2}{983.2 \text{ kg/m}^3 9.8 \text{ m/s}^2} = -2.40 \text{ m}$$

For the new pipe circuit,

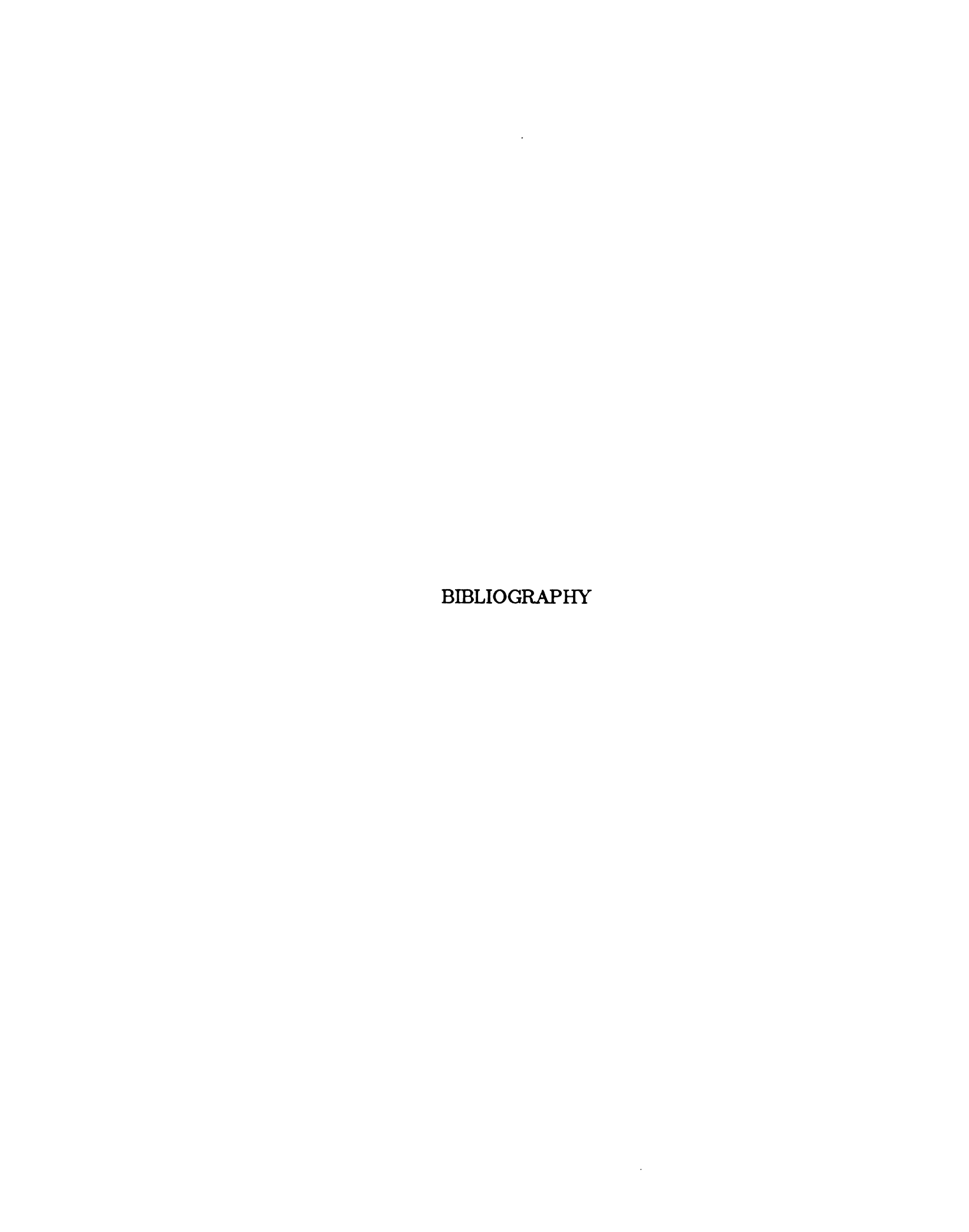
$$\Delta P_{b2} = - (0.289) (10) = -2.9 \text{ KPa}$$

$$\Delta H_{b2} = -\frac{2900 \text{ kg/m} \cdot \text{s}^2}{983.2 \text{ kg/m}^3 9.8 \text{ m/s}^2} = -0.30 \text{ m}$$

3) Comparison with typical and new pipe circuit

Head loss	Typical pipe circuit	New pipe circuit
Loss due to wall friction Loss in pipe bending	- 6.55 m - 2.40 m	- 5.45 m - 0.30 m
Total head loss	- 8.95 m	- 5.75 m

The result shows the new pipe circuit reduced the head loss by 35.8 %. The loss in pipe bending of new pipe circuit was negligible while that of typical pipe circuit occupied a large portion of total loss.

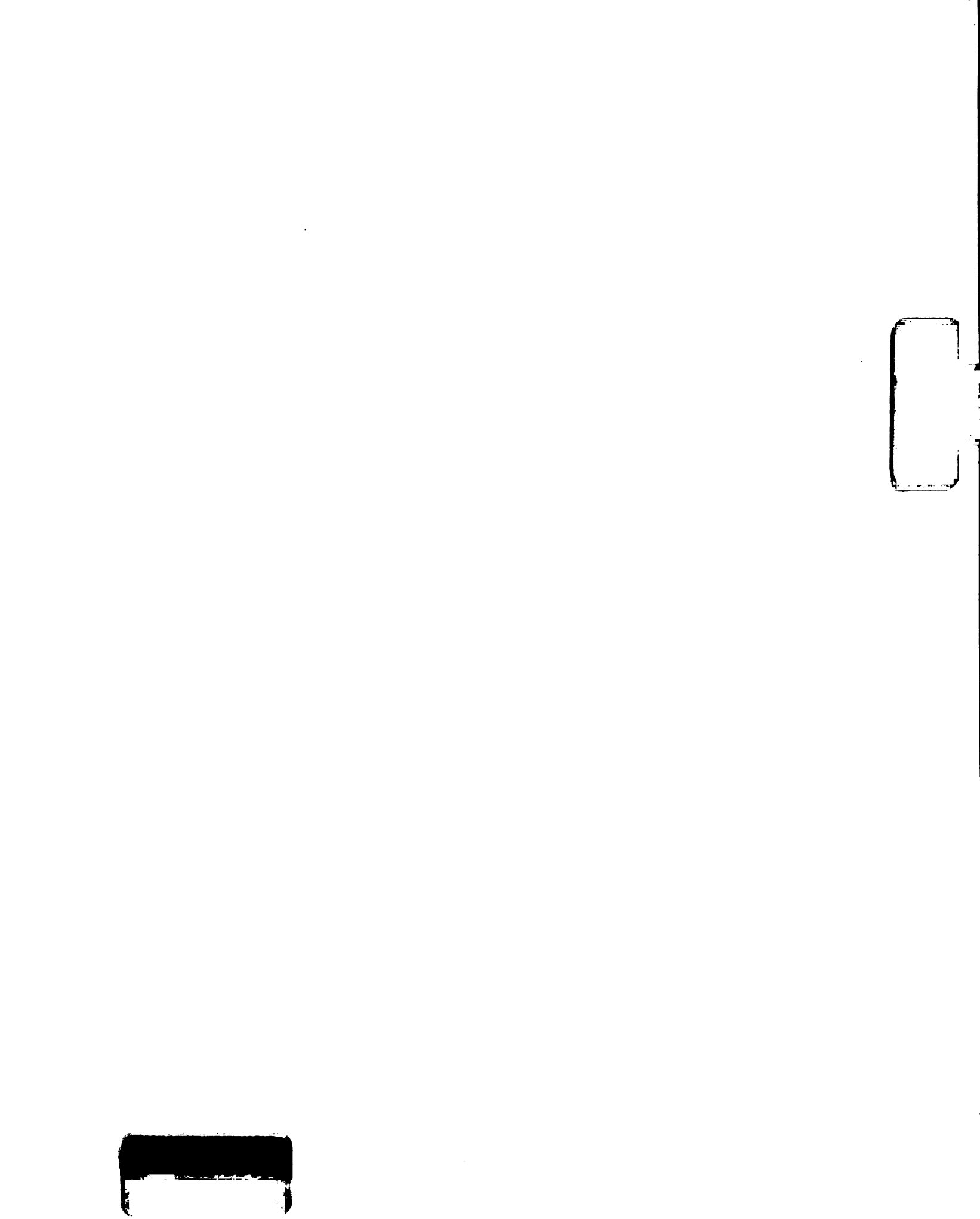


BIBLIOGRAPHY

- Agricultural Engineers Yearbook. 1986. The American Society of Agricultural Engineers, St. Joseph, MI.
- Akyuz, F. A. 1970. Natural Coordinate systems, An Automatic Input Data Generation Scheme for a Finite Element Method. Nuclear Engineering and Design. Vol. 11, pp 195 207.
- Allaire, P. E. 1985. Basics of the Finite Element Method. Wm. C. Brown Publishers.
- Beckett, F. E. and R. F. Barron. 1972. Heat Transfer from a Pig to the Floor. Transactions of the ASAE, Vol. 15, No. 4, pp. 700 703.
- Butchbaker, A. F. and M. D. Shanklin. 1965. Development of Homeothermic Regulation in Young Pigs. Transactions of the ASAE, Vol. 8, No. 4, pp. 481-485.
- Cavendish, J. C., D. A. Field and W. H. Frey. 1985. An Approach to Automatic Three Dimensional Finite Element Mesh Generation. International Journal for Numerical Methods in Engineering, Vol. 21, pp. 329 347.
- Collins, R. J. 1973. Bandwidth Reduction by automatic Renumbering. International Journal for Numerical Methods in Engineering, Vol. 6, pp. 345 356.
- Curtis, S. E. 1981. The Environment in Swine Housing. Extension Bulletin E-1284. Michigan State University, Cooperative Extension Service.
- England, D. C., H. W. Johnes and S. Pollmann. 1987. Care of the Sow During Farrowing and Lactation. Extention Bulletin E-1232. Michigan State University, Cooperative Extension Service.
- Ergatoudis, I., B. M. Irons and O. C. Zienkiewicz. Curved, Isoparametric, Quadrilateral Elements for Finite Element Analysis. International Journal Solids Structures, Vol.4, pp. 31 42.

- Grooms, H. R. 1972. Algorithm for Matrix Bandwidth Reduction. American Society of Civil Engineers, Vol. 98, No. ST1, pp. 203 214.
- Hart, D. P. and R. Couvillion. 1986. Earth Coupled Heat Transfer. National Water Well Association, Dublin, Ohio. pp. 84 85.
- John, J. E. A. and W. L. Haberman. 1980. Introduction to Fluid Mechanics. Second Edition. Prentice-Hall, Inc., Englewood Cliffs, New Jersey.
- Karhnak, J. M. and R. A. Aldrich. 1971. Environmental Control in a Farrow-to-Finish Facility, Transactions of ASAE, Vol. 14, No. 2, pp. 260 - 262.
- Kelly, C. F., H. Heitman and J. R. Morris. 1948. Effect of Environment on Heat Loss from Swine. Agricultural Engineering, Vol. 29, No. 12, pp. 525 529.
- Kreith, F. 1965. Principles of Heat Transfer. Second Edition, International Textbook Company, Scranton, Pennsylvania.
- Lardner, T. J. 1963. Biot's Variational Principle in Heat Conduction. AIAA Journal, Vol. 1, pp. 196 206.
- Laura, P. A. A., J. A. Reyes and R. E. Rossi. 1974. A Comparison of Analytical and Numerical Solutions in Heat Conduction Problems. Nuclear Engineering and Design, Vol. 31, pp. 379 382.
- Liptrap, D. O., J. H. Bailey and J. O'Neal. 1987. Baby Pig Management Birth to Weaning. Extension Bulletin E-1095. Michigan State University, Cooperative Extension Service.
- Mahan, D. C. 1985. Cold Facts on Nursery Environments. Hog Farm Management, pp. 26 28.
- Meyer, V. M. and R. W. Hansen. 1980. Insulation for Swine Housing. Extension Bulletin E-1396. Michigan State University, Cooperative Extension Service.
- Muehling, A. J. and C. M. Stanislaw. 1979. Swine Farrowing Units. Extension Bulletin E-1087. Michigan State University, Cooperative Extension Service.
- Segerlind, L. J. 1984. Applied Finite Element Analysis. Second Edition. John Welley & Sons, Inc., New York.

- Spillman, C. K. and C. N. Hinkle. 1969. Conduction Heat Transfer from Swine to Controlled Temperature Floors. ASAE paper No. 69 441. ASAE, St. Josept, MI.
- Spillman, C. K. and J. P. Murphy. 1976. Effect of Farrowing House temperature on Energy Use and Litter Size. ASAE Paper No. 76-4044. ASAE, St. Joseph, MI.
- Stainsbury, D. 1970. Pig Housing. Fifth Edition, Farm Press Ltd..
- Van Fossen, L. and D. G. Overhults. 1980. Floor Heat for Swine. Extension Bulletin E-1397. Michigan State University, Cooperative Extension Service.
- Wilson, E. L. and R. E. Nickell. 1966. Application of the Finite Method to Heat Conduction Analysis. Nuclear Engineering and Design, Vol. 4, pp. 276-286.
- Zienkiewicz, O. C. and Y. K. Cheung. 1965. Finite Elements in the solution of field problems. The Engineer, Vol. 220, p 507.
- Zienkiewicz, O. C., A. K. Bahrani and P. L. Arlett. 1967. Solution of Three Dimensional Field Problems by the Finite Element Method. The Engineer, Vol. 224, No. 5830, pp. 547 550.
- Zienkiewicz, O. C. 1977. The Finite Element Method. Third Edition. McGraw-Hill Publications, New York.



MICHIGAN STATE UNIV. LIBRARIES
31293005518851